CRC Report No. A-125

THE RISING IMPORTANCE OF NON-COMBUSTION EMISSIONS IN URBAN ATMOSPHERES

Final Report

November 2024

COORDINATING RESEARCH COUNCIL, INC.
5755 NORTH POINT PARKWAY • SUITE 265 • ALPHARETTA, GA 30022

The Coordinating Research Council, Inc. (CRC) is a non-profit corporation supported by the petroleum and automotive equipment industries with participation from other industries, companies, and governmental bodies on research programs of mutual interest. CRC operates through the committees made up of technical experts from industry and government who voluntarily participate. The five main areas of research within CRC are: air pollution (atmospheric and engineering studies); aviation fuels, lubricants, and equipment performance; heavy-duty vehicle fuels, lubricants, and equipment performance (e.g., diesel trucks); light-duty vehicle fuels, lubricants, and equipment performance (e.g., passenger cars); and sustainable mobility (e.g., decarbonization). CRC's function is to provide the mechanism for joint research conducted by industries that will help in determining the optimum combination of products. CRC's work is limited to research that is mutually beneficial to the industries involved. The final results of the research conducted by, or under the auspices of, CRC are available to the public.

1. Executive Summary

Urban air pollution is characterized by significant spatial variability (Harrison, 2018; Yang et al., 2020; Liang & Gong, 2020; Wang et al., 2020). For instance, areas adjacent to highways often exhibit elevated levels of traffic emissions, which serve as major sources of primary pollutants (Filigrana et al., 2020; Jeong et al., 2022; Jiang et al., 2021; Moutinho et al., 2020). Conversely, urban background areas such as parks typically demonstrate lower concentrations (Xu et al., 2020). Typically, it is anticipated that air pollution levels will be closely linked to the specific nature of human activity at any given time, such as anthropogenic emission-generating activities, including the operation of motor vehicles or power plants (Li et al., 2020; Yang et al., 2020). Therefore, pollution characteristics and levels can markedly differ across specific locations and time points of air sample collection, depending on where and when most anthropogenic emissions occur.

The goal of this project was to improve the understanding of how anthropogenic emissions from multiple source sectors vary spatially and temporally in dense urban areas, and how the emissions of both organic species and NOx from these sources impact $PM_{2.5}$ and O_3 concentrations at the urban scale. We were particularly interested in quantifying the impacts of non-combustion sources including volatile chemical products (VCPs) and restaurant cooking. Emissions from these source categories scale with population, are lightly regulated (or not regulated at all), and therefore may be increasing. In contrast, combustion emissions from motor vehicles are decreasing due to regulation.

We tested the following primary hypotheses:(1) Spatiotemporal trends in ambient $PM_{2.5}$ mass and composition, specifically organic aerosol (OA), are coupled to the movement of people throughout the day. Movement of people drives spatial and temporal trends in emissions from both traditional (e.g., vehicles) and nontraditional (e.g., VCPs) sources. (2) "Nontraditional" anthropogenic sources of O_3 and secondary $PM_{2.5}$, including non-combustion volatile chemical products and restaurant emissions, are equal to or greater in importance than vehicular traffic in urban areas.

We tested these hypotheses by performing a series of measurements using a mobile laboratory equipped with a suite of state-of-the-art instrumentation to quantify concentrations of organics ranging from low and extremely low volatility (LVOC and ELVOC) to volatile (VOCs), particle size, and particle composition. We used land use and other geospatial data to guide selection of sampling locations that have varying impacts from our source categories of interest. For example, we sampled in areas of high and low restaurant density to quantify impacts of cooking sources.

The key results of this project are: (1) We demonstrated that in urban locations, contributions of fresh emissions from non-combustion sources such as cooking and asphalt paving to $PM_{2.5}$ are equal to or larger than fresh traffic emissions, (2) Cooking emissions can be an important source of organic nitrogen in urban environments, and that reduced nitrogen species emitted from cooking can rapidly partition into the vapor phase upon dilution of cooking emissions, (3) Spatial variations of OH reactivity, and hence O_3 production potential, are smaller than day-to-day variations driven by emissions and meteorology.

While the results of this report are based on data collected in a single city, the results are applicable to cities across the United States. The same set of anthropogenic emissions sources (e.g., traffic, restaurant cooking, and asphalt paving) are important in cities nationwide (Saha et al., 2020). Therefore, similar temporal and spatial patterns of $PM_{2.5}$ concentrations, driven by spatial and temporal changes in anthropogenic activities, are likely to be found in most cities. Further reductions in urban $PM_{2.5}$ could therefore be achieved by controlling or limiting emissions from these non-combustion sources.

Each of the following three sections of this report addresses one of the key findings. Section 2 discusses measurements and source apportionment of organic aerosols in urban locations impacted by different source mixes. Section 3 discusses the presence of organic nitrogen in emissions from cooking sources. Section 4 examines spatial and temporal variations in OH reactivity.

2. Spatiotemporal Analysis of Traffic, Cooking, and Asphalt Contributions to Ambient Particulate Matter in and Urban Area

2.1 Introduction

One of the most commonly utilized tools for measuring emissions generated by human activity is the Aerosol Mass Spectrometer (AMS) (Crippa et al., 2014a; in 't Veld et al., 2023; Setyan et al., 2012; Tsimpidi et al., 2016; Zhou et al., 2020), which quantifies real-time measurement of vehicle emissions (Cross et al., 2012; J. Wang et al., 2020; Zhang et al., 2021c, 2021c). Factor analysis of the AMS datasets with positive matrix factorization (PMF) routinely identify a Hydrocarbon-like Organic Aerosol (HOA) factor attributable to vehicle exhaust (Mohr et al., 2011; Yao et al., 2021; Ye et al., 2018b; Zhang et al., 2005).

Studies by Alfarra et al. (2004) and Brook et al. (2007) have highlighted anthropogenic origins of primary emissions from gasoline and diesel engines (DeWitt et al., 2015; Hayes et al., 2013; B. P. Lee et al., 2017; Marjanen et al., 2022). The composition of HOAs is significantly complex and diverse, including a wide array of organic compounds like alkanes, polycyclic aromatic hydrocarbons (PAHs), and other hydrocarbon-like substances (Pye and Pouliot, 2012). Despite the variability in its origins, the composition of the HOA factor remains one of the most stable and consistent across the AMS datasets worldwide (Crippa et al., 2014a; Jimenez et al., 2009).

However, the majority of $PM_{2.5}$ is composed of secondary components that are produced as byproducts of the chemical reactions in the atmosphere; this includes secondary organic aerosols (SOAs) and secondary sulfate and nitrate salts (Surratt et al., 2007). Recent research has identified volatile chemical products (VCPs), including personal care products like deodorant, printing inks, and asphalt paving, as an important source for subsequent SOAs in the atmosphere (Coggon et al., 2018; Humes et al., 2023; Seltzer et al., 2022). In addition, prior papers found that a massive amount of Volatile Organic Chemicals (VOCs) can be emitted from hot asphalt mixtures. For example, Khare et al., 2020 showed that asphalt is producing higher SOA yield on average compared with gasoline and diesel emissions. Emissions from these source categories scale with population and are only lightly regulated in the U.S (McDonald et al., 2018), in part due to their complexity and limited studies conducted in this area. This is unlike other conventional forms of air pollution, such as traffic, which has been routinely identified and incorporated into substantial environmental policies (Black, 1991; Chow et al., 2007; Reitze, 1999; Samuelsen et al., 2021, 2021).

Polycyclic Aromatic Hydrocarbons (PAHs) are a specific class of organic compounds characterized by compounds containing aromatic rings in their chemical structure. These compounds are normally identified from various sources from both natural and anthropogenic sources (Dat and Chang, 2017; Kicińska and Dmytrowski, 2023; Stout et al., 2001). High temperatures during the asphalt paving process leads to the volatilization and emission of the PAHs (Birgisdóttir et al., 2007); the specific PAH signature from paving can also differ by the asphalt type and the temperature while paving (Cavallari et al., 2012). Common PAHs associated with asphalt paving include naphthalene, phenanthrene, anthracene, fluoranthene, pyrene among others. These compounds are of particular concern due to their potential impact on the human health (Campo et al., 2006) and some PAHs (benzo[a]anthrancene [BaA], benzo[a]pyrene [BaP], and dibenzo[a,h,]anthracene) are categorized as probable carcinogens according to IARC (Campo et al., 2006).

While there were a few trials of incorporating PAHs sources with the source apportionment method (Zhang et al., 2015; S et al., 2006; Valotto et al., 2017), limited research has been conducted using the AMS. We investigated PAHs potentially present at paving locations, with a focus on identifying and analyzing PAHs-related fragments within environmental samples. The first phase of this approach involved a detailed examination of two paving site samples to identify the presence of PAHs-related fragments. To ensure a comprehensive analysis, we expanded our peak fitting range to include higher ranges of mass-to-charge (*m/z*) values up to 210. In the next phase, we employed PMF analysis, to separate the factors specifically associated with PAHs and their larger mass counterparts. This approach was anticipated to yield more refined separations of the asphalt factor, thereby improving our understanding of PAHs role and sources at paving sites.

In this section, we aim to examine the intra-city source contribution from multiple sectors including both traditional (e.g., traffic) and non-traditional (e.g., asphalt and cooking) sources across space and time from a field campaign in the summer and winter of 2021-2022. The comparative analysis of the non-traditional sources along with the traditionally well-recognized sources will provide insights into their contributions in the urban atmosphere.

2.2 Materials and Methods

2.2.1 Site selection and sampling method

A field campaign was conducted in Pittsburgh in the summer and winter of 2021-2022. Samples were collected via stationary sampling at 9 sites. We collected real-time measurements of non-refractory PM composition with an AMS (aerosol mass spectrometer) and BC with an aethalometer. Filter samples were also collected for offline analysis with a chemical ionization mass spectrometer (CIMS).

The sampling sites were selected to capture influences from different mixtures of anthropogenic sources. To determine the sampling sites of interest, we categorized source characteristics into two groups: those dominated by non-traditional (e.g., Volatile Chemical Products (VCPs) and cooking emissions) sources and those dominated by traditional (e.g., vehicular traffic emissions) sources. Each site was classified based on the intensity of each variable into either a "high" or "low" exposure category, a methodology commonly adopted in air pollution exposure assessment research. Our selection of sampling locations was guided by the hypothesis that areas with high concentrations of restaurants and traffic, as identified in a prior analysis conducted by our team, would exhibit elevated levels of relevant pollutants. This assumption is visually represented in Figure 2.1, where colored regions denote areas with significant restaurant densities. Except for two sites designated for asphalt paving analysis, our selected sampling locations are predominantly situated within areas highlighted in yellow (Figure 2.1), indicating a substantial presence of dining establishments.

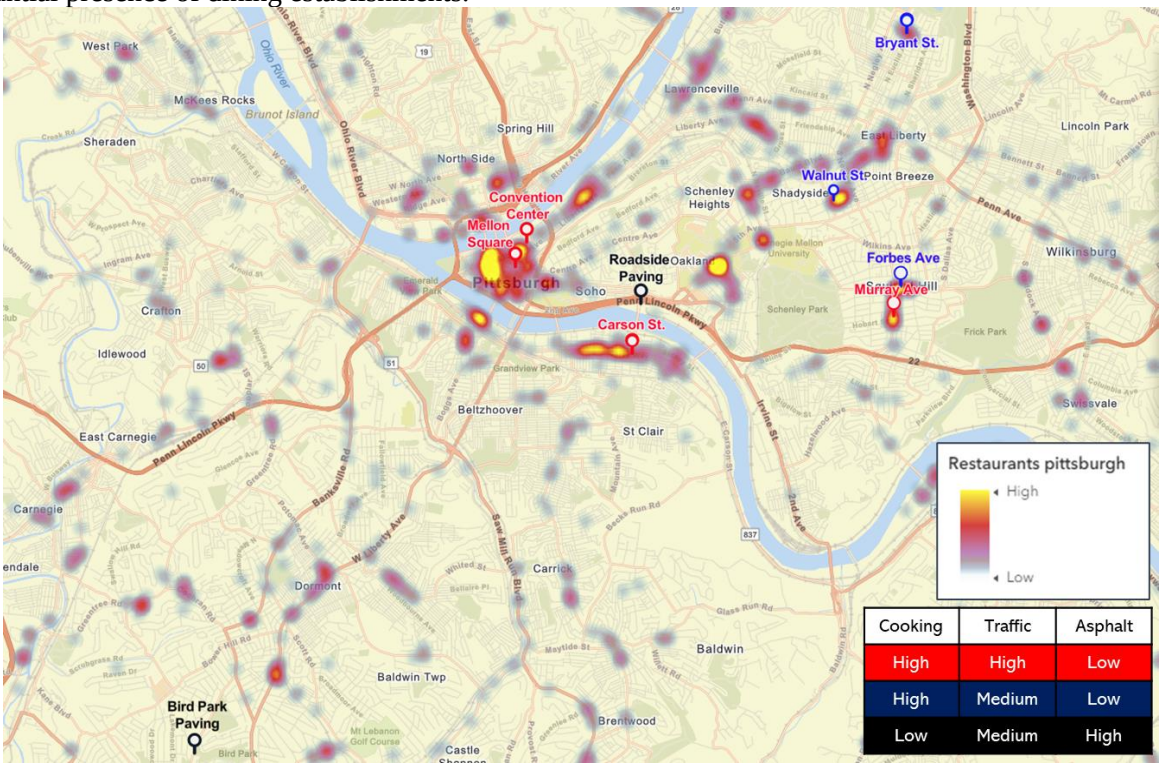

Figure 2.1 Overview of the sampling locations in summer 2021 field campaign in Pittsburgh. The figure includes a detailed map marked with the locations of our sampling sites, which are categorized into three unique groups for clarity.

For example, Convention Center and Mellon Square in downtown Pittsburgh are impacted by sources of VCPs from people, traffic and cooking. Unlike those two sites, Bryant St near Highland Park is not close to main highways, but several restaurants were gathered. For this reason, we mainly expect cooking emissions when we collect samples at Bryant St.

In this study, locations were chosen based on a categorization system derived from the findings from a previous report in our group, which identified areas of high traffic and restaurant density using a range of several land use variables. Traffic variables encompassed vehicle miles traveled, traffic lights, and road length. To evaluate restaurant density, data from Allegheny County Health Department restaurant inspections were utilized. Sampling sites were then classified based on their primary source category, such as VCPs from asphalt paving, traffic, and cooking.

Figure 2.2 shows the sampling schematic used for collecting real-time and integrated samples. Sampling was conducted by parking a mobile laboratory at the selected sampling sites (Figure 2.3)

Sampling occurred at different times of the day at locations anticipated to have significant variations in human activity, facilitating the study of their temporal changes. The time frames were defined as morning (8 am to 10 am), midday (11 am to 1 pm), afternoon (2 pm to 4 pm), and evening (5 pm to 7 pm), all in Eastern Standard Time (EST).

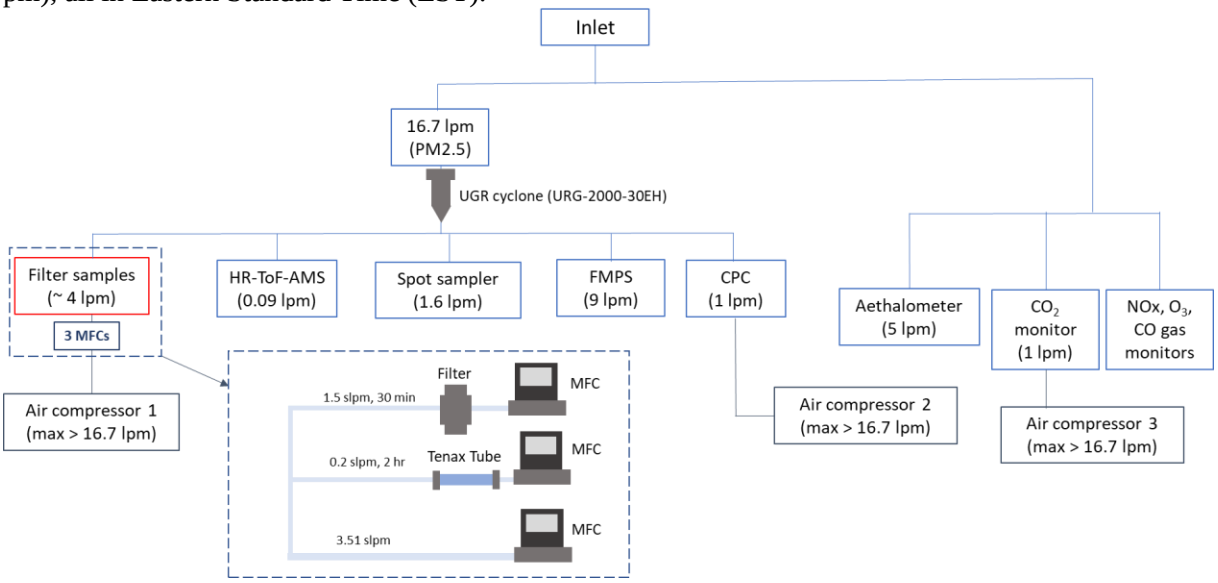

Figure 2.2 Schematic representation of the analytical instrument configuration within the van, employed for sample collection during 2021 field campaigns.

Figure 2.3 Photographs of a sampling site in downtown Pittsburgh (left) and a site targeting asphalt paving emissions (right).

2.2.2 Source apportionment using Positive Matrix Factorization (PMF)

The Positive Matrix Factorization (PMF) model, initially developed by Paatero (Paatero and Tapper 1993), was used for source apportionment of AMS data. It defines source contributions based on the principles of mass conservation and mass balance analysis. In this approach, ambient chemical concentrations data from receptors are utilized to formulate the mass balance equation (Hopke, 2000). PMF is frequently combined with the AMS due to its extensive application in the source apportionment of organic constituents in non-refractory fine particulate matter (NR-PM_1) (Al-Naeema et al., 2018).

For source apportionment of NR-PM_1 organics, the PMF Evaluation Tool (PET) v3.06B was employed. Input for the PMF was provided in the form of high-resolution organic matrix and its corresponding error matrix files, which were generated after fitting the mass spectra between *m/z* 12 to 120. This processing was carried out with PIKA toolkit ver 1.16 I in Igor Pro 8.04. To identify the optimal solutions from the PMF analysis, our group adhered to the general steps outlined in Zhang et al., 2011. Prior to running the model, "bad runs" defined as those with Signal to Noise Ratio (SNR) below 0.2 were removed from the calculation. Weak *m/z* with SNR below 2 and duplicated ions, such as *m/z* 44-related ions, were down weighted with a magnitude of 2. Each PMF factor was assessed using the $Q/Q_{expected}$ to determine the solutions that best describes the dataset, by altering FPEAK values (ranging from -1 to 1 with increments of 0.2) (Ulbrich et al., 2009).

2.3 Results and Discussion

2.3.1 Overview of the chemical composition and sources of NR-PM_1.

Table 2.1 Mass concentration of the chemical species (μg m^{-3}) measured by the AMS and Aethalometer.

Sample sites	Category	Sampling period	Org	SO_4^{2-}	NO_3^-	NH_4^+	Chl^-	Black Carbon
Murray Avenue	Cooking, Traffic	Sep 17th, 2021 Morning-Evening	6.31±2.1	2.16±0.44	0.24±0.06	0.61±0.33	0.01±0.01	-
Bryant Street	Cooking	Sep 2nd, 2021 Evening	15.13±9.7	0.20±0.14	0.21±0.06	1.60±0.09	0.04±0.03	2.35±4.16
		Mar 30th, 2022 Afternoon-Evening	2.58±1.48	0.23±0.06	0.07±0.02	0.09±0.05	0.01±0.01	0.70±0.47
Walnut Street	Cooking	Aug 27th, 2021 Afternoon-Evening	13.37±5.81	7.55±0.99	0.44±0.09	2.52±0.32	0.03±0.02	2.57±3.05
Forbes Avenue	Cooking, Traffic	Sep 16th, 2021 Morning-Evening	7.89±4.31	2.34±0.65	0.21±0.16	0.67±0.24	0.01±0.13	-
Convention Center	Cooking, Traffic	Aug 26th, 2021 Morning-Evening	11.83±1.51	6.23±1.04	1.09±0.91	2.12±0.28	0.03±0.02	1.23±1.08
		Mar 24th, 2022 Morning-Evening	1.14±0.55	0.25±0.07	0.05±0.01	0.07±0.03	0.01±0.00	0.47±0.43
Mellon Square	Cooking, Traffic	Aug 5th, 2021 Morning-Evening	14.52±6.02	2.50±0.27	0.80±0.62	0.91±0.32	0.04±0.05	1.09±0.58
		Mar 22nd, 2022 Morning-Evening	1.78±1.34	0.35±0.15	0.13±0.05	0.12±0.05	0.08±0.01	1.11±0.93
Carson Street	Cooking, Traffic	Sep 1st, 2021 Evening	17.29±22.20	0.54±0.33	0.30±0.14	0.15±0.14	0.04±0.08	9.94±35.34
		Mar 29th, 2022 Evening	3.71±3.47	0.22±0.08	0.69±0.10	0.23±0.04	0.02±0.02	0.81±0.61
Bird Park Paving	Asphalt	Nov 19th, 2021 Midday	3.00±9.07	0.38±0.10	0.88±0.23	0.33±0.14	0.02±0.02	0.89±4.29
Roadside Paving	Asphalt	Aug 30th, 2021 Morning	11.97±7.55	3.91±0.55	0.37±0.07	1.13±0.02	0.02±0.02	6.97±14.70

The primary chemical species of NR-PM_1, including organics, sulfate, nitrate, ammonium, chloride, and black carbon mass concentrations at each sample site are summarized in Table 2.1. The summer field campaign recorded an average organic mass concentration of 12.3 μg m^{-3}. This figure surpasses the annual average criteria of the EPA health-based standard of $PM_{2.5}$ of 12 μg m^{-3}, though it remains below the 24-hour standard of 35 μg m^{-3}. The measured concentrations are similar to the average $PM_{2.5}$ concentration of 10.3 μg m^{-3} recorded in Pittsburgh in 2021.

Among the four species identified from the AMS, the average organic concentration was highest at Carson Street (17.3 μg m^{-3}) followed by Bryant Street (15.1 μg m^{-3}). Both of these sites are heavily impacted by cooking emissions. The lowest organic concentration was noted at the Bird Park paving site

(3.00 µg m^{-3}). Out of the nine sample sites, the Bird Park and Roadside paving sites are largely influenced by asphalt emissions. In contrast, the Bryant and Walnut Street sites are mainly affected by cooking sources. The remaining four sites, characterized by high restaurant density and traffic, represent varied influences on their respective organic concentrations.

It is essential to acknowledge that each sampling site was visited either once or twice, meaning the values present in Table 2.1 likely do not represent long-term concentrations at each site. However, the measurements should be sufficient to examine site-to-site variations in source impacts and source profiles.

2.3.2 Resolved PMF factors and contributions to organic aerosols.

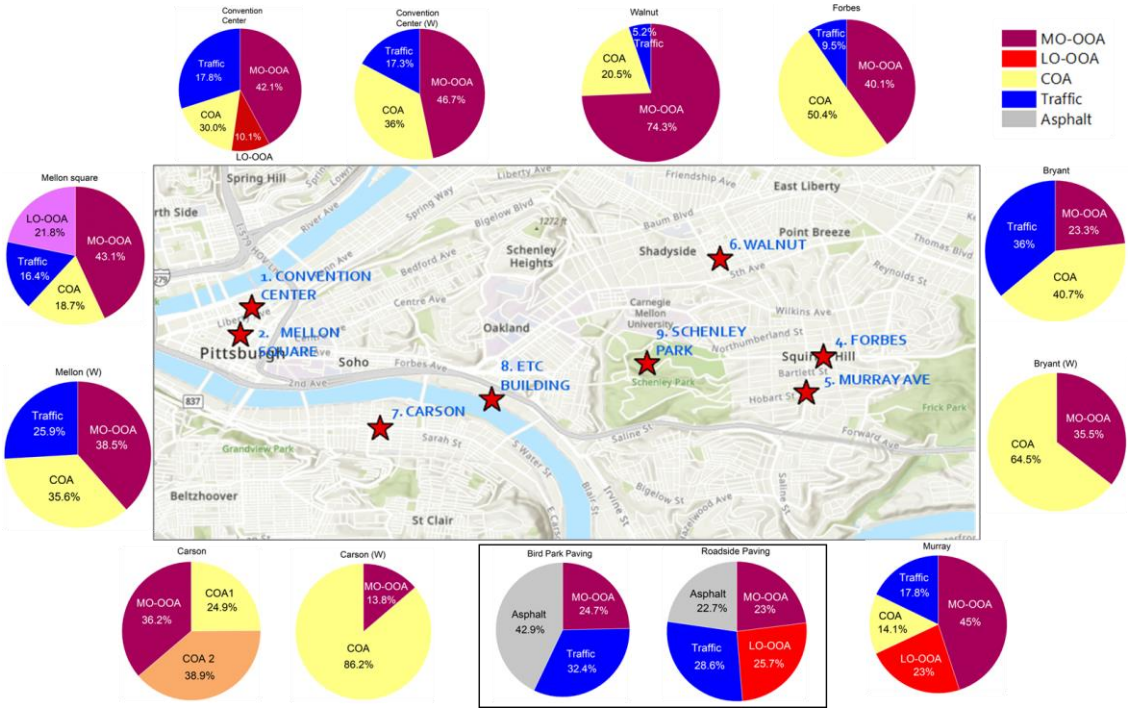

Figure 2.4 Summary of the source apportionment using AMS-PMF analysis. The pie charts show apportionment of organic aerosol among primary sources from cooking (COA), traffic (HOA), and asphalt along with secondary organic aerosol (MO-OOA and LO-OOA).

The comprehensive overview of the PMF source strengths at various sampling sites visited during the field campaign and their contributions to OA are presented in Figure 2.4. At sampling sites, the analysis identified factors corresponding to secondary organic aerosol (oxygenated OA – OOA), Traffic (hydrocarbon-like OA – HOA), cooking (COA), and Asphalt factors.

Excluding the two paving sites, the average COA contribution from each site constituted approximately 38% of the total OA. This is consistent with prior research that indicates substantial contribution from cooking sources to OA emissions in urban areas globally (He et al., 2019). For instance, studies from Canada and Greece found that cooking sources accounted for 15% and 11% of organic aerosol fractions, respectively (Jeong et al., 2016b; Manousakas et al., 2020). This underscores the persistent presence of COA emissions in urban settings and their non-negligible contribution to the total organic compounds. The contribution of COA to total OA in our samples is likely skewed high because we deliberately selected several sampling sites with high cooking influence.

Previous work has correlated the COA concentration with indicators of land use, including the number of nearby restaurants. In our data, while COA was higher in locations with more restaurants, there was not a clear correlation. In the summer, the COA factor contributed 50.4 % of OA at Forbes, followed by 40.7 % at Bryant, 30 % at Convention Center, 24.9 % at Carson, 18.7 % at Mellon square, and 14.1 %

at Murray Street. Although restaurant density within a 1 km boundary of these sites reveals that there is no direct correlation, the data suggests that high COA concentration is likely to be linked to a high number of restaurants observed at the sampling locations. For example, Mellon Square and the Convention center have the higher density with approximately 102 restaurants, followed by Forbes and Murry with 44 each, Carson Street with 43, Walnut Street with 25, and Bryant with 8. However, locations such as Mellon Square and Convention Center experience heavy traffic and high volume of pedestrians, which could contribute to various human-made air pollution sources impacting OA at these sites, traffic emissions.

For example, Figure 2.5 shows the high contributions of HOA (OA associated with traffic emissions) and BC at Mellon Square and Convention Center. Both sites are in downtown Pittsburgh along major bus routes. At these high traffic sites, the contributions of HOA and COA to total OA are nearly equal. This contrasts with several other sites with less intense traffic (e.g., Forbes, Bryant, Carson), where COA concentrations are larger than HOA.

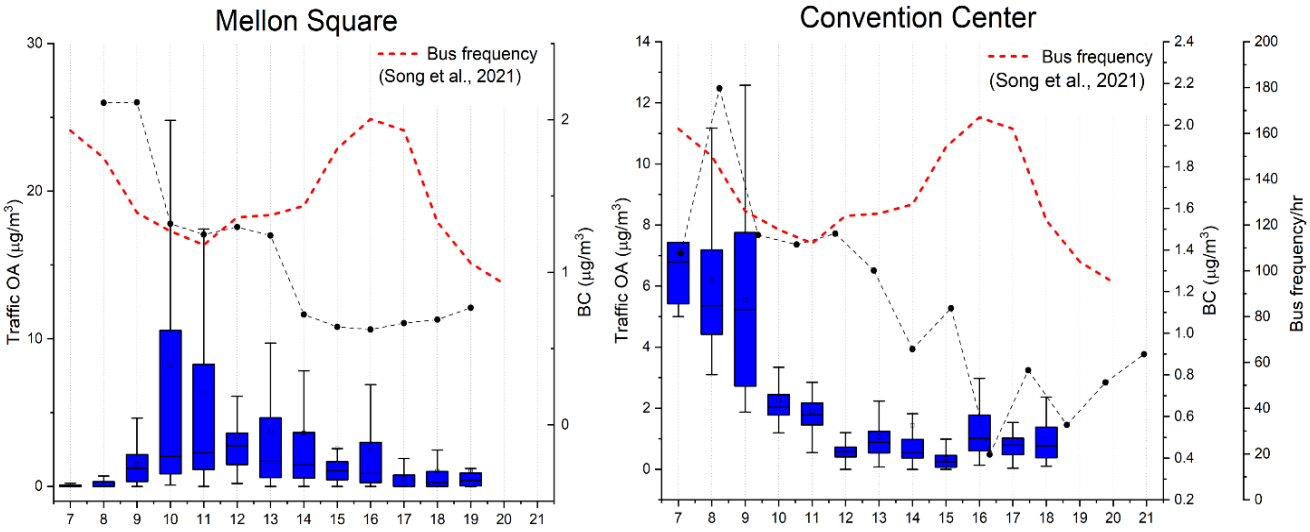

Figure 2.5 Plots depict the relationship between black carbon (BC) and traffic-related factor from PMF over time at Mellon square (left) and Convention center (right). The box plots show the range of hourly concentrations for the Traffic OA factor at each site (the box shows the interquartile range, the line in the center of the box shows the median, and the whiskers show the 10th and 90th percentiles). The black dots show the hourly mean concentrations of BC.

In Figure 2.6, time series plots for COA and Traffic factor identified through PMF analysis are presented. During the sample collection, our group recorded information from the activity log to track potential factors that could influence the sampling data. Interestingly, the temporal pattern revealed that COA concentrations tended to increase around 10 am, reaching their lowest point at 5 pm, and then peaking again between 6-7 pm. This trend suggests high emissions from restaurants during these peak times. At Mellon Square, Forbes, and Murray, the van was parked at locations without close proximity to any particular restaurant. Of the four sites visited during summer, the Convention Center and Mellon Square were revisited in winter, showing a distinct temporal change in COA mass with increases around noon and 6 pm.

Similarly, we observed temporal patterns in traffic emissions. Overall, traffic emissions peaked in the morning when people typically start work, with the lowest concentrations around 3-4 pm.

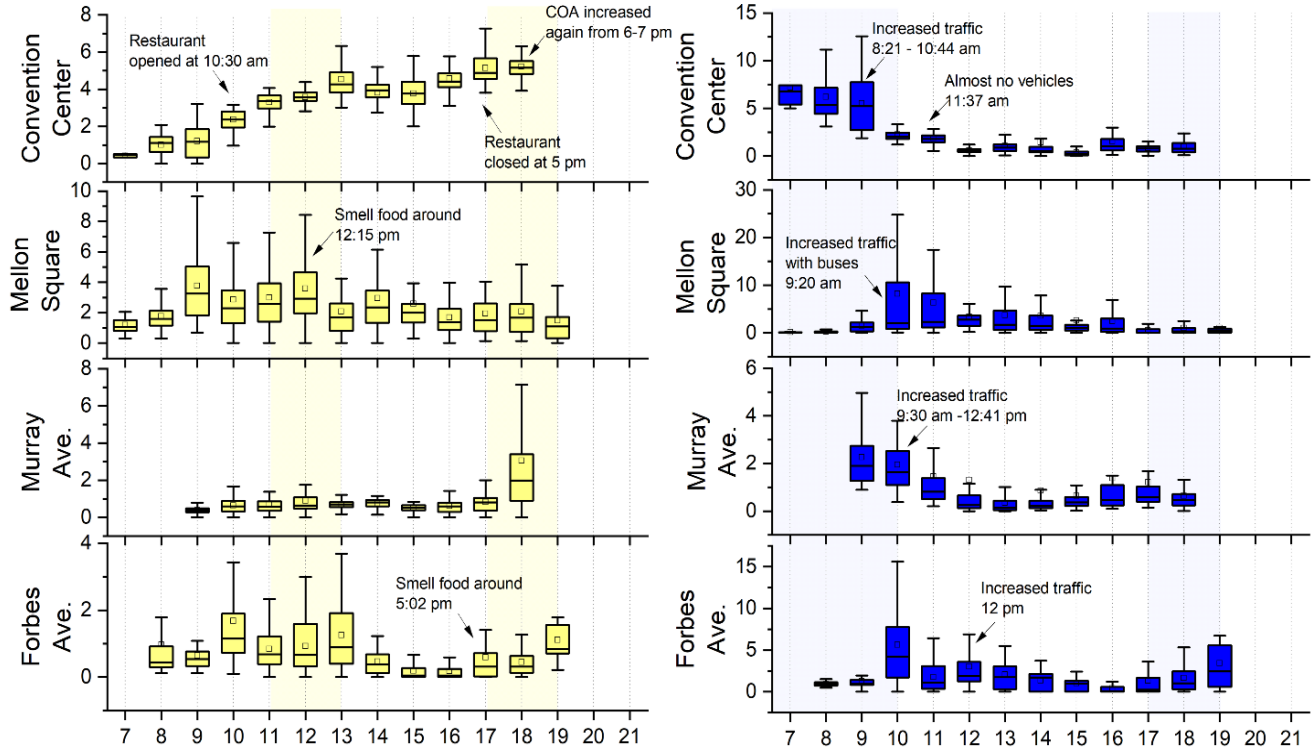

Figure 2.6 Time series box plot illustrating temporal pattern of (a) COA and (b) Traffic emissions identified from PMF at four sample sites monitored from morning to evening.

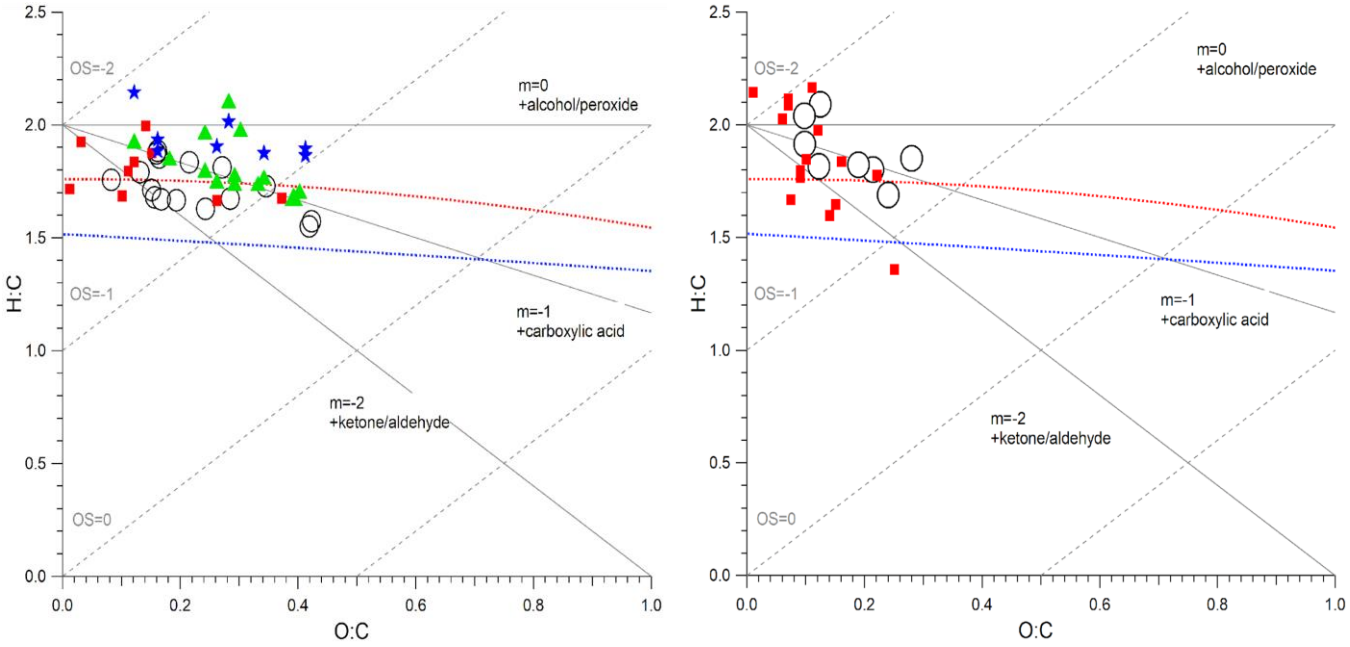

Figure 2.7 Van Krevelen diagram of COA (Left) and Traffic/HOA (Right) factors in field campaigns and previous literature. Black large circular markers show the COA or Traffic-related factors from both summer and winter field campaign conducted in 2021. Light green triangles on the left panel represent the results from cooking emissions data collected during a 2019 summer field campaign in Pittsburgh and Baltimore. Laboratory cooking experiments are indicated by blue markers. Red rectangular markers highlight ambient COA or HOA factors identified from prior literature.

As shown in Figure 2.7, the O:C and H:C ratios of COA obtained in this study were compared with those reported in prior literature, including both field studies and laboratory experiments (Dai et al., 2019; Ge et al., 2012; Huang et al., 2021b; Katz et al., 2021; Mohr et al., 2012; Rivellini et al., 2020; Shah et al., 2018b; Xu et al., 2014; Zhang et al., 2021b). Traffic factors from the 2021 campaign and ambient HOA factors in prior literature (Aiken et al., 2009; Al-Naiema et al., 2018; Bottenus et al., 2018; Dai et al., 2019, 2019; Ge et al., 2012, 2012; Guo et al., 2024, 2024; Hayes et al., 2013; Hu et al., 2016b; Li et al., 2015; Rivellini et al., 2020; Saarikoski et al., 2012; Shah et al., 2018b) are shown on the right in Fig 2.7. Both Traffic and HOA factors show generally lower O:C and demonstrate relatively less variability in comparison to COA factors. In contrast, COA-related factors were observed across a much broader range. Although most COA factors exhibit O:C ratios below 0.4, certain Oxidized COA factors in our field campaign and lab experiments in a prior study displayed higher O:C ranges demonstrating the substantial variability inherent in cooking emissions. For instance, Stir-fried Cabbage SOA and Kung Pao Chicken SOA, two distinct SOA factors derived from cooking emissions, shows the highest O:C ratios among eight data points in their respective experiments (Zhang et al., 2021b). In our 2021 field campaign, Oxidized-COA from Forbes Avenue and Convention Center COA exhibited more oxidized characteristics compared to the COAs from other sampling sites. Among the ambient COA factors, Houston Texas (Dai et al., 2019) displayed the highest O:C ratio, highlighting significant variability in the oxidative properties of ambient cooking organic aerosols.

2.3.3 Separation of Asphalt Paving factor in PMF

This study also aimed to quantify the impact of asphalt paving on ambient air quality. Two of the sampling sites were targeted at asphalt sources. The Bird Park site, shown in Figure 2.3, was adjacent to an active road paving project. The site was on a road with low traffic in a suburban park. Thus, the dominant anthropogenic sources at this location were the asphalt paving and associated diesel equipment.

The Roadside Paving site was located near the entrance to a large asphalt plant. This location also has significant traffic influence, as the asphalt plant is located under an elevated portion of Interstate 376 in the City of Pittsburgh. Also, there was significant diesel truck traffic into and out of the asphalt plant, as large trucks arrived at the plant to be filled with hot asphalt.

A major challenge in separating asphalt from traffic OA with the AMS is that these sources produce similar mass spectra. Both vehicle and asphalt emissions are derived from petroleum – asphalt emissions are from vaporization of hydrocarbons, while vehicle emissions contain major contributions from partially combusted fuel and direct emissions of motor oil. Both Khare et al (2020) and Humes et al (2023) showed in the laboratory that asphalt OA emissions are chemically similar to traffic and motor oil emissions.

In this work, we used concurrent measurements of BC and NOx to separate traffic OA from asphalt OA. Briefly, we expect that asphalt emissions at both Bird Park and Roadside Paving would have weak correlations with BC and NOx. On the other hand, vehicle emissions, especially those associated with diesel vehicles, emit BC and NOx.

For both sites, PMF was used to separate two factors dominated by reduced hydrocarbons. For example, the HOA mass spectrum typically assigned to traffic emissions has large contributions from *m/z* 43, 57, and 69. These peaks are also present in the asphalt mass spectrum (Figure 2.7). We then computed the temporal correlation between each of these reduced PMF factors and NOx and BC. The factor with the higher correlation with NOx and BC was assigned as the HOA factor, whereas the factor with the weaker (or no) correlation was assigned as the asphalt factor. The average asphalt and HOA factors determined from all sites are shown in Figure 2.7.

After separating the asphalt and HOA factors, additional steps were taken to examine and better verify that the asphalt factor was indeed representative of asphalt OA. Previous work by Humes et al (2023) showed that asphalt OA contained peaks from polycyclic aromatic hydrocarbons (PAHs) that are not present in HOA or in vehicle emissions. The presence of these PAH peaks also means that asphalt OA emissions have a greater fraction of their mass at $m/z > 100$ than HOA or vehicle emissions. We observe

these features in our asphalt factor determined from ambient sampling. The asphalt factor in Figure 2.7 contains contributions from ions associated with PAHs, including *m/z* 128 and 152. Additionally, the asphalt factor is enriched in fragments with larger *m/z* compared to the HOA factor. This is shown in the cumulative mass fraction plot in Figure 2.8.

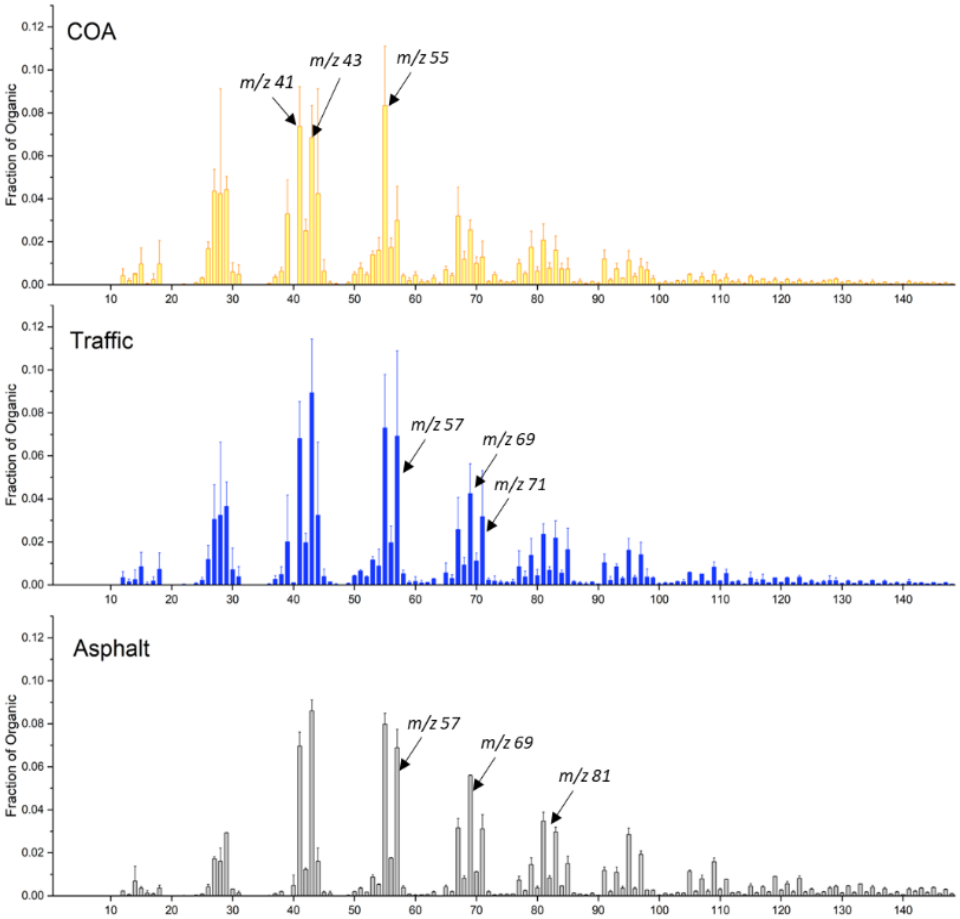

Figure 2.7 Average mass spectra for different PMF factors: COA, Traffic (HOA), and asphalt. There is a high correlation in the mass spectra of the HOA and traffic factors.

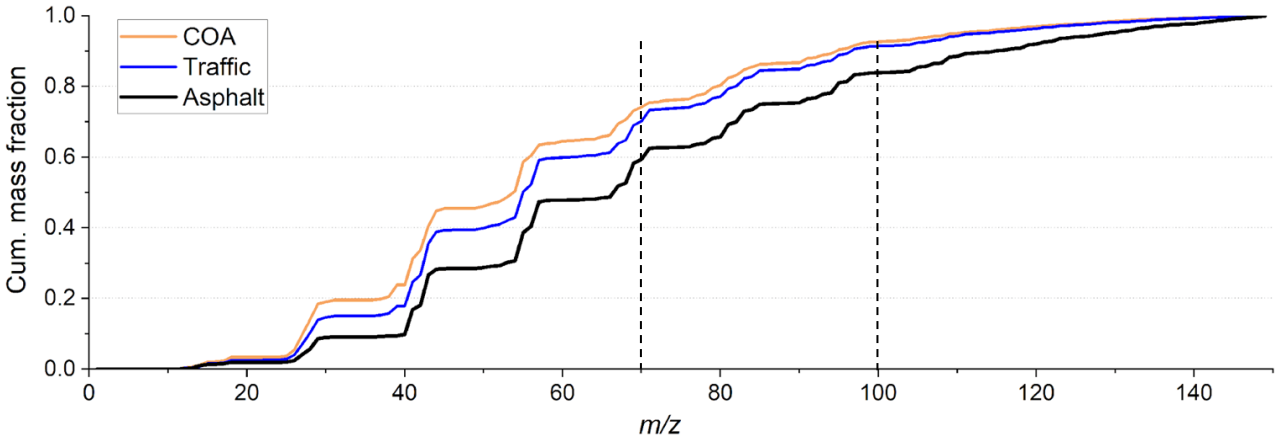

Figure 2.8 Cumulative mass fraction of COA, Traffic, and Asphalt factors at various *m/z* ranges. At *m/z* 70, the cumulative mass fraction of the Traffic factor begins to approach that of COA, achieving near-identical alignment at *m/z* 100. The Asphalt factor's cumulative mass fraction exhibits a distinct profile, remaining significantly different even at *m/z* 100, indicating a unique contribution to the mass spectrum at higher mass ranges. This divergence highlights the Asphalt factor's potential for a significant contribution from polycyclic aromatic hydrocarbons (PAHs) at higher *m/z* values.

We attempted to leverage the presence of PAH peaks in the asphalt mass spectrum to better separate the asphalt OA from HOA. However, this approach yielded only minor improvements in the separation. Further, it did not enable us to identify an asphalt OA factor in locations that did not have large impacts from asphalt emissions.

Figure 2.4 shows that the asphalt factor was only identified at the two asphalt-focused sites. This is due to the difficulty in separating the asphalt factor from the HOA factor. In most ambient sampling, these two factors are too similar to separate. Additionally, the traffic emissions that make up most of HOA are generally the dominant source of reduced OA to the urban atmosphere. This likely means that previous studies have over accounted for traffic emissions, and assigned other sources of reduced OA, including asphalt, as traffic emissions.

2.4 Conclusions

This section used an aerosol mass spectrometer to examine spatial and temporal variations in both OA concentration and source contributions across Pittsburgh. We observed significant spatial and temporal variations in OA, and these variations are coupled to changes in anthropogenic activities. Anthropogenic emissions sources include both combustion sources, with vehicle traffic creating higher concentration zones in high traffic areas and during the morning rush hours, and non-combustion sources. We identified asphalt emissions as a potentially important contributor to urban air pollution and highlighted some of the challenges present in quantifying the impact of this widely distributed source that generates PM with a similar composition as vehicle emissions. We also observed that the chemical signatures of common sources such as vehicle traffic and restaurant cooking do not display strong spatial or temporal variations at the city scale.

The results of this section of the report demonstrate that further reductions in urban PM concentrations can be achieved by targeting non-combustion and combustion source emissions. While this data was collected in one city, we expect that a similar source mix, especially vehicles and restaurants, will be important in cities nationwide.

3. Characterization of Nitrogen-Containing Cooking Organic Aerosols with a Non-targeted Approach Using the Offline FIGAERO-CIMS

3.1 Introduction

Section 2 used real-time aerosol mass spectrometry to demonstrate the importance of non-traffic related sources to urban OA. In many sampling locations, cooking was equal to or greater in importance as a source of primary OA. While these data are useful, the harsh conditions of the AMS mean that molecular information is loss.

Application of Chemical Ionization Mass Spectrometry (CIMS) can provide additional molecular insights into cooking emissions through the minimal fragmentation of molecular compounds (Hearn and Smith, 2006, 2004; Isaacman-VanWertz et al., 2017; Ye et al., 2021; Zhang et al., 2018). While the AMS has been broadly utilized for measuring chemical composition of aerosols in both field (Crippa et al., 2014; Dzepina et al., 2007; Jimenez et al., 2003; Lee et al., 2013; Takegawa et al., 2009) and laboratory settings (Bruns et al., 2015; Chen et al., 2019; Cross et al., 2007; Hu et al., 2017; Xu et al., 2018), it often leads to substantial fragmentation of organic species due to hard ionization processes such as Electron Ionization (EI). Although EI can provide high sensitivity to organics (Hartner et al., 2022), the fragmentation of the parent ion can limit our understanding of the specific molecular composition of the ambient samples (Hartner et al., 2022; Niu et al., 2024; Schueneman et al., 2021; Zhang et al., 2023).

The CIMS has been mainly used in gas phase analysis of the samples; however, the FIGAERO (Filter Inlet for Gases and AEROsols), coupled with the CIMS, enables the measurement of the ambient aerosol particles (Lopez-Hilfiker et al., 2014). FIGAERO is equipped to function in two distinct modes for both gas-phase and particle-phase sample collection and their analysis. The first mode for the particle-phase sample is via a metal port and particle sample collection on a filter. Following this, the second mode includes thermal desorption of the particles using heated nitrogen (N_2). The movable tray of the FIGAERO facilitates the transition from sample collection to thermal desorption mode. During thermal desorption, the gas-phase port is blocked by the movable tray, ensuring that only particle samples collected on the filter are analyzed (Bannan et al., 2019). While FIGAEO-CIMS has been used in multiple aerosol studies in both laboratory (Bannan et al., 2019; D'Ambro et al., 2019; Graham et al., 2023; Masoud and Ruiz, 2021; Yang et al., 2021) and field campaigns (Brown et al., 2021; Chen et al., 2020; Lopez-Hilfiker et al., 2016; Thompson et al., 2017; Ye et al., 2021), several recent trials have established methods for offline analysis with the FIGAERO-CIMS (Cai et al., 2022; Huang et al., 2019; Siegel et al., 2021). The current study leverages the benefits of the offline CIMS method for field campaigns, where filter samples are collected in situ and subsequent analyzed in the primary laboratory by iodide based CIMS utilizing a FIGAERO inlet. The implementation of this innovative method will facilitate the efficient collection of multiple samples without necessitating the on-site installation of the instrument.

The role of nitrogen in COAs has acquired less attention, despite some recognition of its natural and anthropogenic sources. (Yu et al., 2024). While specific contribution of nitrogen from cooking activities has been relatively unexplored, recent studies have unveiled the presence of nitrogen containing compounds in both gas and particle phases from either food itself or during the cooking process (Klein et al., 2019; Reyes-Villegas et al., 2018b). Exploring the origins of nitrogen in food sources, studies highlight its origins from the use of nitrogen fertilizers (Dimkpa et al., 2020; Ladha et al., 2005; Wood et al., 1993), critical to produce amino acids in plants, and subsequently, as sources of protein in animals (Liu et al., 2022; Ochieng' et al., 2021; The et al., 2021). In addition, the essential role of nitrogen in food production has been studied in prior research. For instance, nitrogen from yeast fermentation process, such as those involved in making wine and bread, contributes to the nitrogen content in foods (A. A. O. Ahmed et al., 2023; Kessi-Pérez et al., 2020; Utami et al., 2024). The levels of nitrogen emissions can also vary based on cooking methods or the type of stove used, with gas and electric stoves known to influence the concentration of NOx differently (Dėdelė and Miškinytė, 2016; Dennekamp et al., 2001b; Paulin et al., 2014). Although the focus on nitrogen from cooking emissions has been relatively limited, the presence of nitrogen in the atmosphere carries substantial implications for environmental health and global warming (Haque et al., 2023; J. Wang et al., 2023; Zixuan Wang et al., 2023). For instance, impact

of nitrogen on ecosystems, such as its detrimental effects on coral reef environments, has been documented by several findings (Donovan et al., 2020; Vaughan et al., 2021; Zhao et al., 2021).

Here, we aim to identify cooking originated compounds detected from the Iodide-FIGAERO-CIMS, both a predefined list of cooking markers from existing research and a non-targeted list of compounds. A key objective is to understand why reduced-N compounds, observed in near-source cooking plumes, are not present in ambient COA factors determined from PMF analysis of the 2021 field campaign. By employing both the CIMS and AMS, this research intends to provide a comprehensive overview of nitrogen in cooking emissions, examining potential factors that influence their detection. This integrated approach will offer a clearer understanding of COAs and illustrate how the CIMS complements molecular information detected by the AMS.

3.2 Methods and Measurement

3.2.1 Sample collection setup and measurement site.

Figure 2.2 above shows the sampling setup used in the mobile lab. We sampled $PM_{2.5}$ onto PTFE filters from SKC (2.0 µm pore size, 25 mm, Cat. No. 225-3726) in parallel with real-time AMS measurements presented in Section 2. The filters underwent a pre-baking process in the oven, set at 100 °C, overnight prior to the campaign. This step was carried out to eliminate any organic contaminations present on filters.

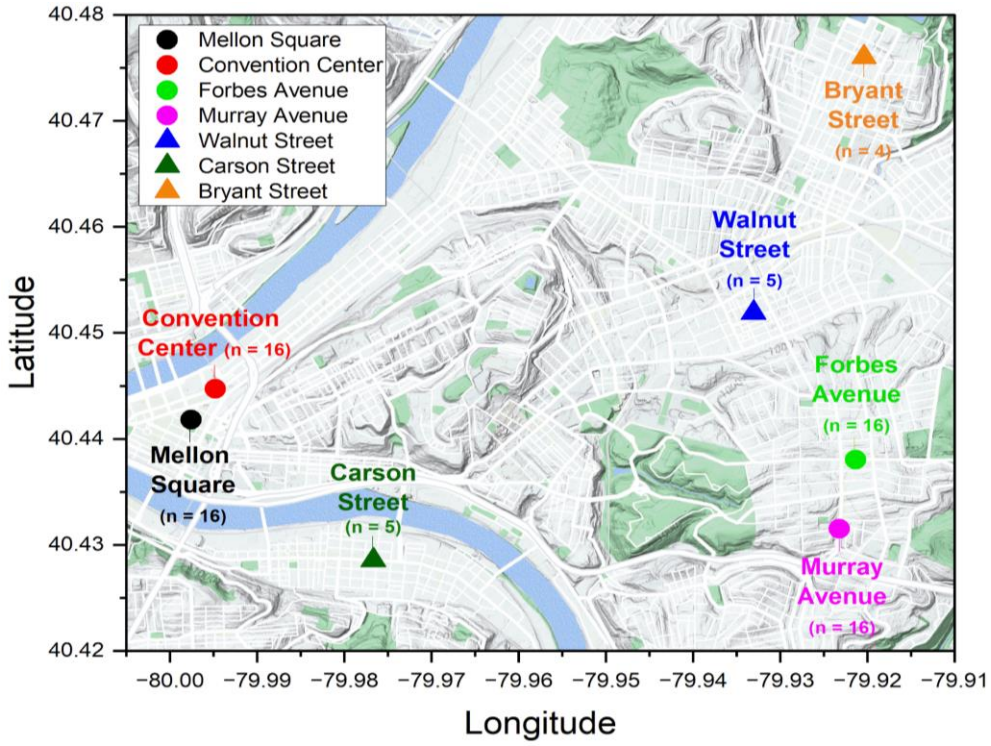

Figure 3.1 Overview of the sampling sites for the Offline FIGAERO-CIMS analysis. The map illustrates the geographical distribution of our sampling locations. Four sites sampled from morning to evening for diurnal analysis are marked with circles, while locations expected to mainly yield cooking emissions are denoted with triangles. Each location is accompanied by the name of the sampling location and the number of filter samples collected there during the study period.

Figure 3.1 illustrates the locations of the sampling sites visited during the study period in the Pittsburgh area. Details on criteria for site selection are discussed in the preceding chapter. Among the seven cooking-focused sampling locations, filter samples were collected from morning to evening at four

of these locations. Thus, the diurnal patterns observed, reflecting characteristics from morning to evening, are based on the results from these four locations, which are indicated with circle dots in Figure 3.1.

Our data collection involved 16 filter samples from each location, including Mellon Square, Convention Center, Forbes Avenue, and Murray Avenue. Samples were collected at regular intervals throughout the day, from morning to evening. To provide a comprehensive dataset, samples were gathered every 30 minutes between 8 am to 7 pm Eastern Time, resulting in a set of four filters for each time window. Although we did not anticipate a significant diurnal pattern in anthropogenic emissions at Walnut Street, Carson Street and Bryant Street, they remained of interest due to their potential as substantial sources of cooking emissions. As a result, we collected between four to five filters samples at each of these locations, which contributed to our overall dataset.

While both online and offline measurements have their benefits in certain situations, prior studies have been restricted in its online measurements of the CIMS in the analysis of the field campaign data. This is primarily due to the high cost of the instrument and the lack of skilled human resources to operate instruments in multiple locations. As result, applications of the CIMS in field campaigns become challenging. Therefore, a system to collect filter samples was specifically designed for the offline data collection in the field campaign. To determine the optimal duration for sufficient mass loading on the filters for the CIMS analysis, laboratory tests were conducted using ambient samples obtained in the campus area. The durations tested included 30 minutes, 1 hour and 2 hours, respectively. Based on the preliminary analysis, it was determined that a 30-minute sampling period, accompanied by a flow rate of 5 standard liters per minute (slpm), was the most suitable for effective sample collection. Throughout the campaign, Mass Flow Controllers (MFCs) were employed to maintain a consistent flow rate during the sample collection period. Detailed information regarding the instrumental setup and operational conditions can be found in the previous chapter, as it provides comprehensive details regarding the mobile laboratory utilized during the summer field campaign of 2021 (see Chapter 3, 3.2.1 Site selection and sampling method). The campaign employed the consistent framework and setting to gather the filters samples, which were subsequently utilized for laboratory analysis using the iodide FIGAERO-CIMS.

3.2.2 FIGAERO-CIMS setup and analysis protocols

The chemical ionization method employs an ionized reagent gas, requiring less energy compared to Electron Impact (EI) (Dayhuff and Wells, 2005). The CIMS can utilize various reagent ions, such as acetate, iodide, nitrate, and methane, allowing for interchangeable ionization sources and selective detection of different chemical classes. This indicates the importance of choosing an appropriate reagent ion when selectively choosing targeted ions in samples (Aljawhary et al., 2013). In our research, we chose to employ iodide, as its widespread deployment for the measurement of atmospheric trace gases and its selective preference for oxygenated organic compounds (Dörich et al., 2021), especially, given the unpredictability of real-world urban atmospheric measurements. The extent of fragmentation and the detection sensitivity can be precisely managed by employing a diverse array of reagent ions. (Marcy et al., 2005; Rissanen et al., 2019; Xu et al., 2022).

The FIGAERO-inlet was specifically designed to enable the continuous detection of particle-phase and gas-phase compounds in conjunction with a Time-of-Flight Chemical Ionization Mass Spectrometer (ToF-CIMS). Its design allows for easy interchange with the standard gas-phase inlet of the CIMS, facilitating alternating sampling cycles between gas-phase and particle phase measurements during aerosol collection and thermal desorption for mass spectral analysis of collected aerosol. During the thermal desorption process, the filters is moved to a designated position in the program, and a flow of ultra-high purity (UHP) nitrogen gas at a rate of 2 slpm is heated programmatically and directed across the filter to desorb the compounds present. The particles on filters are thermally desorbed by the nitrogen flow, and the desorbed compounds are ionized by clustering with iodide anions generated through exposure to the radioactive source Polonium-210.

The sample analysis process involves automated switching between aerosol and blank sampling, accompanied by a programmable thermal desorption ramp. The temperature ramping protocol used in this study ranged from approximately 35 °C to 150 °C and lasted for a total of 15 minutes in total.

Specifically, within the employed FIGAERO-CIMS, the filter samples were initially analyzed at around 35 °C for 1 minute before being gradually heated up to 150 °C over a period of 14 minutes. This temperature protocol was implemented to observe any signal changes correlating with the desorption temperature.

Blank correction is a critical procedure for ensuring accurate measurements by eliminating background noise or contamination present in the environment. Field blanks have been widely employed in aerosol research to follow the same sampling procedure as actual sample collection, with the key difference being that they do not directly collect particulate matter (Bhardwaj and Sunder Raman, 2022; Vodička et al., 2022; Yoon et al., 2021; W. Zhang et al., 2022). This study's approach to background correction was specifically adapted from May et al., 2013 to mitigate potential contamination during sample collection. The same type of PTFE filters was used, which were prepared in the oven with a pre-baking process at 100 °C overnight. Field blank filers were used throughout the field campaign to expose the field conditions to capture environmental conditions, mirroring all procedures except the direct collection of particulate matter samples.

Four field blank samples were utilized to determine the background concentration of pollutants. These blanks underwent the same data analysis process as the collected samples. The background-corrected signal for each sample was calculated by subtracting the summed signal intensities of all compounds identified in the field blank samples from the total original signal intensity of the samples. To accurately measure the concentration of compounds in the study samples, it was essential to distinguish the true signal from background noise. This was achieved by subtracting the background noise, measured using field blank samples, from the raw signal detected in each sample.

3.3 Results and discussion

3.3.1 Early insights from targeted analysis

To employ cooking markers that signify the emissions from culinary activities, compound peak lists of the CIMS from two research papers were referenced. The chosen studies utilized iodide as the reagent in their investigation of indoor cooking aerosols, measured through the HR-ToF FIGAERO-CIMS. Reyes-Villegas et al. (2018) focused on measuring both particulate matter and gaseous emissions generated while cooking a typical English breakfast, involving an array of food preparation techniques and ingredients. Another study by Masoud et al. (2022) simulated cooking activities within a realistic kitchen and home environment setup. The results of these experiments led to a list of compounds identified in both the gas and particle phases. After careful comparison and exclusion of overlapping compounds from the two studies, a total of 32 distinct compounds were identified. This collection of compounds, therefore, represents the emissions originating from the specific cooking scenarios scrutinized in previous studies, and subsequently examined in this study. This research focused on the analysis of the top 10 compounds that showed the highest signal intensity from a set of 32 markers associated with cooking emissions, utilizing the FIGAERO-CIMS instrument.

Table 3.1 Table of compounds selected for targeted-analysis, with their chemical formulas, mass-to-charge ratios (*m/zs*) and proposed chemical names. The name of the chemical species and phase classification of these compounds into either particle or gas phase are informed by findings reported by Reyes-Villegas et al., 2018, and Masoud et al., 2022.

Formula	m/z	Name	
$C_2H_2O_4$	216.900	Oxalic acid	
$C_3H_8O_3$	218.952	Glycerol	
$C_5H_8O_3$	242.952	Levulinic acid	
$C_4H_6O_4$	244.934	Succinic acid	
$C_6H_6O_3$	252.937	Maltol	
$C_5H_8O_4$	258.947	Glutaric acid	
$C_6H_9N_3O_2$	281.9745	Histidine	
$C_9H_{18}O_2$	285.036	Palmitic acid	
$C_7H_{12}O_4$	286.979	Pimelic acid	
$C_6H_{10}O_5$	288.958	Levoglucosan	
$C_6H_{12}O_5$	290.974	Fucose	Particle phase
$C_{10}H_{12}O_2$	290.989	Propanoic acid	
$C_8H_{14}O_4$	300.994	Suberic acid	
$C_9H_{14}O_4$	312.994	Pinic acid	
$C_9H_{16}O_4$	315.010	Azelaic acid	
$C_{10}H_{18}O_4$	329.026	Sebacic acid	
$C_{12}H_{22}O_4$	357.057	Dodecanedioic	
$C_{16}H_{32}O_2$	383.145	Palmitic acid	
$C_{17}H_{34}O_2$	397.161	Margaric acid	
$C_{17}H_{26}O_3$	405.0932	Paradol	
$C_{18}H_{32}O_2$	407.145	Linoleic acid	
$C_{18}H_{34}O_2$	409.161	Oleic acid	
$C_{18}H_{36}O_2$	411.177	Stearic acid	
$C_{18}H_{34}O_3$	425.156	Ricinoleic acid	
CHNO	169.911	Isocyanic acid	
CH_2O_2	172.911	Formic acid	
$C_3H_4O_2$	198.926	Acrylic acid	Gas phase
$C_3H_6O_2$	200.942	Propionic acid	
$C_3H_6O_3$	216.937	Lactic acid	
$C_3H_4O_4$	230.916	Malonic acid	
$C_6H_{10}O_2$	240.973	Hexanoic acid	
$C_6H_{10}O_4$	272.963	Adipic acid	

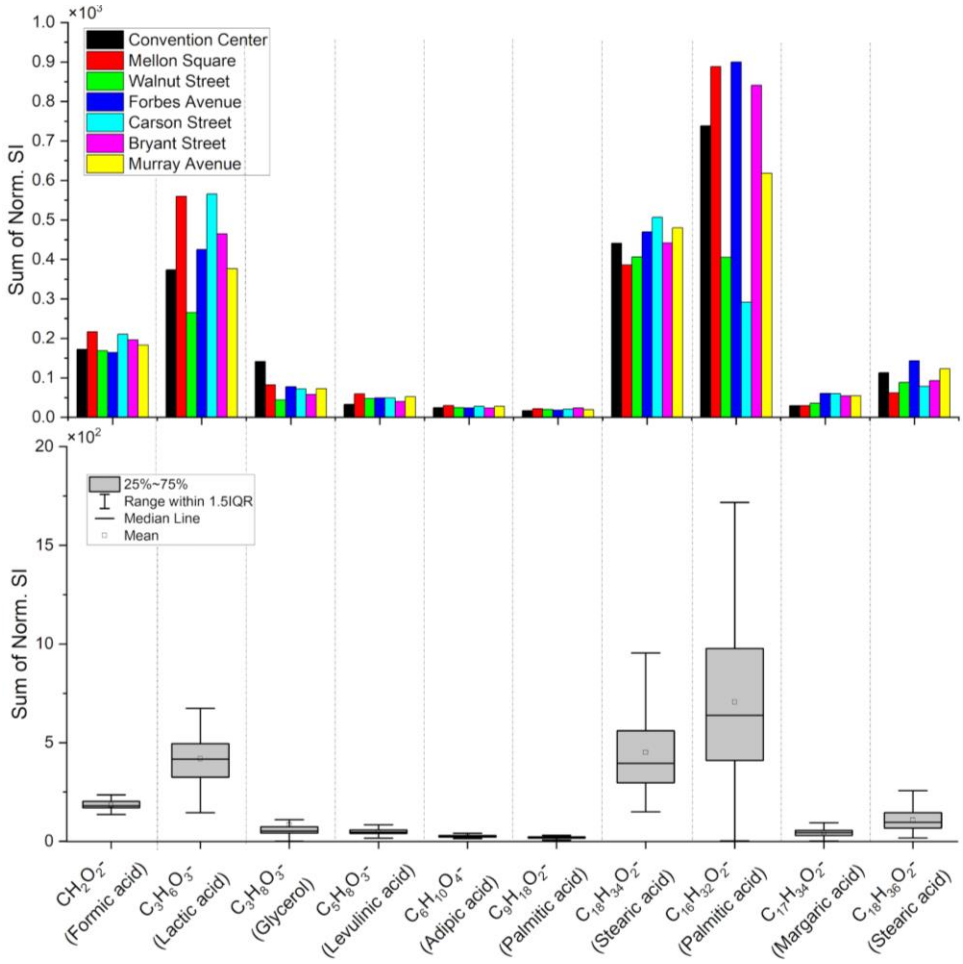

Figure 3.2 Selection of 10 compounds based on their high signal levels throughout the day.

In Figure 3.2, palmitic acid emerged as the compound with the highest signal intensity. Previous literature has identified the presence of palmitic acid in the cooking emissions of meat, dairy products like butter, and some plant oils (Rogge et al., 1991; Masoud et al., 2022). Following palmitic acid, the compounds showing the highest signal intensity were oleic and stearic acid, predominantly found in olive oil and animal fats, respectively (Liu and Jiang, 2020; Martínez et al., 2014; Monfreda et al., 2014). Due to the inherent limitations of the CIMS in distinguishing compounds with identical chemical formulas at the same *m/z* (Hammes et al., 2019; Siegel et al., 2021), it was inferred that the detected signals likely correspond to oleic and stearic acids. This is because previous studies have shown that they are highly prevalent in cooking emissions (Alves et al., 2021; Huang et al., 2021b; Lyu et al., 2021; Robinson et al., 2006; Schauer et al., 2002b; Zhao et al., 2007c).

Lactic acid, identified as the third major compound, is predominantly emitted from cheese and fermented foods (Alves et al., 2020; Rocchetti et al., 2019; Weidner et al., 2023; Zareie et al., 2023). Among the analyzed compounds, palmitic acid, oleic acid, and lactic acid demonstrated the highest concentrations. These three compounds collectively accounted for 64.6% to 78.5% of the mass across all sampling sites, highlighting their significant contribution to cooking emissions. Other potential compounds with the highest signal intensity included formic acid, glycerol, glutaric acid, etc.

The samples were collected from various locations at different times, days, and with varying weather conditions, the variability in compounds concentrations across sites suggests the influence environmental factors on emission profiles. This finding emphasizes the dynamic nature of cooking emissions in real-world scenarios.

However, focusing solely on these markers provides limited insight into the broader spectrum of cooking emissions. Previous applications of the FIGAERO-CIMS have identified a wide range of organic compounds across diverse environments, extending from indoor settings to the Arctic Ocean (Brown et al., 2021; Chen et al., 2020; Siegel et al., 2021; Ye et al., 2021; Zhang et al., 2018). Such diversity underscores the potential of a non-targeted analysis approach in uncovering a broader array of compounds at low concentrations, including previously unidentified chemical species.

Prompted by this understanding, the current research process included completing a non-targeted analysis of cooking emission samples collected during the summer 2021 field campaign. This comprehensive approach enabled the assignment of 2242 compound masses based on the observed spectral peaks. Of these, 1364 compounds were identified by specific chemical formulas. The findings revealed that a targeted analysis, while informative, may overlook a substantial portion of the emissions' chemical composition. Indeed, the 32 initial compounds represented just a fraction of the total compounds detected across the samples in the current research (3.8%), advocating for the necessity to take a broader analytical scope in environmental studies on cooking emissions.

3.3.2 Overview of the non-targeted compounds identified.

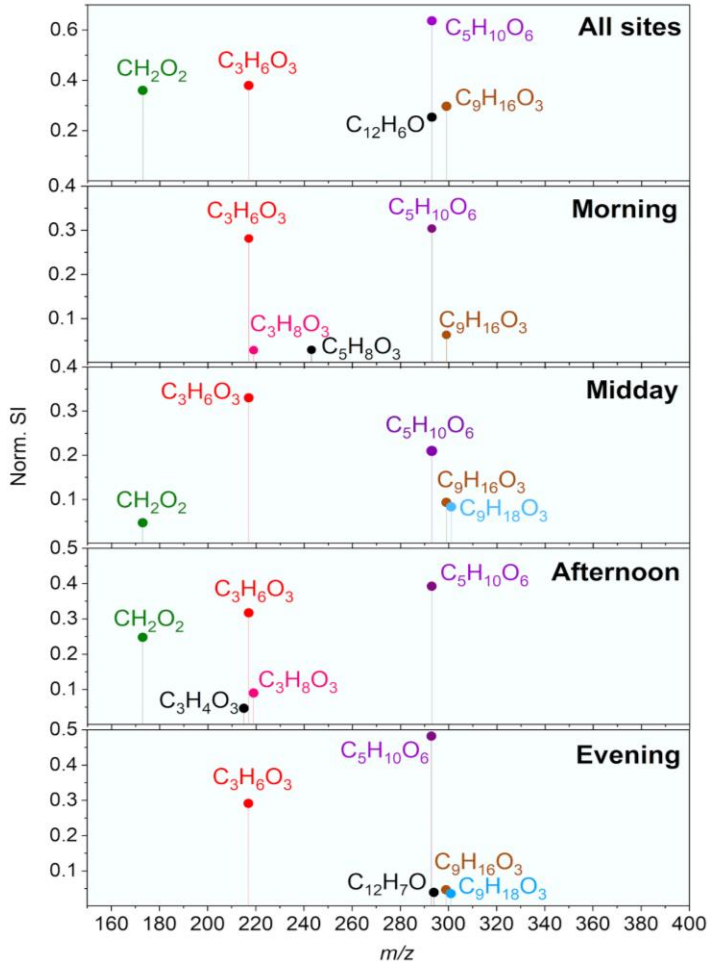

Figure 3.3 Top five compounds by signal intensity after blank correction. In the top panel covering all seven sites, the most significant compounds were identified from a total of 1363 chemical compounds. The two most prevalent compounds identified ($C_5H_6O_8$ and $C_3H_6O_4$) remained consistent across different times of the day, indicating that dominant compounds show similar patterns throughout the day.

Within the targeted compounds listed in Table 3.1, $C_3H_6O_3^-$ (lactic acids), CH_2O_2 (formic acid), and $C_3H_8O_3^-$- (glycerol) were notable for their high intensities, featuring among the top five compounds. Lactic acid ($C_3H_6O_3^-$) was specifically identified as one of the major contributors, ranking among the top five compounds with high signal intensity from morning to evening at four sites, as well as in the overall site average (Fig. 4.3). This compound, highlighted in our targeted analysis and recognized for its significance in the gas phase according to Reyes-Villegas et al., 2018, emerged as one of the dominant compounds during these times. The dominance of the compounds $C_3H_6O_3^-$ significantly contributed to the overall signal intensity observed in the blank samples. However, the contribution of $C_3H_6O_3^-$ remained markedly higher in comparison to other chemical species even after subtracting the background signal.

Following lactic acid, formic acid ($CH_2O_2^-$) is featured in both Table 3.1 and Figure 3.3. It was observed during both midday and afternoon periods, significantly contributing to the overall signals at all sites. Formic acid has been documented in various atmospheric particle and gaseous-phase studies (Allen and Miguel, 1995; Takhar et al., 2021; Wang et al., 2007; Yokelson et al., 1999), with its formation from photochemical reactions. Cooking-related emissions, such as those from meat charbroiling (Kaltsonoudis et al., 2017b) and the use of soybean and peanut oils (L. Wang et al., 2020), have been noted for their formic acid compounds content.

Glycerol ($C_3H_8O_3^-$) appeared in the top five compounds during morning and afternoon periods. Its significant signal contributions can be attributed to its presence in food additives, as identified in a prior study by Masoud et al., 2022. This compound can be naturally found in a wide range of food sources, including both plant and animal-based products. It is commonly present in fats and oils, dairy products, and various processed foods, highlighting its ubiquity in dietary substances (Wang et al., 2007). It also serves as a sweetener in sugar-free food products, typically sourced from vegetables, and is employed as a humectant or a preservative in processed foods (Larrea-Wachtendorff et al., 2020). These various roles of glycerol in food production could potentially explain its elevated presence in the morning and afternoon.

Among the top five compounds identified, the most notable were potentially sugar alcohol derivatives or xylonic acid $C_5H_{10}O_6^-$, despite not being included in the targeted compound list in Table 3.1. This compounds, which can arise from the breakdown or transformation of carbohydrates from chemical reactions (Jin et al., 2022). When sugars or sugar alcohol derivatives are heated to high temperatures, they undergo caramelization or Maillard reactions, which result in browning and complex flavors; these reactions are influenced by several factors including heating time, temperature, and the presence of oxygen (Ames, 1998; Jaeger et al., 2010; Lc, 1912). Another potential source of xylonic acid could be the decomposition of plant cell wall polysaccharides. When heated, these polysaccharides can break down into smaller sugar acids or compounds with similar formulas (C. C. Lee et al., 2017; Lekshmi Sundar and Madhavan Nampoothiri, 2022). In addition, fermented foods contain byproducts like sugar acids that could emit xylonic acid (Cao and Xu, 2019; Zhang et al., 2017). Their emissions sources can also vary based on food ingredients, leading to a significant presence in the samples collected.

Fatty acids or $C_9H_{16}O_3^-$ was also commonly observed in the midday and evening samples, which are potentially from vegetable oils (F. A. Ahmed et al., 2023; Boukhebti et al., 2016).

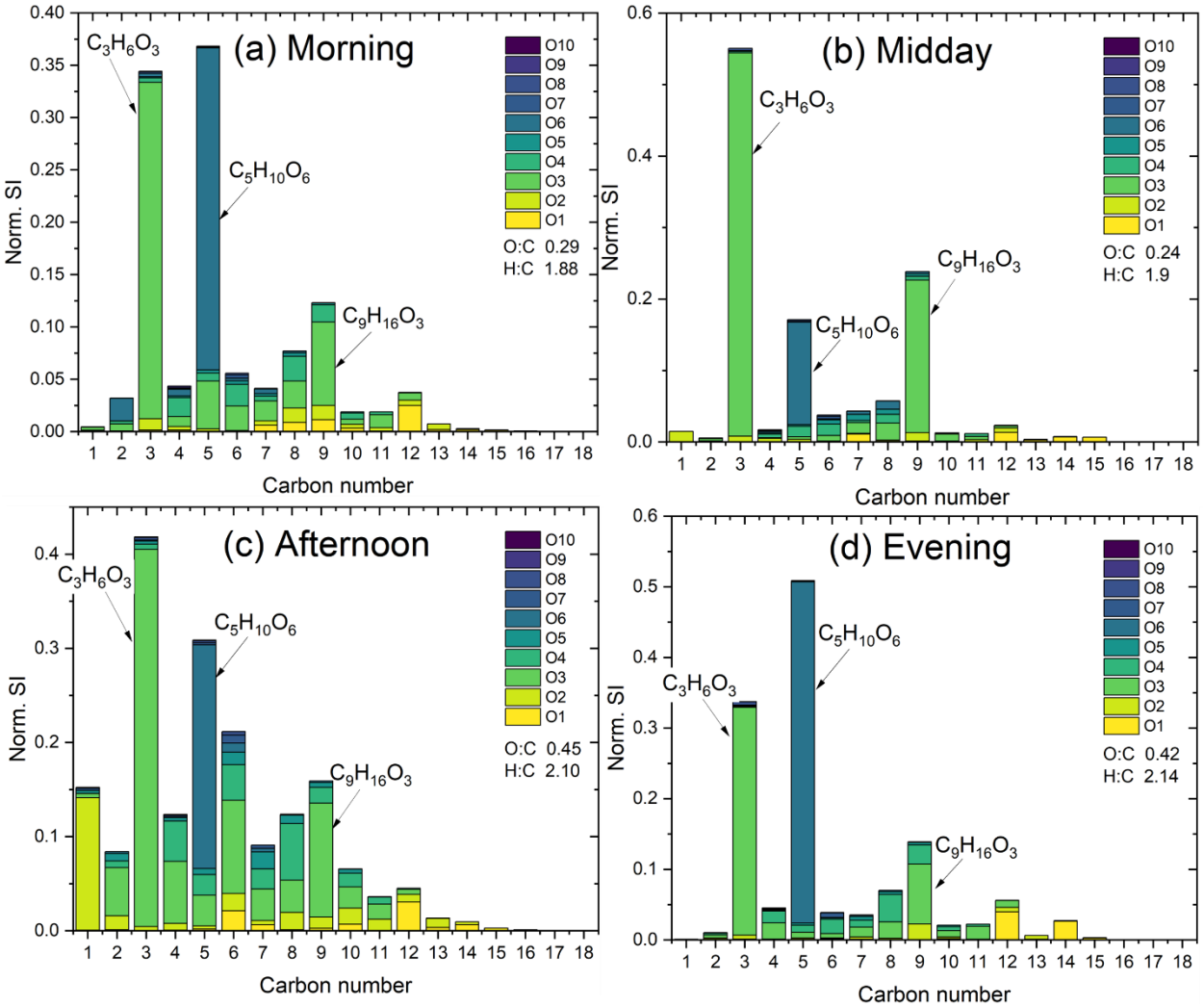

Figure 3.4 Normalized signal intensity (Norm. SI) of identified compounds over the course of a day from morning to evening after applying background correction. Lactic acid ($C_3H_6O_3^-$), sugar alcohol derivative ($C_5H_{10}O_6^-$), and fatty acid ($C_9H_{16}O_3^-$) were the most significant compounds, regardless of the time of day. The influence of $C_5H_{10}O_6^-$ was more pronounced in the morning and evening, while $C_3H_6O_3^-$ dominated at midday and in the afternoon.

The soft ionization in the CIMS allows us to quantify species by the number of carbon and oxygen atoms in the molecular formula. This is shown in Figure 3.4, which categorizes compounds based on their carbon and oxygen atom count with normalized signal intensity of each chemical compound. The color coding used in the chart represents the quantity of oxygen atoms per compound, highlighting the most prevalent compositions among the 1,364 compounds detected.

The distribution shows that the majority of the compounds contain more than one oxygen atom in their formulas. Compounds classified into the O3 and O6 groups collectively constitute more than 60% of the total signal intensity throughout the day. The prevalence of compounds with O3 or O6 functional groups is due to the dominant contributions of lactic acid ($C_3H_6O_3^-$), a sugar alcohol derivative ($C_5H_{10}O_6^-$), and a fatty acid ($C_9H_{16}O_3^-$). Following O3 and O6, compounds with O2 and O4 functional groups constituted 6-27 %, bringing the sume of O2 to O6 compounds to approximately 90 % of the total signal.

The analysis indicates that compounds with carbon chains ranging from C2 to C6 accounted for 75 % of the total signal in the morning and 65 % at midday. During the afternoon and evening periods,

compounds within the C2-C6 carbon range constituted 62 % and 71 % of the total signal, respectively. This pattern suggests a higher volatility for compounds with fewer carbon bonds, such as those within C2-C6 range, are likely more volatile compared to those with more than six carbon atoms in their formulas (Kroll and Seinfeld, 2008).

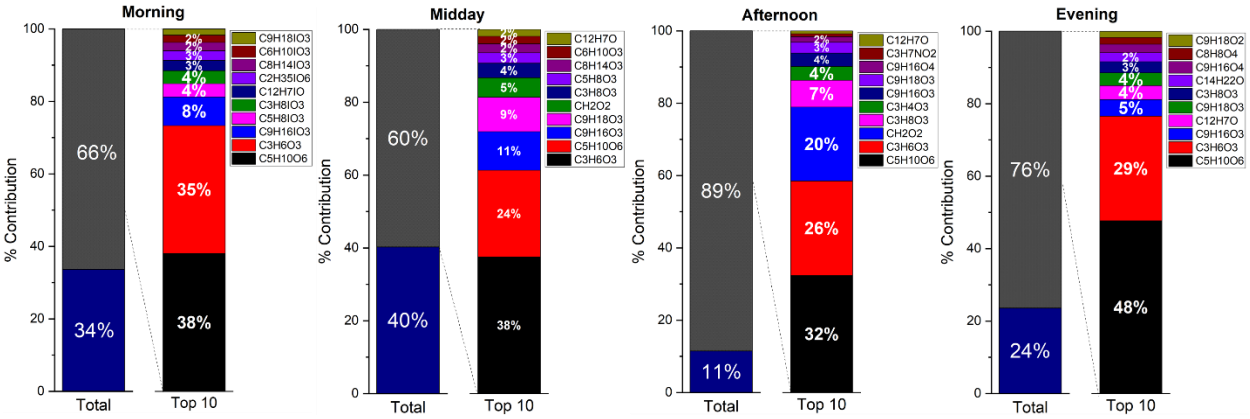

Figure 3.5 Variability in signal contribution of the top 10 compounds with the highest signal intensity as measured by the FIGAERO-CIMS. Each compound listed contains oxygen in the formula identified as either CHO or CHOx throughout the day. The compounds within the top 10 significant signals accounted for more than 60 % of the mass.

In Figure 3.5, each graph displays the total contributions of all compounds compared to the top 10 most significant compounds during morning, midday, afternoon, and evening periods. The signal intensity contribution of the top compounds collectively accounted for a substantial portion (60 % to 89 %) of the total signal throughout the day. Specifically, the dominant compounds $C_3H_6O_3^-$ and $C_5H_{10}O_6^-$ consistently appear in significant proportions across all time periods, though their relative abundance shifts.

Figures 3.4 and 3.5 show the average signal across all times of day. However, the relative abundance of different species changed over the course of the day. For example, during the midday hours (11 am to 1 pm ET), the top two significant compounds were consistent with those identified in the morning, afternoon and evening, though their order of prominence changed. Lactic acid or $C_3H_6O_3^-$ is likely associated with fermented foods, emerged as the leading compound across all sites in the midday, followed by $C_5H_{10}O_6^-$. Mellon Square was distinguished by contributing the most substantial portion of the total signal among the four sites. Although the spatial proximity of the Convention Center and Mellon Square, their location did not significantly influence the distribution of contributions from major chemical compounds.

In the afternoon (2 pm to 4 pm ET), the percentage contribution of the top three significant compounds was relatively consistent across the sites compared to other times of the day, indicating their widespread presence. The samples from the Convention Center collected in the afternoon were excluded due to experimental errors. The afternoon samples highlighted the prevalent compounds and their proportions, even though the field samples were collected on different days and from various locations. This consistency indicates that the variations in compound presence are likely not attributable to the emission characteristics of any particular day.

The evening samples (5 pm to 7 pm ET) at the Convention Center provide further insights into the sources driving variations in aerosol characteristics throughout the day. This analysis of organic compositions was conducted using both the AMS and the FIGAERO-CIMS. As discussed in the previous chapter, the diurnal pattern of traffic-related OA factors shows fluctuations in mass concentrations over time but no noticeable increase in traffic emission concentrations between 5 pm and 7 pm. On the other hand, COA factor demonstrates a clear increase specifically between 6 pm and 7 pm, suggesting that the

rise in glycerol ($C_3H_8O_3^-$) could likely be linked to cooking-related emissions at the Convention Center site during the evening hours.

3.3.3 Contribution of N-containing compounds

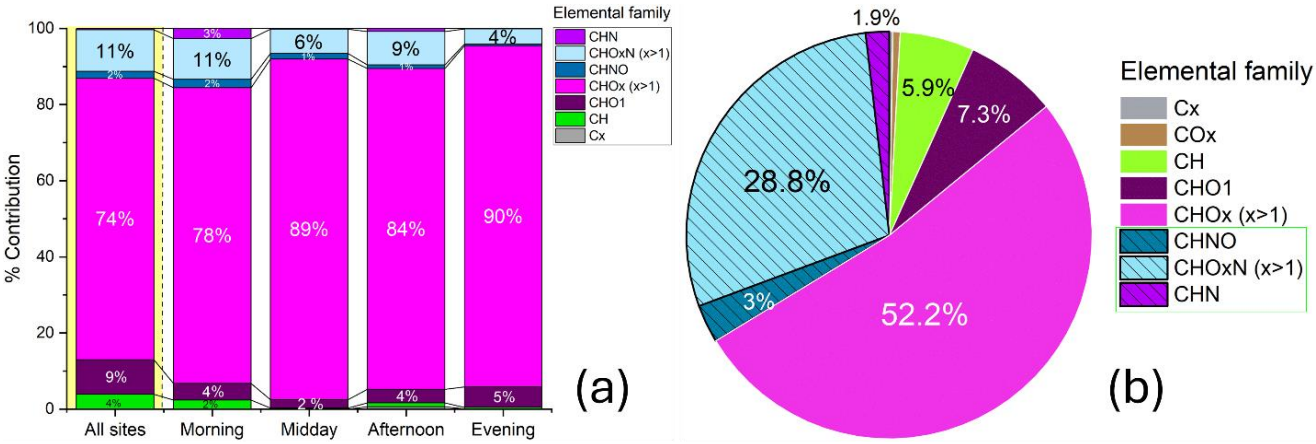

Figure 3.6 Contribution of each elemental family group to the overall chemical profile and the fraction of nitrogen-containing compounds identified in this study. (a) Variations in elemental contributions (CHN, CHOxN, CHNO, CHOx, CHO1, CH, Cx) measured by the FIGAERO-CIMS throughout a day. The contribution of each elemental family group reveals that CHOx has the highest overall contribution (all sites), followed by CHOxN (nitrogen-containing compounds with more than one oxygen). CHOxN contributions accounted for more than 10 % of the total during the morning hours. The composition analysis of identified ions depicted in (b) reveals that out of the corrected samples, 33.7 % of the total ions contain nitrogen.

To estimate the proportions of nitrogen-containing compounds identified through the FIGAERO-CIMS, the molecular formulas of identified chemical compounds were classified into seven groups based on their elemental compositions. These groups are groups CHN, CHOxN, CHNO, CHOx, CHO_1, CH, and Cx, reflecting variations in the presence of carbon (C), hydrogen (H), oxygen (O), and nitrogen (N). The percentage contribution was calculated from the sum of the normalized signal intensities of each identified chemical compound.

Daily variations at the restaurant-focused locations are shown in Figure 3.6 (a) in the first column. It reveals that CHOx was the most significant elemental group across all sites (74 %) and maintained a high contribution throughout the day (78-90%). Previous online CIMS particle measurements have demonstrated that the CHOx and CHON groups are dominant in SOA formation under photo-oxidation conditions in a smog chamber experiments (Du et al., 2022; Shao et al., 2022). This trend characterized by more than 50 % of CHO and CHOx contents followed by the CHON group was observed in the global atmosphere during field campaign measurements at various sample sites (Cai et al., 2022; Dall'Osto et al., 2012; Siegel et al., 2021). As illustrated in Figure 3.6 (a), the contribution of nitrogen-containing compounds (both CHN and CHOxN) did not differ significantly throughout the day, with the most pronounced proportions observed in the morning at 16 % of the total aggregated signal intensity. The selection of sample sites was based on the high density of restaurants and cooking sources in the area, indicting similar daily patterns in the influence of nitrogen-containing particles during these times.

Figure 3.6 (b) presents a pie chart that categorizes compounds into each elemental family group based solely on the number of detected ions. This chart highlights the contribution of reduced (1.9 %) and oxidized (31.8 %) nitrogen-containing compounds after CHOx, which contributes 52.2 % of detected peaks. Our previous measurements in restaurant exhaust plumes (Kim et al, 2024) showed a high abundance of reduced nitrogen ions (~10% of OA mass). However, our CIMS measurements here do not

reflect a large amount of reduced N. The possible reasons for that discrepancy are discussed in more detail below.

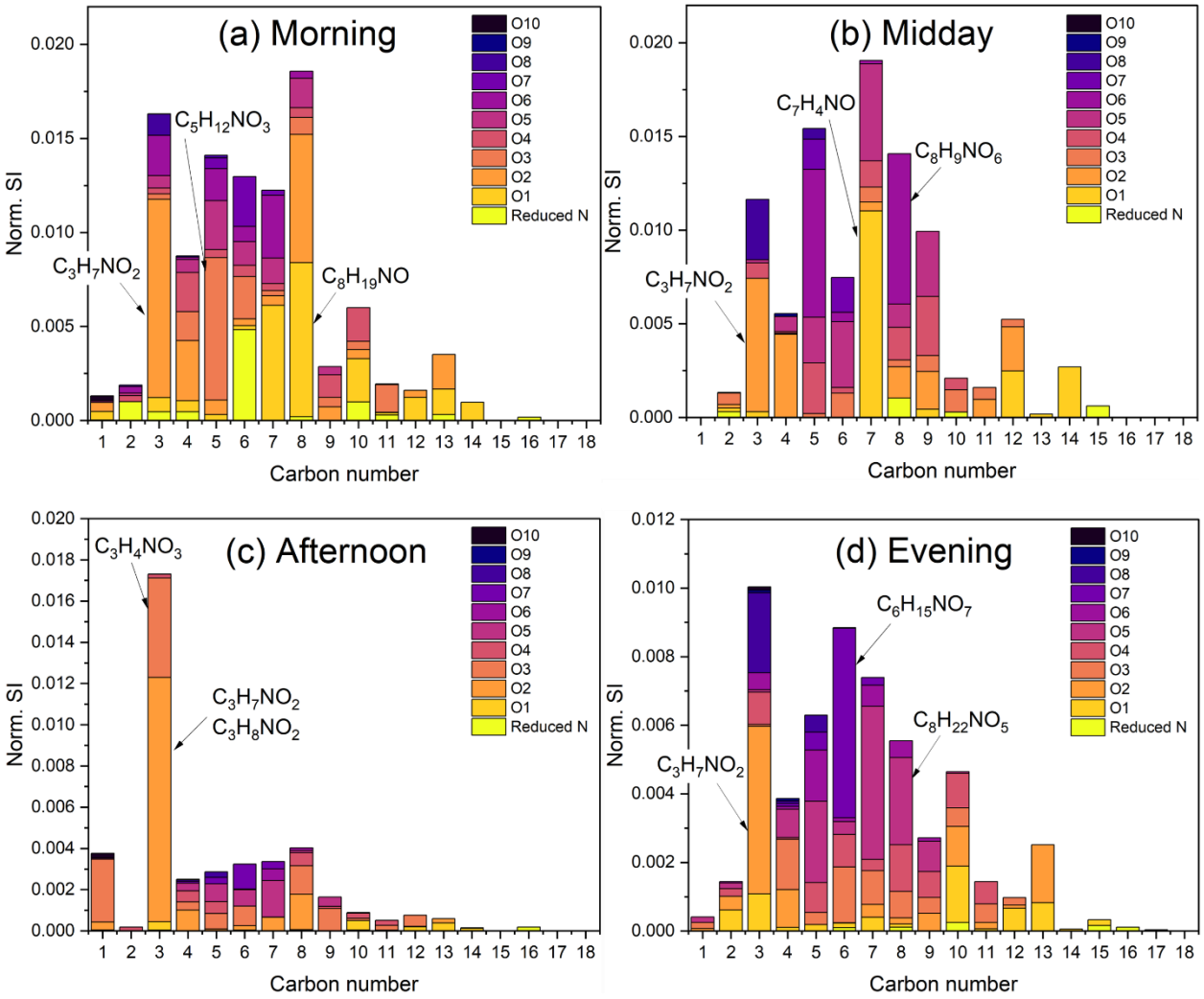

Figure 3.7 Normalized signal intensity (Norm. SI) for nitrogen containing compounds identified measured from morning through evening. Oxidized nitrogen (O ≥ 1) accounted for 91 to 98 % of the total signal intensity of nitrogen-containing compounds.

Nitrogen-containing compounds were not among the top five, but $C_3H_7NO_2^-$ was included in the top 10 compounds, as shown in Figure 3.5. $C_3H_7NO_2^-$ was the only N-containing compound identified among the top three highest signals across morning to evening samples, potentially corresponding to amino acid alanine (Figure 3.7). Alanine is naturally occurring amino acid found in various protein-rich foods including meat, seafood and beans (Alexander et al., 1953; Jiang et al., 2014; Kralik et al., 2015; Zhibo Wang et al., 2023) While the observed signal may represent a fragment originating from the degradation of parent ions (Abd El-Kareem et al., 2016), the pronounced signal intensity of the nitrogen-containing compounds support their actual presence in the collected particulate matter samples.

While our previous AMS measurements (Kim et al, 2024; Figure 3.8a) highlighted the contribution of CHN, oxidized nitrogen compounds accounted for more than 90 % of the total signal intensity from nitrogen-containing compounds here (Figure 3.7). The presence of oxidized nitrogen compounds peaked in the afternoon at 98.9%, followed by midday at 97.6 %, the evening at 97.2 %, and

morning at 91.5 % of the nitrogen compounds signal. This observation significantly contrasts with the summer 2019 field campaign, where high contributions from the CHN family were observed by the AMS.

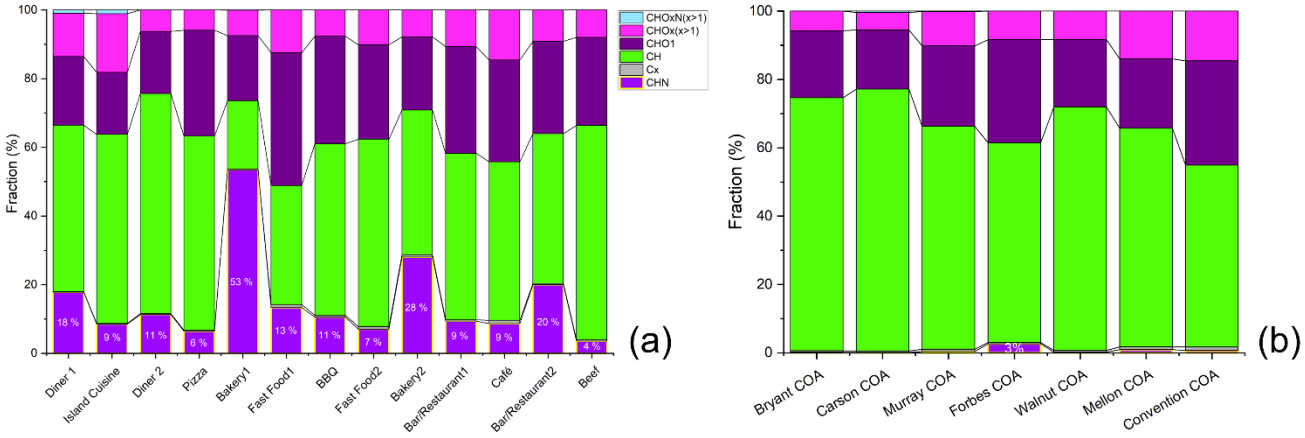

Figure 3.8 Fractional distribution of CHO_XN, CHON, CHN, CHO_X, CHO_1, CH, and C_X families across sampling sites during summer field campaigns. Measurements from the 2019 summer field campaign are displayed in (a), where the CHN family shows predominant proportions at Bakery 1 and Bakery 2, using the HR-ToF-AMS. Measurements using the same instrument during the 2021 summer field campaign are presented in (b), showing less than 1 % of COAs in ambient air.

During measurements inside of restaurant plumes in 2019, cooking OA from various restaurant sites demonstrated notable contributions from ions containing reduced nitrogen (Fig. 4.8a). Despite variability across sites, nitrogen-containing fragments accounted for an average of 15.8 %, of the total cooking OA mass, marking a significant contribution. Figure 3.8 (a) indicates that two bakery sites had higher proportions of the CHN family group (53 % and 28 %). Subsequent 2021 field campaigns aimed to compare CHN contributions to those observed in 2019, given their substantial impact on the earlier findings. As shown in Figure 3.8 (b), fractional distribution found in summer 2021 campaign showed the average CHN contribution to cooking OA, as identified through PMF analysis, was less than 1 % of the total OA concentration.

To address the significant discrepancy in CHN fractions observed between two summer field campaigns, several factors were evaluated. Initially, the possibility that higher ambient temperatures in 2021 could accelerate the chemical reactions of CHN in the air was considered. This hypothesis was dismissed after analyzing the CHN levels from the 2021 winter field campaign, which showed no significant seasonal variation of N-containing compounds. Furthermore, the detection limit of the AMS for CHN compounds was assessed, confirming that CHN concentrations from samples were significantly above its threshold. After ruling out these initial considerations, the study posits that the compounds in the CHN family exhibit high volatility, leading to their rapid dispersion from the immediate vicinity of exhaust pipes and resulting in low atmospheric persistence. To investigate this volatility further, the two-dimensional volatility basis set (2D-VBS) diagram was employed across nitrogen-containing compounds measured by the AMS and the CMS measurements.

3.3.3 Oxidation and volatility of nitrogen containing compounds.

Figure 3.9 illustrates the two-dimensional volatility basis set (2D-VBS) for nitrogen-containing compounds with oxidation state (2*O:C-H:C) on the y-axis and the logarithm of the saturation concentration reported in C* on the x-axis. Following background correction, N-containing compounds were allocated into volatility classes according to their saturation concentration. Figure 3.9 depicts the distribution of N-containing compounds as measured by the FIGAERO-CIMS . O/N ratios were depicted

with varying circle sizes based on their values: O/N < 3, 3 ≤ O/N < 6, 6 ≤ O/N ≤ 9. N-containing species with O/N < 3 indicates that the nitrogen containing species that are not likely to be organic nitrate but indicating the existence of structural features associated with reduced nitrogen (Kim et al., 2024). Additionally, the peak areas of CHON (CHON + CHOxN) and CHN groups were distinguished by colors, with CHN family peaks shown in blue.

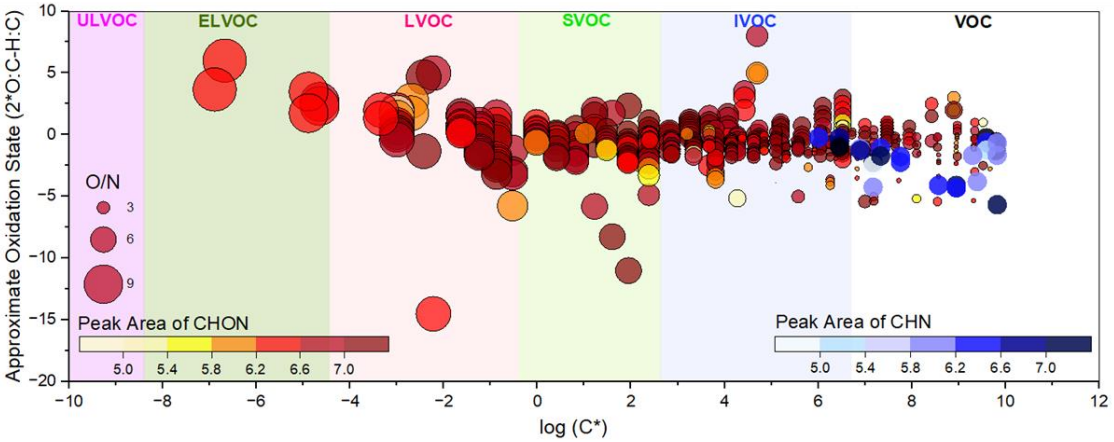

Figure 3.9 Comparative analysis of the 2D-Volatility Basis Set (2D-VBS), focusing on the saturation concentration and the approximate oxidation state of nitrogen containing compounds, as measured by FIGAERO-CIMS for 2021 summer field campaign. Ions were classified into volatility classes after background: Ultra-Low volatile Volatility Organic Compounds (ULVOC) below negative 8.3, Extremely Low-Volatility Organic Compounds (ELVOC) within a $\log_{10}$C* range of -8.3 to -4.3, Low-Volatility Organic Compounds (LVOC) with a $\log_{10}$C* between -4.3 and -0.3, Semi-Volatile Organic Compounds (SVOC) fall in the $\log_{10}$C* range of -0.3 to 2.7, Intermediate-Volatility Organic Compounds (IVOC) between the $\log_{10}$C* range between 2.7 to 6.7, and Volatility Organic Compounds (VOC) with a $\log_{10}$C* greater than 6.7.

The 2D-VBS advances beyond the traditional one-dimensional VBS by tracking both the oxidation state and saturation concentration of model species as detailed by Donahue et al., 2011. Unlike the 2D-VBS, earlier models focused solely on saturation vapor concentration (C*) and differentiated species based on their oxidation status without considering never-oxidized species (Murphy et al., 2011).

In this study, we adopted the updated parameterization from Donahue et al., 2011 with the assumption that OH oxidation significantly affects our samples. For the calculation of saturation vapor concentration, equation (1) from (Stolzenburg et al., 2022) was used to determine the saturation concentration value for all species based on their elemental content. Here, n_C, n_O, and n_N represent the counts of carbon, oxygen, and nitrogen atoms respectively in the organic compounds.

$$C^* = b_C(n^0{}_C - n_C) - b_O(n_O - 3n_N) - 2b_{CO}\frac{n_C(n_O-3n_N)}{(n_C+n_O-3n_N)} - n_N b_N \qquad (1)$$

The approach for nitrogen-containing compounds presumes inclusion of the nitrate (-ONO_2) group, requiring that the number of oxygen atoms to be at least triple the number of nitrogen atoms ($n_O \geq 3n_N$). The parameterization criterion, stating that compounds must have $n_C + n_O - 3n_N \leq 0$ be considered, excludes certain compounds from the volatility estimation framework. The volatility calculations were based on assumption of saturation concentration at 300 K (C^0=C*).

Compounds with higher O/N ratios primarily grouped in the lower volatility range (ELVOC to LVOC), yet the majority were classified as IVOC (46.5 %) and SVOC (25.5 %), with VOC accounting for 13.1 % of the total (Figure 3.10). Prior experimental studies have demonstrated that organonitrates (ONs), characterized by a nitrate (-ONO_2) group, often exhibit low volatility (Berkemeier et al., 2020; Brean et al., 2019). Specifically, Highly Oxygenated Organic Molecules (HOMs) typically fall into the Extremely Low Volatility Organic Compounds (ELVOC) category (Mohr et al., 2019; Peräkylä et al., 2020) due to their molar mass and reduced volatility, enhancing their propensity to condense onto particle surfaces (Li et al., 2016; Räty et al., 2021).

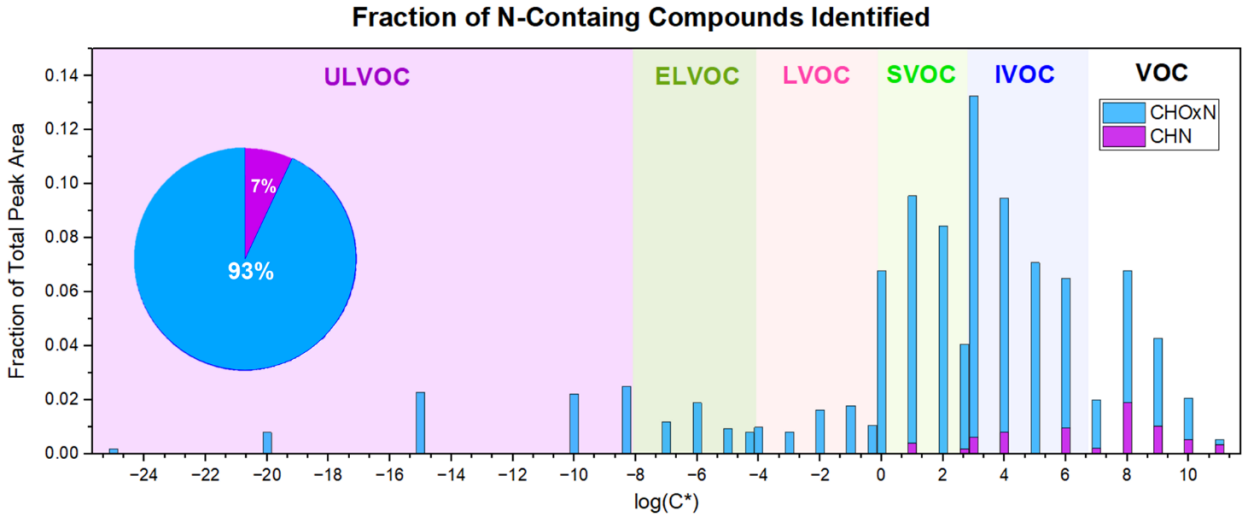

Figure 3.10 Normalized fraction of N-containing compounds in the 2D-VBS diagram. The fraction of the total peak area of N-containing compounds were normalized to the total iodide signal after background subtraction, ensures that fractions add up to 1. Stacked bar charts and a pie chart within the plot show that CHOxN compounds represent the majority of the signal from N-containing compounds, accounting for 93 % of the total.

The notable fractional contribution from CHN in Figure 3.8 highlights the discrepancy in CHN contributions between the summer campaigns of 2019 and 2021. In addition, both CHON and CHN compounds predominantly fell within the high volatile ranges in Figure 3.10, but CHN compounds were specifically placed a in higher VOC volatility category.

The most likely explanation for the discrepancy in the CHN family abundance between our 2019 and 2021 samples is therefore partitioning. The 2019 samples (Fig 3.8a) were collected inside of restaurant emission plumes. Concentrations were often high (OA > 50 μg m^{-3} in several cases) and the plumes were measured a few seconds after emission. Our 2021 measurements sampled diluted cooking emissions in areas with high restaurant density but were not collected inside of the emission plumes. The higher volatility of CHN family ions compared to CHON family ions suggests that the CHN species, which are in the particle phase in the near-source plume, evaporated during dilution away from the emissions source and are therefore in the gas phase in the 2021 measurements.

The difference in detection of CHON group compounds by the CIMS and the AMS can indeed be attributed to the differing sensitivities of these instruments to certain chemicals. CHON contributions in the atmosphere have been investigated in several studies using the CIMS (Guo et al., 2022; Haslett et al., 2023; Huang et al., 2024; Mehra et al., 2021; Siegel et al., 2021). CIMS is known for its high sensitivity to a wide range of organic and inorganic compounds, including those with low volatility and functionalized nitrogen-containing species (like CHON compounds), due to its soft ionization technique (Hearn and Smith, 2004; Iyer et al., 2016; Lee et al., 2014). This method minimizes fragmentation and

allows for the detection of molecular ions, making it particularly effective for identifying specific compounds in complex mixtures. AMS, while highly effective for quantifying the overall composition of non-refractory submicron aerosol particles (Aljawhary et al., 2013), may have lower sensitivity to certain compounds (Allan et al., 2004) due to its ionization technique, which can lead to fragmentation of parent molecules (Jimenez et al., 2003). This means that the AMS might not detect certain species as efficiently as the CIMS, especially if those compounds break down into fragments that are not easily attributed to their original molecules. The varying sensitivities of the CIMS and the AMS to specific chemical compounds could explain why the CIMS detects a higher contribution of CHO_XN group compounds compared to the AMS.

3.4 **Conclusions**

Section 2 used AMS data to show that cooking is an important source of urban PM and that cooking sources contribute to the spatial and temporal variations in urban PM concentrations. This section used chemical ionization mass spectrometry (CIMS) to examine cooking emissions at a molecular level. Targeted analysis demonstrated the importance of common cooking markers including fatty acids. We demonstrated the value of a non-target analysis, as the common species used in the targeted analysis represented a minority of the overall number of compounds and mass of compounds emitted from cooking sources.

Our previous work had demonstrated that cooking sources can be a source of organic nitrogen in urban environments. The CIMS measurements showed that ~10% of cooking emissions, by mass, contain organic nitrogen groups. These organic nitrogen containing species include a mixture of oxygen-containing and reduced (non-oxygen-containing) nitrogen functional groups. We demonstrated that the reduced nitrogen compounds are generally IVOCs or more volatile species, and that these compounds, while possibly emitted as particles in the concentrated cooking plume emitted by restaurants, rapidly evaporate to the vapor phase. The impacts of these organic nitrogen species on both ambient PM concentrations and human exposure and health require further study to fully understand.

4. Spatial variations in ozone-forming potential of VOCs

4.1 Overview and introduction

The prior two sections of this report focused on emissions of PM from various urban sources. Urban sources that emit PM, especially OA, co-emit organic vapors. These vapors can participate in chemical reactions that generate ozone and secondary organic aerosol. This chapter of the report focuses on the spatial variation of VOC concentrations and their potential to form secondary pollutants like ozone.

O_3 is formed by the coupled reactions of NOx (nitrogen oxides) and VOCs (volatile organic compounds). Oxidation of VOCs by the hydroxyl radical (OH) produces peroxy radicals (ROO) that react with NO to form NO_2. NO_2 is subsequently photolyzed in sunlight, and the resulting O radical produces O_3 via reaction with O_2. While the specific O_3 production rate and maximum daytime O_3 concentration in an area depends on the concentrations of NOx and VOCs, OH reactivity is a simple metric to evaluate the abundance of VOCs that can recycle NO to NO_2.

The goal of this portion of the project was to quantify spatial variations in OH reactivity, and hence the ability of the ambient VOC mixture to produce O_3. We hypothesized that OH reactivity would demonstrate significant spatial variations, and that these spatial variations would echo the spatial distribution of anthropogenic sources in different city neighborhoods.

The previous two sections of the report showed that PM mass and composition varied spatially due in part of the presence (or absence) of local sources. As we show in this section of the report, OH reactivity exhibited less spatial variability. This is in large part to OH reactivity having large contributions from small, secondary, oxygenated organic molecules that constitute part of the VOC background. Local enhancements in OH reactivity are minor, and would therefore be expected to generate small spatial variations in ambient O_3.

4.2 Methods

4.2.1 OH reactivity and VOC measurements

OH reactivity is defined as: $R_{OH} = \sum(k_{oH+VOC}[VOC])$. Here k is the rate constant for the reaction of each VOC with OH. This is summed across all species to determine a total reactivity. The units of OH reactivity are inverse time (e.g., 1/s).

We measured VOC concentrations in different areas of Pittsburgh with a proton-transfer-reaction mass spectrometer (PTR-MS). The PTR-MS can quantify concentrations of VOCs in real time. The PTR-MS relies on "soft" ionization through proton reaction, so species are quantified at their molecular weight plus one for the attached proton:

$$X + H_3^+O \rightarrow XH^+ + H_2O$$

The PTR-MS is only sensitive to species with a higher proton affinity than water. This means that it is insensitive to major inorganic gases like CO and CO_2, which could overwhelm the VOC signal. It is also insensitive to small aliphatic species like methane and ethane, though these are minor contributors to overall OH reactivity.

4.2.2 Mobile sampling approach

Sections 2 and 3 of this report focused on stationary measurements at specific sampling sites. The PTR-MS was not available for those measurements because of maintenance issues. Instead, for OH reactivity, we conducted in-motion sampling with our mobile laboratory. The approach followed our previous mobile sampling work (e.g., Shah et al, 2018). We defined a sampling route through Pittsburgh that included many of the same land use types identified for the stationary sampling in Sections 3 and 4 of the report. For example, our mobile sampling route included areas of high and low traffic density and high and low restaurant density. It included the downtown central business district, areas dominated by heavy industry, and residential areas in the urban background.

The sampling route was driven on multiple days to generate a dataset that is representative of long-term average conditions. Previous work by our group and others has shown that a minimum of seven repeat mobile sampling trips on different days are required to capture long-term trends in concentrations with mobile sampling. Further, we subdivided the mobile sampling route into three sub-routes. On each

sampling day, we sampled the sub-routes in a different order. This prevents the dataset from developing temporal biases (e.g., the dataset would be biased if we always sampled a specific sub-route in the morning and another sub-route in the afternoon).

4.3 Results and Discussion

Our mobile sampling results show that OH reactivity had larger inter-day temporal variability than intra-day spatial variability. Figure 4.1 shows box and whisker plots of measured OH reactivity on 11 separate mobile sampling days. The entire driving route was sampled on each day, so the data from each day represent the spatial variation in OH reactivity on a given day.

In general, inter-day variations in OH reactivity are larger than intra-day (spatial) variations. The daily median OH reactivity varies by about a factor of 5, from ~3 to ~15 s^{-1}. In contrast, the intra-day interquartile range in OH reactivity is typically around a factor of 2. This suggests that spatial variations in emission sources and strengths have a smaller impact on OH reactivity and O_3 formation than inter-day variations in emissions and meteorology.

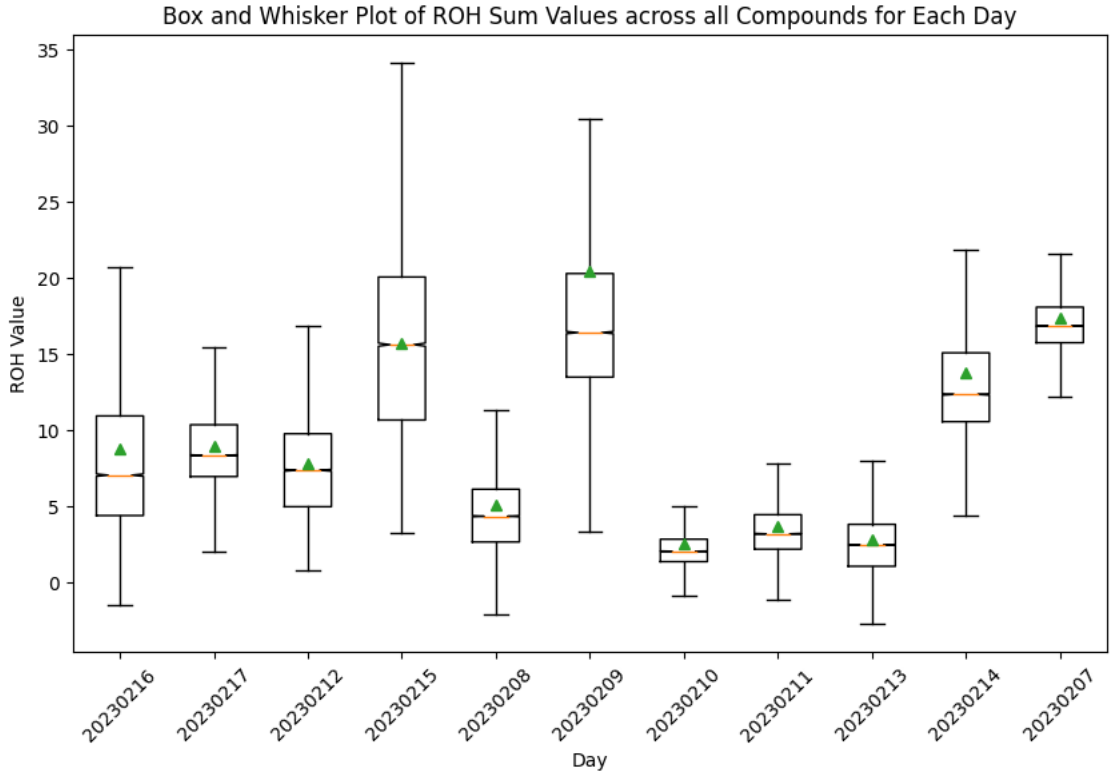

Figure 4.1 Box plots of OH reactivity measured on 11 separate mobile sampling days. The entire sampling route was driven on each day. There are generally larger differences between days than within days.

The relative lack of spatial variation in OH reactivity is because OH reactivity is dominated by small, oxygenated molecules rather than fresh emissions. The local, neighborhood-scale, differences in emissions make up a smaller fraction of overall OH reactivity than of PM mass. Thus, while neighborhood-scale variations in emissions impact PM mass and composition, they have a smaller impact on OH reactivity.

An example of neighborhood-scale variations in OH reactivity is shown in Figure 4.2. It compares OH reactivity in two neighborhoods along the mobile sampling route on a single day. The left pie chart shows the OH reactivity on Neville Island, an area with several large industrial emissions

sources and heavy diesel traffic. The right pie chart shows OH reactivity in the Oakland neighborhood of Pittsburgh, which is a city neighborhood with high traffic and restaurant density. In each neighborhood, OH reactivity is dominated by small, oxygenated molecules. The single most important VOC to OH reactivity in each location is C_2H_4O, which is likely acetaldehyde. Acetaldehyde is a secondary species formed by oxidation chemistry, and it therefore has small spatial variations across Pittsburgh.

There are differences in the VOC mix in the two neighborhoods shown in Figure 4.2. Concentrations of aromatic VOCs are higher on Neville Island (left). However, these differences have a small impact on OH reactivity, which is dominated by the small oxygenated species.

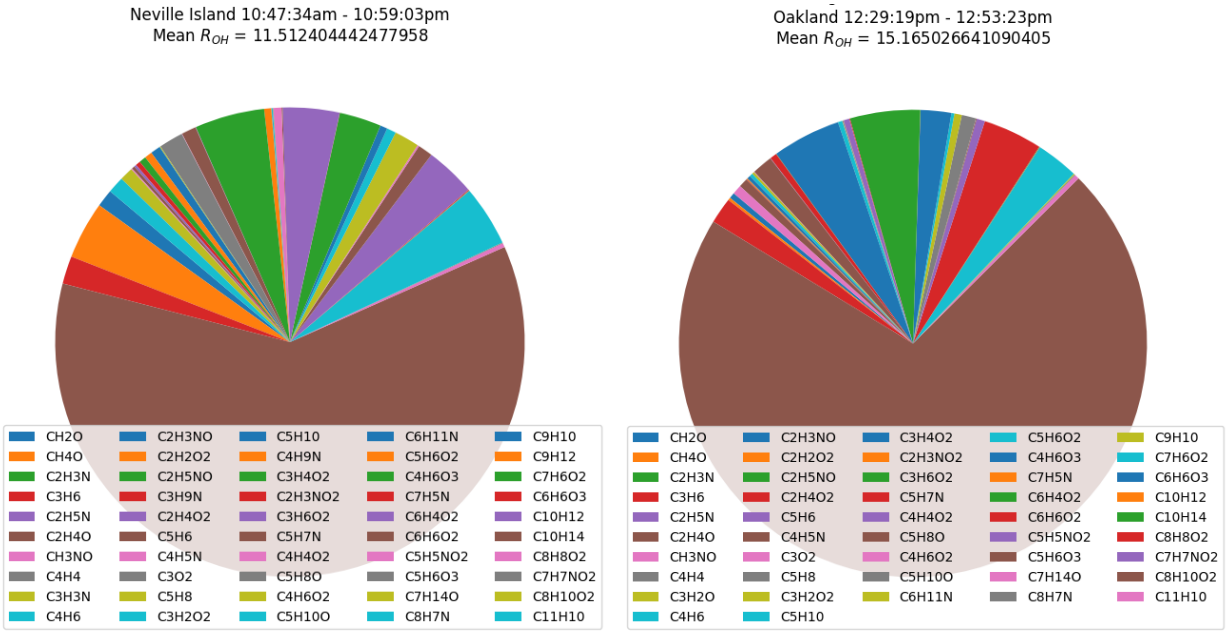

Figure 4.2. OH reactivity in an industrial neighborhood (left) and a mixed urban neighborhood (right) as measured with PTR-MS.

Overall, the PTR-MS results indicate that spatial variations in OH reactivity, and hence O_3 production, seem to be smaller than spatial variations in PM mass and composition. OH reactivity is dominated by small oxygenated molecules. The local-scale variations in VOC emissions have a minor impact on OH reactivity. Thus we would expect that local-scale impacts of VOC emissions on O_3 production would also be small. It is very possible that local-scale O_3 production depends more strongly on NOx, and corresponding impacts to the VOC:NOx ratio, than the speciation of VOCs.

4.3 Conclusions

We measured the concentrations of a suite of VOCs across Pittsburgh and converted those concentrations to OH reactivities. Overall, OH reactivity was significantly less spatially variable than temporally variable, and significantly less spatially variable than PM concentrations and source contributions presented in Sections 2 and 3 of this report. The majority of OH reactivity variation was temporal, and OH reactivity was dominated by small, oxygenated molecules. This suggests that urban ozone production potential is both less spatially variable than PM concentrations. It also suggests that there is less ability to locally reduce ozone concentrations, whereas $PM_{2.5}$ concentrations can be reduced at a neighborhood scale via reductions in local emissions.

References

Abd El-Kareem, M., Rabbih, M., Selim, E., 2016. Identification of zingiber components by gas chromatograph/mass spectrometer and semi-empirical calculations. International Journal of Physical Research 4, 20. https://doi.org/10.14419/ijpr.v4i1.6052

Abdullahi, K.L., Delgado-Saborit, J.M., Harrison, R.M., 2013. Emissions and indoor concentrations of particulate matter and its specific chemical components from cooking: A review. Atmospheric Environment 71, 260–294. https://doi.org/10.1016/j.atmosenv.2013.01.061

Actkinson, B., Ensor, K., Griffin, R.J., 2021. SIBaR: a new method for background quantification and removal from mobile air pollution measurements. Atmospheric Measurement Techniques 14, 5809–5821. https://doi.org/10.5194/amt-14-5809-2021

Ahmed, A.A.O., Salah, A., Sedik, F., Ghanim, A., 2023. Effect of foliar treatment with yeast and nitrogen fertilization on the productivity of sesame. Aswan University Journal of Environmental Studies 4, 15–24. https://doi.org/10.21608/aujes.2023.165031.1097

Ahmed, F.A., Baraka, D.M., Essawy, H.S., Badawy, H., Abdel-Mawgoud, M., 2023. VOLATILE OILS, LIPID CONSTITUENTS AND CHARACTERIZATION OF GREEN SILVER NANOPARTICLES OF SOME PLANTS BELONGING TO FAMILY APIACEAE. Egyptian Journal of Desert Research 73, 489–511. https://doi.org/10.21608/ejdr.2023.220150.1147

Äijälä, M., Heikkinen, L., Fröhlich, R., Canonaco, F., Prévôt, A.S.H., Junninen, H., Petäjä, T., Kulmala, M., Worsnop, D., Ehn, M., 2017. Resolving anthropogenic aerosol pollution types – deconvolution and exploratory classification of pollution events. Atmospheric Chemistry and Physics 17, 3165–3197. https://doi.org/10.5194/acp-17-3165-2017

Aiken, A.C., Salcedo, D., Cubison, M.J., Huffman, J.A., DeCarlo, P.F., Ulbrich, I.M., Docherty, K.S., Sueper, D., Kimmel, J.R., Worsnop, D.R., Trimborn, A., Northway, M., Stone, E.A., Schauer, J.J., Volkamer, R.M., Fortner, E., de Foy, B., Wang, J., Laskin, A., Shutthanandan, V., Zheng, J., Zhang, R., Gaffney, J., Marley, N.A., Paredes-Miranda, G., Arnott, W.P., Molina, L.T., Sosa, G., Jimenez, J.L., 2009. Mexico City aerosol analysis during MILAGRO using high resolution aerosol mass spectrometry at the urban supersite (T0) – Part 1: Fine particle composition and organic source apportionment. Atmospheric Chemistry and Physics 9, 6633–6653. https://doi.org/10.5194/acp-9-6633-2009

Alexander, J.C., Beckner, C.W., Elvehjem, C.A., 1953. The Alanine, Cystine, Glycine and Serine Content of Meat1. The Journal of Nutrition 51, 319–328. https://doi.org/10.1093/jn/51.3.319

Alfarra, M.R., Coe, H., Allan, J.D., Bower, K.N., Boudries, H., Canagaratna, M.R., Jimenez, J.L., Jayne, J.T., Garforth, A.A., Li, S.-M., Worsnop, D.R., 2004. Characterization of urban and rural organic particulate in the Lower Fraser Valley using two Aerodyne Aerosol Mass Spectrometers. Atmospheric Environment, The Pacific 2001 Air Quality Study 38, 5745–5758. https://doi.org/10.1016/j.atmosenv.2004.01.054

Aljawhary, D., Lee, A.K.Y., Abbatt, J.P.D., 2013. High-resolution chemical ionization mass spectrometry (ToF-CIMS): application to study SOA composition and processing. Atmospheric Measurement Techniques 6, 3211–3224. https://doi.org/10.5194/amt-6-3211-2013

Allan, J.D., Delia, A.E., Coe, H., Bower, K.N., Alfarra, M.R., Jimenez, J.L., Middlebrook, A.M.,

Drewnick, F., Onasch, T.B., Canagaratna, M.R., Jayne, J.T., Worsnop, D.R., 2004. A generalised method for the extraction of chemically resolved mass spectra from Aerodyne aerosol mass spectrometer data. Journal of Aerosol Science 35, 909–922. https://doi.org/10.1016/j.jaerosci.2004.02.007

Allan, J.D., Williams, P.I., Morgan, W.T., Martin, C.L., Flynn, M.J., Lee, J., Nemitz, E., Phillips, G.J., Gallagher, M.W., Coe, H., 2010. Contributions from transport, solid fuel burning and cooking to primary organic aerosols in two UK cities. Atmospheric Chemistry and Physics 10, 647–668. https://doi.org/10.5194/acp-10-647-2010

Allen, A.G., Miguel, A.H., 1995. Indoor organic and inorganic pollutants: In-situ formation and dry deposition in Southeastern Brazil. Atmospheric Environment 29, 3519–3526. https://doi.org/10.1016/1352-2310(95)00172-U

Al-Naiema, I.M., Hettiyadura, A.P.S., Wallace, H.W., Sanchez, N.P., Madler, C.J., Cevik, B.K., Bui, A.A.T., Kettler, J., Griffin, R.J., Stone, E.A., 2018. Source apportionment of fine particulate matter in Houston, Texas: insights to secondary organic aerosols. Atmos. Chem. Phys. 18, 15601–15622. https://doi.org/10.5194/acp-18-15601-2018

Alves, C.A., Evtyugina, M., Vicente, E., Vicente, A., Gonçalves, C., Neto, A.I., Nunes, T., Kováts, N., 2022. Outdoor charcoal grilling: Particulate and gas-phase emissions, organic speciation and ecotoxicological assessment. Atmospheric Environment 285, 119240. https://doi.org/10.1016/j.atmosenv.2022.119240

Alves, C.A., Vicente, E.D., Evtyugina, M., Vicente, A.M., Nunes, T., Lucarelli, F., Calzolai, G., Nava, S., Calvo, A.I., Alegre, C. del B., Oduber, F., Castro, A., Fraile, R., 2020. Indoor and outdoor air quality: A university cafeteria as a case study. Atmospheric Pollution Research 11, 531–544. https://doi.org/10.1016/j.apr.2019.12.002

Alves, C.A., Vicente, E.D., Evtyugina, M., Vicente, A.M.P., Sainnokhoi, T.-A., Kováts, N., 2021. Cooking activities in a domestic kitchen: Chemical and toxicological profiling of emissions. Science of The Total Environment 772, 145412. https://doi.org/10.1016/j.scitotenv.2021.145412

Ames, J.M., 1998. Applications of the Maillard reaction in the food industry. Food Chemistry 62, 431–439. https://doi.org/10.1016/S0308-8146(98)00078-8

Amouei Torkmahalleh, M., Ospanova, S., Baibatyrova, A., Nurbay, S., Zhanakhmet, G., Shah, D., 2018. Contributions of burner, pan, meat and salt to PM emission during grilling. Environmental Research 164, 11–17. https://doi.org/10.1016/j.envres.2018.01.044

Bak, U.G., Nielsen, C.W., Marinho, G.S., Gregersen, Ó., Jónsdóttir, R., Holdt, S.L., 2019. The seasonal variation in nitrogen, amino acid, protein and nitrogen-to-protein conversion factors of commercially cultivated Faroese Saccharina latissima. Algal Research 42, 101576. https://doi.org/10.1016/j.algal.2019.101576

Bannan, T.J., Le Breton, M., Priestley, M., Worrall, S.D., Bacak, A., Marsden, N.A., Mehra, A., Hammes, J., Hallquist, M., Alfarra, M.R., Krieger, U.K., Reid, J.P., Jayne, J., Robinson, W., McFiggans, G., Coe, H., Percival, C.J., Topping, D., 2019. A method for extracting calibrated volatility information from the FIGAERO-HR-ToF-CIMS and its experimental application. Atmospheric Measurement Techniques 12, 1429–1439. https://doi.org/10.5194/amt-12-1429-2019

Berkemeier, T., Takeuchi, M., Eris, G., Ng, N.L., 2020. Kinetic modeling of formation and evaporation of secondary organic aerosol from NO3 oxidation of pure and mixed monoterpenes. Atmospheric Chemistry and Physics 20, 15513–15535. https://doi.org/10.5194/acp-20-15513-2020

Bhardwaj, A., Sunder Raman, R., 2022. Evaluation of organic aerosol filter sampling artefacts and implications to gravimetric PM2.5 mass at a COALESCE network site - Bhopal, India. Journal of Environmental Management 319, 115749. https://doi.org/10.1016/j.jenvman.2022.115749
Black, F.M., 1991. Control of motor vehicle emissions‐the U.S. experience. Critical Reviews in Environmental Control 21, 373–410. https://doi.org/10.1080/10643389109388423

Bottenus, C.L.H., Massoli, P., Sueper, D., Canagaratna, M.R., VanderSchelden, G., Jobson, B.T., VanReken, T.M., 2018. Identification of amines in wintertime ambient particulate material using high resolution aerosol mass spectrometry. Atmospheric Environment 180, 173–183. https://doi.org/10.1016/j.atmosenv.2018.01.044

Boukhebti, H., Chaker, A., Belhadj, H., Harzallah, D., 2016. Longue time storage at room temperature increases the chemical composition of olive oil 8, 73–78.

Bozzetti, C., El Haddad, I., Salameh, D., Daellenbach, K.R., Fermo, P., Gonzalez, R., Minguillón, M.C., Iinuma, Y., Poulain, L., Elser, M., Müller, E., Slowik, J.G., Jaffrezo, J.-L., Baltensperger, U., Marchand, N., Prévôt, A.S.H., 2017. Organic aerosol source apportionment by offline-AMS over a full year in Marseille. Atmospheric Chemistry and Physics 17, 8247–8268. https://doi.org/10.5194/acp-17-8247-2017
Brean, J., Harrison, R.M., Shi, Z., Beddows, D.C.S., Acton, W.J.F., Hewitt, C.N., Squires, F.A., Lee, J., 2019. Observations of highly oxidized molecules and particle nucleation in the atmosphere of Beijing. Atmospheric Chemistry and Physics 19, 14933–14947. https://doi.org/10.5194/acp-19-14933-2019

Brook, J.R., Graham, L., Charland, J.P., Cheng, Y., Fan, X., Lu, G., Li, S.M., Lillyman, C., MacDonald, P., Caravaggio, G., MacPhee, J.A., 2007. Investigation of the motor vehicle exhaust contribution to primary fine particle organic carbon in urban air. Atmospheric Environment 41, 119–135. https://doi.org/10.1016/j.atmosenv.2006.07.050

Brown, W.L., Day, D.A., Stark, H., Pagonis, D., Krechmer, J.E., Liu, X., Price, D.J., Katz, E.F., DeCarlo, P.F., Masoud, C.G., Wang, D.S., Hildebrandt Ruiz, L., Arata, C., Lunderberg, D.M., Goldstein, A.H., Farmer, D.K., Vance, M.E., Jimenez, J.L., 2021. Real-time organic aerosol chemical speciation in the indoor environment using extractive electrospray ionization mass spectrometry. Indoor Air 31, 141–155. https://doi.org/10.1111/ina.12721

Bruns, E.A., El Haddad, I., Keller, A., Klein, F., Kumar, N.K., Pieber, S.M., Corbin, J.C., Slowik, J.G., Brune, W.H., Baltensperger, U., Prévôt, A.S.H., 2015. Inter-comparison of laboratory smog chamber and flow reactor systems on organic aerosol yield and composition. Atmospheric Measurement Techniques 8, 2315–2332. https://doi.org/10.5194/amt-8-2315-2015

Cai, J., Daellenbach, K., Wu, C., Zheng, Y., Zheng, F., Du, W., Haslett, S., Chen, Q., Kulmala, M., Mohr, C., 2022. Characterization of offline analysis of particulate matter with FIGAERO-CIMS. Atmospheric Measurement Techniques Discussions 1–22. https://doi.org/10.5194/amt-2022-248

Cai, M., Ye, C., Yuan, B., Huang, S., Zheng, E., Yang, S., Wang, Z., Lin, Y., Li, T., Hu, W., Chen, W., Song, Q., Li, W., Peng, Y., Liang, B., Sun, Q., Zhao, J., Chen, D., Sun, J., Yang, Z., Shao, M., 2024. Enhanced daytime secondary aerosol formation driven by gas-particle partitioning in downwind urban plumes. EGUsphere 1–30. https://doi.org/10.5194/egusphere-2024-887

Canagaratna, M.R., Jimenez, J.L., Kroll, J.H., Chen, Q., Kessler, S.H., Massoli, P., Hildebrandt Ruiz, L., Fortner, E., Williams, L.R., Wilson, K.R., Surratt, J.D., Donahue, N.M., Jayne, J.T., Worsnop, D.R., 2015. Elemental ratio measurements of organic compounds using aerosol mass spectrometry: characterization, improved calibration, and implications. Atmospheric Chemistry and Physics 15, 253–272. https://doi.org/10.5194/acp-15-253-2015

Canonaco, F., Crippa, M., Slowik, J.G., Baltensperger, U., Prévôt, A.S.H., 2013. SoFi, an IGOR-based interface for the efficient use of the generalized multilinear engine (ME-2) for the source apportionment: ME-2 application to aerosol mass spectrometer data. Atmospheric Measurement Techniques 6, 3649–3661. https://doi.org/10.5194/amt-6-3649-2013

Cao, R., Xu, Y., 2019. Efficient Preparation of Xylonic Acid from Xylonate Fermentation Broth by Bipolar Membrane Electrodialysis. Appl Biochem Biotechnol 187, 396–406. https://doi.org/10.1007/s12010-018-2827-y

Castillo, M.D., Kinney, P.L., Southerland, V., Arno, C.A., Crawford, K., van Donkelaar, A., Hammer, M., Martin, R.V., Anenberg, S.C., 2021. Estimating Intra-Urban Inequities in PM2.5-Attributable Health Impacts: A Case Study for Washington, DC. GeoHealth 5, e2021GH000431. https://doi.org/10.1029/2021GH000431

Chen, Y., Takeuchi, M., Nah, T., Xu, L., Canagaratna, M.R., Stark, H., Baumann, K., Canonaco, F., Prévôt, A.S.H., Huey, L.G., Weber, R.J., Ng, N.L., 2020. Chemical characterization of secondary organic aerosol at a rural site in the southeastern US: insights from simultaneous high-resolution time-of-flight aerosol mass spectrometer (HR-ToF-AMS) and FIGAERO chemical ionization mass spectrometer (CIMS) measurements. Atmospheric Chemistry and Physics 20, 8421–8440. https://doi.org/10.5194/acp-20-8421-2020

Chen, Y., Xu, L., Humphry, T., Hettiyadura, A.P.S., Ovadnevaite, J., Huang, S., Poulain, L., Schroder, J.C., Campuzano-Jost, P., Jimenez, J.L., Herrmann, H., O'Dowd, C., Stone, E.A., Ng, N.L., 2019. Response of the Aerodyne Aerosol Mass Spectrometer to Inorganic Sulfates and Organosulfur Compounds: Applications in Field and Laboratory Measurements. Environ. Sci. Technol. 53, 5176–5186. https://doi.org/10.1021/acs.est.9b00884

Cheng, B., Wang-Li, L., Meskhidze, N., Classen, J., Bloomfield, P., 2019. Spatial and temporal variations of PM2.5 mass closure and inorganic PM2.5 in the Southeastern U.S. Environ Sci Pollut Res 26, 33181–33191. https://doi.org/10.1007/s11356-019-06437-8

Chow, J.C., Chen, L.-W.A., Watson, J.G., Lowenthal, D.H., Magliano, K.A., Turkiewicz, K., Lehrman, D.E., 2006. PM2.5 chemical composition and spatiotemporal variability during the California Regional PM10/PM2.5 Air Quality Study (CRPAQS). Journal of Geophysical Research: Atmospheres 111. https://doi.org/10.1029/2005JD006457

Chow, J.C., Watson, J.G., Feldman, H.J., Nolen, J.E., Wallerstein, B., Hidy, G.M., Lioy, P.J., McKee, H., Mobley, D., Baugues, K., Bachmann, J.D., 2007. Will the Circle Be Unbroken: A History of the U.S. National Ambient Air Quality Standards. Journal of the Air & Waste Management Association 57, 1151–1163. https://doi.org/10.3155/1047-3289.57.10.1151

Coggon, M.M., McDonald, B.C., Vlasenko, A., Veres, P.R., Bernard, F., Koss, A.R., Yuan, B., Gilman, J.B., Peischl, J., Aikin, K.C., DuRant, J., Warneke, C., Li, S.-M., de Gouw, J.A., 2018. Diurnal Variability and Emission Pattern of Decamethylcyclopentasiloxane (D5) from the Application of Personal

Care Products in Two North American Cities. Environ. Sci. Technol. 52, 5610–5618. https://doi.org/10.1021/acs.est.8b00506

Crippa, M., Canonaco, F., Lanz, V.A., Äijälä, M., Allan, J.D., Carbone, S., Capes, G., Ceburnis, D., Dall'Osto, M., Day, D.A., DeCarlo, P.F., Ehn, M., Eriksson, A., Freney, E., Hildebrandt Ruiz, L., Hillamo, R., Jimenez, J.L., Junninen, H., Kiendler-Scharr, A., Kortelainen, A.-M., Kulmala, M., Laaksonen, A., Mensah, A.A., Mohr, C., Nemitz, E., O'Dowd, C., Ovadnevaite, J., Pandis, S.N., Petäjä, T., Poulain, L., Saarikoski, S., Sellegri, K., Swietlicki, E., Tiitta, P., Worsnop, D.R., Baltensperger, U., Prévôt, A.S.H., 2014a. Organic aerosol components derived from 25 AMS data sets across Europe using a consistent ME-2 based source apportionment approach. Atmospheric Chemistry and Physics 14, 6159–6176. https://doi.org/10.5194/acp-14-6159-2014

Crippa, M., Canonaco, F., Lanz, V.A., Äijälä, M., Allan, J.D., Carbone, S., Capes, G., Ceburnis, D., Dall'Osto, M., Day, D.A., DeCarlo, P.F., Ehn, M., Eriksson, A., Freney, E., Hildebrandt Ruiz, L., Hillamo, R., Jimenez, J.L., Junninen, H., Kiendler-Scharr, A., Kortelainen, A.-M., Kulmala, M., Laaksonen, A., Mensah, A.A., Mohr, C., Nemitz, E., O'Dowd, C., Ovadnevaite, J., Pandis, S.N., Petäjä, T., Poulain, L., Saarikoski, S., Sellegri, K., Swietlicki, E., Tiitta, P., Worsnop, D.R., Baltensperger, U., Prévôt, A.S.H., 2014b. Organic aerosol components derived from 25 AMS data sets across Europe using a consistent ME-2 based source apportionment approach. Atmospheric Chemistry and Physics 14, 6159–6176. https://doi.org/10.5194/acp-14-6159-2014

Crippa, M., DeCarlo, P.F., Slowik, J.G., Mohr, C., Heringa, M.F., Chirico, R., Poulain, L., Freutel, F., Sciare, J., Cozic, J., Di Marco, C.F., Elsasser, M., Nicolas, J.B., Marchand, N., Abidi, E., Wiedensohler, A., Drewnick, F., Schneider, J., Borrmann, S., Nemitz, E., Zimmermann, R., Jaffrezo, J.-L., Prévôt, A.S.H., Baltensperger, U., 2013. Wintertime aerosol chemical composition and source apportionment of the organic fraction in the metropolitan area of Paris. Atmospheric Chemistry and Physics 13, 961–981. https://doi.org/10.5194/acp-13-961-2013

Crippa, Monica, El Haddad, I., Slowik, J.G., DeCarlo, P.F., Mohr, C., Heringa, M.F., Chirico, R., Marchand, N., Sciare, J., Baltensperger, U., Prévôt, A.S.H., 2013. Identification of marine and continental aerosol sources in Paris using high resolution aerosol mass spectrometry. Journal of Geophysical Research: Atmospheres 118, 1950–1963. https://doi.org/10.1002/jgrd.50151

Cross, E.S., Sappok, A., Fortner, E.C., Hunter, J.F., Jayne, J.T., Brooks, W.A., Onasch, T.B., Wong, V.W., Trimborn, A., Worsnop, D.R., Kroll, J.H., 2012. Real-Time Measurements of Engine-Out Trace Elements: Application of a Novel Soot Particle Aerosol Mass Spectrometer for Emissions Characterization. Journal of Engineering for Gas Turbines and Power 134. https://doi.org/10.1115/1.4005992

Cross, E.S., Slowik, J.G., Davidovits, P., Allan, J.D., Worsnop, D.R., Jayne, J.T., Lewis †, D.K., Canagaratna, M., Onasch, T.B., 2007. Laboratory and Ambient Particle Density Determinations using Light Scattering in Conjunction with Aerosol Mass Spectrometry. Aerosol Science and Technology 41, 343–359. https://doi.org/10.1080/02786820701199736

Dai, Q., Schulze, B.C., Bi, X., Bui, A.A.T., Guo, F., Wallace, H.W., Sanchez, N.P., Flynn, J.H., Lefer, B.L., Feng, Y., Griffin, R.J., 2019. Seasonal differences in formation processes of oxidized organic aerosol near Houston, TX. Atmospheric Chemistry and Physics 19, 9641–9661. https://doi.org/10.5194/acp-19-9641-2019

Dallmann, T.R., Kirchstetter, T.W., DeMartini, S.J., Harley, R.A., 2013. Quantifying On-Road Emissions from Gasoline-Powered Motor Vehicles: Accounting for the Presence of Medium- and Heavy-Duty Diesel Trucks. Environ. Sci. Technol. 47, 13873–13881. https://doi.org/10.1021/es402875u

Dall'Osto, M., Ceburnis, D., Monahan, C., Worsnop, D.R., Bialek, J., Kulmala, M., Kurtén, T., Ehn, M., Wenger, J., Sodeau, J., Healy, R., O'Dowd, C., 2012. Nitrogenated and aliphatic organic vapors as possible drivers for marine secondary organic aerosol growth. Journal of Geophysical Research: Atmospheres 117. https://doi.org/10.1029/2012JD017522

Dall'Osto, M., Paglione, M., Decesari, S., Facchini, M.C., O'Dowd, C., Plass-Duellmer, C., Harrison, R.M., 2015. On the Origin of AMS "Cooking Organic Aerosol" at a Rural Site. Environ. Sci. Technol. 49, 13964–13972. https://doi.org/10.1021/acs.est.5b02922

D'Ambro, E.L., Schobesberger, S., Gaston, C.J., Lopez-Hilfiker, F.D., Lee, B.H., Liu, J., Zelenyuk, A., Bell, D., Cappa, C.D., Helgestad, T., Li, Z., Guenther, A., Wang, J., Wise, M., Caylor, R., Surratt, J.D., Riedel, T., Hyttinen, N., Salo, V.-T., Hasan, G., Kurtén, T., Shilling, J.E., Thornton, J.A., 2019. Chamber-based insights into the factors controlling epoxydiol (IEPOX) secondary organic aerosol (SOA) yield, composition, and volatility. Atmospheric Chemistry and Physics 19, 11253–11265. https://doi.org/10.5194/acp-19-11253-2019

Dat, N.-D., Chang, M.B., 2017. Review on characteristics of PAHs in atmosphere, anthropogenic sources and control technologies. Science of The Total Environment 609, 682–693. https://doi.org/10.1016/j.scitotenv.2017.07.204

Dayhuff, L.-E., Wells, M.J.M., 2005. Identification of fatty acids in fishes collected from the Ohio River using gas chromatography–mass spectrometry in chemical ionization and electron impact modes. Journal of Chromatography A 1098, 144–149. https://doi.org/10.1016/j.chroma.2005.08.049

Dėdelė, A., Miškinytė, A., 2016. Seasonal variation of indoor and outdoor air quality of nitrogen dioxide in homes with gas and electric stoves. Environ Sci Pollut Res 23, 17784–17792. https://doi.org/10.1007/s11356-016-6978-5

Dennekamp, M., Howarth, S., Dick, C. a. J., Cherrie, J.W., Donaldson, K., Seaton, A., 2001a. Ultrafine particles and nitrogen oxides generated by gas and electric cooking. Occupational and Environmental Medicine 58, 511–516. https://doi.org/10.1136/oem.58.8.511

Dennekamp, M., Howarth, S., Dick, C. a. J., Cherrie, J.W., Donaldson, K., Seaton, A., 2001b. Ultrafine particles and nitrogen oxides generated by gas and electric cooking. Occupational and Environmental Medicine 58, 511–516. https://doi.org/10.1136/oem.58.8.511

Devarakonda, S., Sevusu, P., Liu, H., Liu, R., Iftode, L., Nath, B., 2013. Real-time air quality monitoring through mobile sensing in metropolitan areas, in: Proceedings of the 2nd ACM SIGKDD International Workshop on Urban Computing, UrbComp '13. Association for Computing Machinery, New York, NY, USA, pp. 1–8. https://doi.org/10.1145/2505821.2505834

DeWitt, H.L., Hellebust, S., Temime-Roussel, B., Ravier, S., Polo, L., Jacob, V., Buisson, C., Charron, A., André, M., Pasquier, A., Besombes, J.L., Jaffrezo, J.L., Wortham, H., Marchand, N., 2015. Near-highway aerosol and gas-phase measurements in a high-diesel environment. Atmospheric Chemistry and Physics 15, 4373–4387. https://doi.org/10.5194/acp-15-4373-2015

Dimkpa, C.O., Fugice, J., Singh, U., Lewis, T.D., 2020. Development of fertilizers for enhanced nitrogen use efficiency – Trends and perspectives. Science of The Total Environment 731, 139113. https://doi.org/10.1016/j.scitotenv.2020.139113

Ditto, J.C., Abbatt, J.P.D., Chan, A.W.H., 2022. Gas- and Particle-Phase Amide Emissions from Cooking: Mechanisms and Air Quality Impacts. Environ. Sci. Technol. 56, 7741–7750. https://doi.org/10.1021/acs.est.2c01409
Ditto, J.C., Barnes, E.B., Khare, P., Takeuchi, M., Joo, T., Bui, A.A.T., Lee-Taylor, J., Eris, G., Chen, Y., Aumont, B., Jimenez, J.L., Ng, N.L., Griffin, R.J., Gentner, D.R., 2018. An omnipresent diversity and variability in the chemical composition of atmospheric functionalized organic aerosol. Commun Chem 1, 1–13. https://doi.org/10.1038/s42004-018-0074-3
Ditto, J.C., Joo, T., Slade, J.H., Shepson, P.B., Ng, N.L., Gentner, D.R., 2020. Nontargeted Tandem Mass Spectrometry Analysis Reveals Diversity and Variability in Aerosol Functional Groups across Multiple Sites, Seasons, and Times of Day. Environ. Sci. Technol. Lett. 7, 60–69. https://doi.org/10.1021/acs.estlett.9b00702
Donahue, N.M., Epstein, S.A., Pandis, S.N., Robinson, A.L., 2011. A two-dimensional volatility basis set: 1. organic-aerosol mixing thermodynamics. Atmospheric Chemistry and Physics 11, 3303–3318. https://doi.org/10.5194/acp-11-3303-2011
Donovan, M.K., Adam, T.C., Shantz, A.A., Speare, K.E., Munsterman, K.S., Rice, M.M., Schmitt, R.J., Holbrook, S.J., Burkepile, D.E., 2020. Nitrogen pollution interacts with heat stress to increase coral bleaching across the seascape. Proceedings of the National Academy of Sciences 117, 5351–5357. https://doi.org/10.1073/pnas.1915395117
Du, M., Voliotis, A., Shao, Y., Wang, Y., Bannan, T.J., Pereira, K.L., Hamilton, J.F., Percival, C.J., Alfarra, M.R., McFiggans, G., 2022. Combined application of online FIGAERO-CIMS and offline LC-Orbitrap mass spectrometry (MS) to characterize the chemical composition of secondary organic aerosol (SOA) in smog chamber studies. Atmospheric Measurement Techniques 15, 4385–4406. https://doi.org/10.5194/amt-15-4385-2022
Dührkop, K., Fleischauer, M., Ludwig, M., Aksenov, A.A., Melnik, A.V., Meusel, M., Dorrestein, P.C., Rousu, J., Böcker, S., 2019. SIRIUS 4: a rapid tool for turning tandem mass spectra into metabolite structure information. Nat Methods 16, 299–302. https://doi.org/10.1038/s41592-019-0344-8
Dührkop, K., Shen, H., Meusel, M., Rousu, J., Böcker, S., 2015. Searching molecular structure databases with tandem mass spectra using CSI:FingerID. Proceedings of the National Academy of Sciences 112, 12580–12585. https://doi.org/10.1073/pnas.1509788112
Dzepina, K., Arey, J., Marr, L.C., Worsnop, D.R., Salcedo, D., Zhang, Q., Onasch, T.B., Molina, L.T., Molina, M.J., Jimenez, J.L., 2007. Detection of particle-phase polycyclic aromatic hydrocarbons in Mexico City using an aerosol mass spectrometer. International Journal of Mass Spectrometry 263, 152–170. https://doi.org/10.1016/j.ijms.2007.01.010
Filigrana, P., Milando, C., Batterman, S., Levy, J.I., Mukherjee, B., Adar, S.D., 2020. Spatiotemporal variations in traffic activity and their influence on air pollution levels in communities near highways. Atmospheric Environment 242, 117758. https://doi.org/10.1016/j.atmosenv.2020.117758
Florou, K., Papanastasiou, D.K., Pikridas, M., Kaltsonoudis, C., Louvaris, E., Gkatzelis, G.I., Patoulias, D., Mihalopoulos, N., Pandis, S.N., 2017. The contribution of wood burning and other pollution sources to wintertime organic aerosol levels in two Greek cities. Atmospheric Chemistry and Physics 17, 3145–3163. https://doi.org/10.5194/acp-17-3145-2017
Ge, X., Setyan, A., Sun, Y., Zhang, Q., 2012. Primary and secondary organic aerosols in Fresno, California during wintertime: Results from high resolution aerosol mass spectrometry. Journal of Geophysical Research: Atmospheres 117. https://doi.org/10.1029/2012JD018026
Giorio, C., Tapparo, A., Dall'Osto, M., Harrison, R.M., Beddows, D.C.S., Di Marco, C., Nemitz, E., 2012. Comparison of three techniques for analysis of data from an Aerosol Time-of-Flight Mass Spectrometer. Atmospheric Environment 61, 316–326. https://doi.org/10.1016/j.atmosenv.2012.07.054
Graham, E.L., Wu, C., Bell, D.M., Bertrand, A., Haslett, S.L., Baltensperger, U., El Haddad, I., Krejci, R., Riipinen, I., Mohr, C., 2023. Volatility of aerosol particles from NO3 oxidation of various biogenic organic precursors. Atmospheric Chemistry and Physics 23, 7347–7362. https://doi.org/10.5194/acp-23-7347-2023

Gu, P., Li, H.Z., Ye, Q., Robinson, E.S., Apte, J.S., Robinson, A.L., Presto, A.A., 2018. Intracity Variability of Particulate Matter Exposure Is Driven by Carbonaceous Sources and Correlated with Land-Use Variables. Environ. Sci. Technol. 52, 11545–11554. https://doi.org/10.1021/acs.est.8b03833
Guo, F., Bui, A.A.T., Schulze, B.C., Dai, Q., Yoon, S., Shrestha, S., Wallace, H.W., Sanchez, N.P., Alvarez, S., Erickson, M.H., Sheesley, R.J., Usenko, S., Flynn, J., Griffin, R.J., 2024. Airmass history, night-time particulate organonitrates, and meteorology impact urban SOA formation rate. Atmospheric Environment 322, 120362. https://doi.org/10.1016/j.atmosenv.2024.120362
Guo, Y., Yan, C., Liu, Yuliang, Qiao, X., Zheng, F., Zhang, Ying, Zhou, Y., Li, C., Fan, X., Lin, Z., Feng, Z., Zhang, Yusheng, Zheng, P., Tian, L., Nie, W., Wang, Z., Huang, D., Daellenbach, K.R., Yao, L., Dada, L., Bianchi, F., Jiang, J., Liu, Yongchun, Kerminen, V.-M., Kulmala, M., 2022. Seasonal variation in oxygenated organic molecules in urban Beijing and their contribution to secondary organic aerosol. Atmospheric Chemistry and Physics 22, 10077–10097. https://doi.org/10.5194/acp-22-10077-2022
Hammes, J., Lutz, A., Mentel, T., Faxon, C., Hallquist, M., 2019. Carboxylic acids from limonene oxidation by ozone and hydroxyl radicals: insights into mechanisms derived using a FIGAERO-CIMS. Atmospheric Chemistry and Physics 19, 13037–13052. https://doi.org/10.5194/acp-19-13037-2019
Han, Y., Feng, G., Swaney, D.P., Dentener, F., Koeble, R., Ouyang, Y., Gao, W., 2020. Global and regional estimation of net anthropogenic nitrogen inputs (NANI). Geoderma 361, 114066. https://doi.org/10.1016/j.geoderma.2019.114066
Haque, M.M., Akhter, S., Biswas, J.C., Ali, E., Maniruzzaman, M., Akter, S., Solaiman, Z.M., 2023. Influence of nitrogen sources on grain yield of wheat and net global warming potential. Archives of Agronomy and Soil Science 69, 3314–3327. https://doi.org/10.1080/03650340.2023.2228714
Hartner, E., Paul, A., Käfer, U., Czech, H., Hohaus, T., Gröger, T., Sklorz, M., Jakobi, G., Orasche, J., Jeong, S., Brejcha, R., Ziehm, T., Zhang, Z.-H., Schnelle-Kreis, J., Adam, T., Rudich, Y., Kiendler-Scharr, A., Zimmermann, R., 2022. On the Complementarity and Informative Value of Different Electron Ionization Mass Spectrometric Techniques for the Chemical Analysis of Secondary Organic Aerosols. ACS Earth Space Chem. 6, 1358–1374. https://doi.org/10.1021/acsearthspacechem.2c00039
Haslett, S.L., Bell, D.M., Kumar, V., Slowik, J.G., Wang, D.S., Mishra, S., Rastogi, N., Singh, A., Ganguly, D., Thornton, J., Zheng, F., Li, Y., Nie, W., Liu, Y., Ma, W., Yan, C., Kulmala, M., Daellenbach, K.R., Hadden, D., Baltensperger, U., Prevot, A.S.H., Tripathi, S.N., Mohr, C., 2023. Nighttime NO emissions strongly suppress chlorine and nitrate radical formation during the winter in Delhi. Atmospheric Chemistry and Physics 23, 9023–9036. https://doi.org/10.5194/acp-23-9023-2023
Hayes, P.L., Ortega, A.M., Cubison, M.J., Froyd, K.D., Zhao, Y., Cliff, S.S., Hu, W.W., Toohey, D.W., Flynn, J.H., Lefer, B.L., Grossberg, N., Alvarez, S., Rappenglück, B., Taylor, J.W., Allan, J.D., Holloway, J.S., Gilman, J.B., Kuster, W.C., Gouw, J.A. de, Massoli, P., Zhang, X., Liu, J., Weber, R.J., Corrigan, A.L., Russell, L.M., Isaacman, G., Worton, D.R., Kreisberg, N.M., Goldstein, A.H., Thalman, R., Waxman, E.M., Volkamer, R., Lin, Y.H., Surratt, J.D., Kleindienst, T.E., Offenberg, J.H., Dusanter, S., Griffith, S., Stevens, P.S., Brioude, J., Angevine, W.M., Jimenez, J.L., 2013. Organic aerosol composition and sources in Pasadena, California, during the 2010 CalNex campaign. Journal of Geophysical Research: Atmospheres 118, 9233–9257. https://doi.org/10.1002/jgrd.50530
He, Y., Sun, Y., Wang, Q., Zhou, W., Xu, W., Zhang, Y., Xie, C., Zhao, J., Du, W., Qiu, Y., Lei, L., Fu, P., Wang, Z., Worsnop, D.R., 2019. A Black Carbon-Tracer Method for Estimating Cooking Organic Aerosol From Aerosol Mass Spectrometer Measurements. Geophysical Research Letters 46, 8474–8483. https://doi.org/10.1029/2019GL084092
Hearn, J.D., Smith, G.D., 2006. Reactions and mass spectra of complex particles using Aerosol CIMS. International Journal of Mass Spectrometry, Aerosols/Microparticles Special Issue 258, 95–103. https://doi.org/10.1016/j.ijms.2006.05.017
Hearn, J.D., Smith, G.D., 2004. A Chemical Ionization Mass Spectrometry Method for the Online Analysis of Organic Aerosols. Anal. Chem. 76, 2820–2826. https://doi.org/10.1021/ac049948s

Hering, S.V., Lewis, G.S., Spielman, S.R., Eiguren-Fernandez, A., 2019. A MAGIC concept for self-sustained, water-based, ultrafine particle counting. Aerosol Science and Technology 53, 63–72. https://doi.org/10.1080/02786826.2018.1538549
Herring, C.L., Faiola, C.L., Massoli, P., Sueper, D., Erickson, M.H., McDonald, J.D., Simpson, C.D., Yost, M.G., Jobson, B.T., VanReken, T.M., 2015. New Methodology for Quantifying Polycyclic Aromatic Hydrocarbons (PAHs) Using High-Resolution Aerosol Mass Spectrometry. Aerosol Science and Technology 49, 1131–1148. https://doi.org/10.1080/02786826.2015.1101050
Hu, R., Wang, S., Zheng, H., Zhao, B., Liang, C., Chang, X., Jiang, Y., Yin, R., Jiang, J., Hao, J., 2021. Variations and Sources of Organic Aerosol in Winter Beijing under Markedly Reduced Anthropogenic Activities During COVID-2019. Environ. Sci. Technol. https://doi.org/10.1021/acs.est.1c05125
Hu, W., Campuzano-Jost, P., Day, D.A., Croteau, P., Canagaratna, M.R., Jayne, J.T., Worsnop, D.R., Jimenez, J.L., 2017. Evaluation of the new capture vapourizer for aerosol mass spectrometers (AMS) through laboratory studies of inorganic species. Atmospheric Measurement Techniques 10, 2897–2921. https://doi.org/10.5194/amt-10-2897-2017
Hu, Weiwei, Hu, M., Hu, Wei, Jimenez, J.L., Yuan, B., Chen, W., Wang, M., Wu, Y., Chen, C., Wang, Z., Peng, J., Zeng, L., Shao, M., 2016a. Chemical composition, sources, and aging process of submicron aerosols in Beijing: Contrast between summer and winter. Journal of Geophysical Research: Atmospheres 121, 1955–1977. https://doi.org/10.1002/2015JD024020
Hu, Weiwei, Hu, M., Hu, Wei, Jimenez, J.L., Yuan, B., Chen, W., Wang, M., Wu, Y., Chen, C., Wang, Z., Peng, J., Zeng, L., Shao, M., 2016b. Chemical composition, sources, and aging process of submicron aerosols in Beijing: Contrast between summer and winter. Journal of Geophysical Research: Atmospheres 121, 1955–1977. https://doi.org/10.1002/2015JD024020
Huang, D.D., Zhu, S., An, J., Wang, Q., Qiao, L., Zhou, M., He, X., Ma, Y., Sun, Y., Huang, C., Yu, J.Z., Zhang, Q., 2021a. Comparative Assessment of Cooking Emission Contributions to Urban Organic Aerosol Using Online Molecular Tracers and Aerosol Mass Spectrometry Measurements. Environ. Sci. Technol. 55, 14526–14535. https://doi.org/10.1021/acs.est.1c03280
Huang, D.D., Zhu, S., An, J., Wang, Q., Qiao, L., Zhou, M., He, X., Ma, Y., Sun, Y., Huang, C., Yu, J.Z., Zhang, Q., 2021b. Comparative Assessment of Cooking Emission Contributions to Urban Organic Aerosol Using Online Molecular Tracers and Aerosol Mass Spectrometry Measurements. Environ. Sci. Technol. 55, 14526–14535. https://doi.org/10.1021/acs.est.1c03280
Huang, W., Saathoff, H., Shen, X., Ramisetty, R., Leisner, T., Mohr, C., 2019. Seasonal characteristics of organic aerosol chemical composition and volatility in Stuttgart, Germany. Atmospheric Chemistry and Physics 19, 11687–11700. https://doi.org/10.5194/acp-19-11687-2019
Huang, W., Wu, C., Gao, L., Gramlich, Y., Haslett, S.L., Thornton, J., Lopez-Hilfiker, F.D., Lee, B.H., Song, J., Saathoff, H., Shen, X., Ramisetty, R., Tripathi, S.N., Ganguly, D., Jiang, F., Vallon, M., Schobesberger, S., Yli-Juuti, T., Mohr, C., 2024. Variation in chemical composition and volatility of oxygenated organic aerosol in different rural, urban, and mountain environments. Atmospheric Chemistry and Physics 24, 2607–2624. https://doi.org/10.5194/acp-24-2607-2024
Huang, X.-F., He, L.-Y., Hu, M., Canagaratna, M.R., Sun, Y., Zhang, Q., Zhu, T., Xue, L., Zeng, L.-W., Liu, X.-G., Zhang, Y.-H., Jayne, J.T., Ng, N.L., Worsnop, D.R., 2010. Highly time-resolved chemical characterization of atmospheric submicron particles during 2008 Beijing Olympic Games using an Aerodyne High-Resolution Aerosol Mass Spectrometer. Atmospheric Chemistry and Physics 10, 8933–8945. https://doi.org/10.5194/acp-10-8933-2010
Humes, M.B., Machesky, J.E., Kim, S., Oladeji, O.J., Gentner, D.R., Donahue, N.M., Presto, A.A., 2023. Primary and Secondary Organic Aerosol Formation from Asphalt Pavements. Environ. Sci. Technol. 57, 20034–20042. https://doi.org/10.1021/acs.est.3c06037
in ’t Veld, M., Khare, P., Hao, Y., Reche, C., Pérez, N., Alastuey, A., Yus-Díez, J., Marchand, N., Prevot, A.S.H., Querol, X., Daellenbach, K.R., 2023. Characterizing the sources of ambient PM10 organic aerosol in urban and rural Catalonia, Spain. Science of The Total Environment 902, 166440. https://doi.org/10.1016/j.scitotenv.2023.166440

Isaacman-VanWertz, G., Massoli, P., E. O'Brien, R., B. Nowak, J., R. Canagaratna, M., T. Jayne, J., R. Worsnop, D., Su, L., A. Knopf, D., K. Misztal, P., Arata, C., H. Goldstein, A., H. Kroll, J., 2017. Using advanced mass spectrometry techniques to fully characterize atmospheric organic carbon: current capabilities and remaining gaps. Faraday Discussions 200, 579–598. https://doi.org/10.1039/C7FD00021A
Iyer, S., Lopez-Hilfiker, F., Lee, B.H., Thornton, J.A., Kurtén, T., 2016. Modeling the Detection of Organic and Inorganic Compounds Using Iodide-Based Chemical Ionization. J. Phys. Chem. A 120, 576–587. https://doi.org/10.1021/acs.jpca.5b09837
Jaeger, H., Janositz, A., Knorr, D., 2010. The Maillard reaction and its control during food processing. The potential of emerging technologies. Pathologie Biologie, Vieillissement 58, 207–213. https://doi.org/10.1016/j.patbio.2009.09.016
Jeong, C.-H., Hilker, N., Wang, J.M., Debosz, J., Healy, R.M., Sofowote, U., Munoz, T., Herod, D., Evans, G.J., 2022. Characterization of winter air pollutant gradients near a major highway. Science of The Total Environment 849, 157818. https://doi.org/10.1016/j.scitotenv.2022.157818
Jeong, C.-H., Wang, J.M., Evans, G.J., 2016a. Source Apportionment of Urban Particulate Matter using Hourly Resolved Trace Metals, Organics, and Inorganic Aerosol Components. Atmospheric Chemistry and Physics Discussions 1–32. https://doi.org/10.5194/acp-2016-189
Jeong, C.-H., Wang, J.M., Evans, G.J., 2016b. Source Apportionment of Urban Particulate Matter using Hourly Resolved Trace Metals, Organics, and Inorganic Aerosol Components. Atmospheric Chemistry and Physics Discussions 1–32. https://doi.org/10.5194/acp-2016-189
Jiang, L., Kiselova, N., Rosén, J., Ilag, L.L., 2014. Quantification of neurotoxin BMAA (β-N-methylamino-L-alanine) in seafood from Swedish markets. Sci Rep 4, 6931. https://doi.org/10.1038/srep06931
Jiang, L., Xia, Y., Wang, Lu, Chen, X., Ye, J., Hou, T., Wang, Liqiang, Zhang, Y., Li, M., Li, Z., Song, Z., Jiang, Y., Liu, W., Li, P., Rosenfeld, D., Seinfeld, J.H., Yu, S., 2021. Hyperfine-resolution mapping of on-road vehicle emissions with comprehensive traffic monitoring and an intelligent transportation system. Atmospheric Chemistry and Physics 21, 16985–17002. https://doi.org/10.5194/acp-21-16985-2021
Jimenez, J.L., Canagaratna, M.R., Donahue, N.M., Prevot, A.S.H., Zhang, Q., Kroll, J.H., DeCarlo, P.F., Allan, J.D., Coe, H., Ng, N.L., Aiken, A.C., Docherty, K.S., Ulbrich, I.M., Grieshop, A.P., Robinson, A.L., Duplissy, J., Smith, J.D., Wilson, K.R., Lanz, V.A., Hueglin, C., Sun, Y.L., Tian, J., Laaksonen, A., Raatikainen, T., Rautiainen, J., Vaattovaara, P., Ehn, M., Kulmala, M., Tomlinson, J.M., Collins, D.R., Cubison, M.J., E., Dunlea, J., Huffman, J.A., Onasch, T.B., Alfarra, M.R., Williams, P.I., Bower, K., Kondo, Y., Schneider, J., Drewnick, F., Borrmann, S., Weimer, S., Demerjian, K., Salcedo, D., Cottrell, L., Griffin, R., Takami, A., Miyoshi, T., Hatakeyama, S., Shimono, A., Sun, J.Y., Zhang, Y.M., Dzepina, K., Kimmel, J.R., Sueper, D., Jayne, J.T., Herndon, S.C., Trimborn, A.M., Williams, L.R., Wood, E.C., Middlebrook, A.M., Kolb, C.E., Baltensperger, U., Worsnop, D.R., 2009. Evolution of Organic Aerosols in the Atmosphere. Science 326, 1525–1529. https://doi.org/10.1126/science.1180353
Jimenez, J.L., Jayne, J.T., Shi, Q., Kolb, C.E., Worsnop, D.R., Yourshaw, I., Seinfeld, J.H., Flagan, R.C., Zhang, X., Smith, K.A., Morris, J.W., Davidovits, P., 2003. Ambient aerosol sampling using the Aerodyne Aerosol Mass Spectrometer. Journal of Geophysical Research: Atmospheres 108. https://doi.org/10.1029/2001JD001213
Jin, D., Ma, J., Li, Y., Jiao, G., Liu, K., Sun, S., Zhou, J., Sun, R., 2022. Development of the synthesis and applications of xylonic acid: A mini-review. Fuel 314, 122773. https://doi.org/10.1016/j.fuel.2021.122773
J. Schwartz, T., Heiningen, A.R.P. van, Clayton Wheeler, M., 2010. Energy densification of levulinic acid by thermal deoxygenation. Green Chemistry 12, 1353–1356. https://doi.org/10.1039/C005067A
Jung, C.-C., Su, H.-J., 2020. Chemical and stable isotopic characteristics of PM2.5 emitted from Chinese cooking. Environmental Pollution 267, 115577. https://doi.org/10.1016/j.envpol.2020.115577
Kaltsonoudis, C., Kostenidou, E., Louvaris, E., Psichoudaki, M., Tsiligiannis, E., Florou, K., Liangou, A., Pandis, S.N., 2017a. Characterization of fresh and aged organic aerosol emissions from meat charbroiling. Atmospheric Chemistry and Physics 17, 7143–7155. https://doi.org/10.5194/acp-17-7143-2017

Kaltsonoudis, C., Kostenidou, E., Louvaris, E., Psichoudaki, M., Tsiligiannis, E., Florou, K., Liangou, A., Pandis, S.N., 2017b. Characterization of fresh and aged organic aerosol emissions from meat charbroiling. Atmos. Chem. Phys. 17, 7143–7155. https://doi.org/10.5194/acp-17-7143-2017
Kang, S., Fu, J., Zhang, G., 2018. From lignocellulosic biomass to levulinic acid: A review on acid-catalyzed hydrolysis. Renewable and Sustainable Energy Reviews 94, 340–362. https://doi.org/10.1016/j.rser.2018.06.016
Karwowska, M., Kononiuk, A., 2020. Nitrates/Nitrites in Food—Risk for Nitrosative Stress and Benefits. Antioxidants 9, 241. https://doi.org/10.3390/antiox9030241
Katz, E.F., Guo, H., Campuzano-Jost, P., Day, D.A., Brown, W.L., Boedicker, E., Pothier, M., Lunderberg, D.M., Patel, S., Patel, K., Hayes, P.L., Avery, A., Hildebrandt Ruiz, L., Goldstein, A.H., Vance, M.E., Farmer, D.K., Jimenez, J.L., DeCarlo, P.F., 2021. Quantification of cooking organic aerosol in the indoor environment using aerodyne aerosol mass spectrometers. Aerosol Science and Technology 55, 1099–1114. https://doi.org/10.1080/02786826.2021.1931013
Keithly, L., Wayne, G.F., Cullen, D.M., Connolly, G.N., 2005. Industry Research on the Use and Effects of Levulinic Acid: A Case Study in Cigarette Additives. Nicotine & Tobacco Research 7, 761–771. https://doi.org/10.1080/14622200500259820
Kessi-Pérez, E.I., Molinet, J., Martínez, C., 2020. Disentangling the genetic bases of Saccharomyces cerevisiae nitrogen consumption and adaptation to low nitrogen environments in wine fermentation. Biol Res 53, 2. https://doi.org/10.1186/s40659-019-0270-3
Khare, P., Machesky, J., Soto, R., He, M., Presto, A.A., Gentner, D.R., 2020. Asphalt-related emissions are a major missing nontraditional source of secondary organic aerosol precursors. Science Advances 6, eabb9785. https://doi.org/10.1126/sciadv.abb9785

Kicińska, A., Dmytrowski, P., 2023. Anthropogenic impact on soils of protected areas—example of PAHs. Sci Rep 13, 1524. https://doi.org/10.1038/s41598-023-28726-6
Kiendler-Scharr, A., Zhang, Q., Hohaus, T., Kleist, E., Mensah, A., Mentel, T.F., Spindler, C., Uerlings, R., Tillmann, R., Wildt, J., 2009. Aerosol Mass Spectrometric Features of Biogenic SOA: Observations from a Plant Chamber and in Rural Atmospheric Environments. Environ. Sci. Technol. 43, 8166–8172. https://doi.org/10.1021/es901420b
Kim, S., Machesky, J., Gentner, D.R., Presto, A.A., 2024. Real-world observations of reduced nitrogen and ultrafine particles in commercial cooking organic aerosol emissions. Atmospheric Chemistry and Physics 24, 1281–1298. https://doi.org/10.5194/acp-24-1281-2024
Klein, F., Baltensperger, U., Prévôt, A.S.H., El Haddad, I., 2019. Quantification of the impact of cooking processes on indoor concentrations of volatile organic species and primary and secondary organic aerosols. Indoor Air 29, 926–942. https://doi.org/10.1111/ina.12597
Klompmaker, J.O., Montagne, D.R., Meliefste, K., Hoek, G., Brunekreef, B., 2015. Spatial variation of ultrafine particles and black carbon in two cities: Results from a short-term measurement campaign. Science of The Total Environment 508, 266–275. https://doi.org/10.1016/j.scitotenv.2014.11.088
Kostenidou, E., Lee, B.-H., Engelhart, G.J., Pierce, J.R., Pandis, S.N., 2009. Mass Spectra Deconvolution of Low, Medium, and High Volatility Biogenic Secondary Organic Aerosol. Environ. Sci. Technol. 43, 4884–4889. https://doi.org/10.1021/es803676g
Kralik, G., Sak-Bosnar, M., Kralik, Z., Galović, O., Grčević, M., Kralik, I., 2015. EFFECT OF B-ALANINE AND L-HISTIDINE ON CONCENTRATION OF CARNOSINE IN MUSCLE TISSUE AND OXIDATIVE STABILITY OF CHICKEN MEAT. Poljoprivreda 21, 190–194. https://doi.org/10.18047/poljo.21.1.sup.45
Kroll, J.H., Seinfeld, J.H., 2008. Chemistry of secondary organic aerosol: Formation and evolution of low-volatility organics in the atmosphere. Atmospheric Environment 42, 3593–3624. https://doi.org/10.1016/j.atmosenv.2008.01.003
Kumar, L.R., Yellapu, S.K., Tyagi, R.D., Zhang, X., 2019. A review on variation in crude glycerol composition, bio-valorization of crude and purified glycerol as carbon source for lipid production. Bioresource Technology 293, 122155. https://doi.org/10.1016/j.biortech.2019.122155

Ladha, J.K., Pathak, H., J. Krupnik, T., Six, J., van Kessel, C., 2005. Efficiency of Fertilizer Nitrogen in Cereal Production: Retrospects and Prospects, in: Advances in Agronomy. Academic Press, pp. 85–156. https://doi.org/10.1016/S0065-2113(05)87003-8
Lalchandani, V., Kumar, V., Tobler, A., M. Thamban, N., Mishra, S., Slowik, J.G., Bhattu, D., Rai, P., Satish, R., Ganguly, D., Tiwari, Suresh, Rastogi, N., Tiwari, Shashi, Močnik, G., Prévôt, A.S.H., Tripathi, S.N., 2021. Real-time characterization and source apportionment of fine particulate matter in the Delhi megacity area during late winter. Science of The Total Environment 770, 145324. https://doi.org/10.1016/j.scitotenv.2021.145324
Lanz, V.A., Alfarra, M.R., Baltensperger, U., Buchmann, B., Hueglin, C., Prévôt, A.S.H., 2007. Source apportionment of submicron organic aerosols at an urban site by factor analytical modelling of aerosol mass spectra. Atmospheric Chemistry and Physics 7, 1503–1522. https://doi.org/10.5194/acp-7-1503-2007
Larrea-Wachtendorff, D., Di Nobile, G., Ferrari, G., 2020. Effects of processing conditions and glycerol concentration on rheological and texture properties of starch-based hydrogels produced by high pressure processing (HPP). International Journal of Biological Macromolecules 159, 590–597. https://doi.org/10.1016/j.ijbiomac.2020.05.120
Laurenza, A.G., Losito, O., Casiello, M., Fusco, C., Nacci, A., Pantone, V., D'Accolti, L., 2021. Valorization of cigarette butts for synthesis of levulinic acid as top value-added chemicals. Sci Rep 11, 15775. https://doi.org/10.1038/s41598-021-95361-4
Lc, M., 1912. Action des acides amines sur les sucres : formation des melanoidines par voie methodique. C. R. Seances Soc. Biol Fil. 154, 66–68.
Lee, B.H., Lopez-Hilfiker, F.D., Mohr, C., Kurtén, T., Worsnop, D.R., Thornton, J.A., 2014. An Iodide-Adduct High-Resolution Time-of-Flight Chemical-Ionization Mass Spectrometer: Application to Atmospheric Inorganic and Organic Compounds. Environ. Sci. Technol. 48, 6309–6317. https://doi.org/10.1021/es500362a
Lee, B.P., Li, Y.J., Yu, J.Z., Louie, P.K.K., Chan, C.K., 2015. Characteristics of submicron particulate matter at the urban roadside in downtown Hong Kong—Overview of 4 months of continuous high-resolution aerosol mass spectrometer measurements. Journal of Geophysical Research: Atmospheres 120, 7040–7058. https://doi.org/10.1002/2015JD023311
Lee, B.P., Li, Y.J., Yu, J.Z., Louie, P.K.K., Chan, C.K., 2013. Physical and chemical characterization of ambient aerosol by HR-ToF-AMS at a suburban site in Hong Kong during springtime 2011. Journal of Geophysical Research: Atmospheres 118, 8625–8639. https://doi.org/10.1002/jgrd.50658
Lee, B.P., Louie, P.K.K., Luk, C., Chan, C.K., 2017. Evaluation of traffic exhaust contributions to ambient carbonaceous submicron particulate matter in an urban roadside environment in Hong Kong. Atmospheric Chemistry and Physics 17, 15121–15135. https://doi.org/10.5194/acp-17-15121-2017
Lee, C.C., Kibblewhite, R.E., Paavola, C.D., Orts, W.J., Wagschal, K., 2017. Production of D-Xylonic Acid from Hemicellulose Using Artificial Enzyme Complexes. Journal of Microbiology and Biotechnology 27, 77–83. https://doi.org/10.4014/jmb.1606.06041
Lekshmi Sundar, M.S., Madhavan Nampoothiri, K., 2022. An overview of the metabolically engineered strains and innovative processes used for the value addition of biomass derived xylose to xylitol and xylonic acid. Bioresource Technology 345, 126548. https://doi.org/10.1016/j.biortech.2021.126548
Lenschow, P., Abraham, H.-J., Kutzner, K., Lutz, M., Preuß, J.-D., Reichenbächer, W., 2001. Some ideas about the sources of PM10. Atmospheric Environment, Selected Papers Presented at the Venice Conference 35, S23–S33. https://doi.org/10.1016/S1352-2310(01)00122-4
Li, Y., Pöschl, U., Shiraiwa, M., 2016. Molecular corridors and parameterizations of volatility in the chemical evolution of organic aerosols. Atmospheric Chemistry and Physics 16, 3327–3344. https://doi.org/10.5194/acp-16-3327-2016
Li, Y.J., Lee, B.P., Su, L., Fung, J.C.H., Chan, C.K., 2015. Seasonal characteristics of fine particulate matter (PM) based on high-resolution time-of-flight aerosol mass spectrometric (HR-ToF-AMS) measurements at the HKUST Supersite in Hong Kong. Atmospheric Chemistry and Physics 15, 37–53. https://doi.org/10.5194/acp-15-37-2015

Liu, N., Jiang, J., 2020. Valorisation of food waste using salt to alleviate inhibition by animal fats and vegetable oils during anaerobic digestion. Biomass and Bioenergy 143, 105826. https://doi.org/10.1016/j.biombioe.2020.105826
Liu, T., Li, Z., Chan, M., Chan, C.K., 2017. Formation of secondary organic aerosols from gas-phase emissions of heated cooking oils. Atmospheric Chemistry and Physics 17, 7333–7344. https://doi.org/10.5194/acp-17-7333-2017
Liu, T., Wang, Z., Wang, X., Chan, C.K., 2018. Primary and secondary organic aerosol from heated cooking oil emissions. Atmospheric Chemistry and Physics 18, 11363–11374. https://doi.org/10.5194/acp-18-11363-2018
Liu, X., Hu, B., Chu, C., 2022. Nitrogen assimilation in plants: current status and future prospects. Journal of Genetics and Genomics, Special Issue on Rice Biology 49, 394–404. https://doi.org/10.1016/j.jgg.2021.12.006
Lopez-Hilfiker, F.D., Mohr, C., D'Ambro, E.L., Lutz, A., Riedel, T.P., Gaston, C.J., Iyer, S., Zhang, Z., Gold, A., Surratt, J.D., Lee, B.H., Kurten, T., Hu, W.W., Jimenez, J., Hallquist, M., Thornton, J.A., 2016. Molecular Composition and Volatility of Organic Aerosol in the Southeastern U.S.: Implications for IEPOX Derived SOA. Environ. Sci. Technol. 50, 2200–2209. https://doi.org/10.1021/acs.est.5b04769
Lopez-Hilfiker, F.D., Mohr, C., Ehn, M., Rubach, F., Kleist, E., Wildt, J., Mentel, T.F., Lutz, A., Hallquist, M., Worsnop, D., Thornton, J.A., 2014. A novel method for online analysis of gas and particle composition: description and evaluation of a Filter Inlet for Gases and AEROsols (FIGAERO). Atmospheric Measurement Techniques 7, 983–1001. https://doi.org/10.5194/amt-7-983-2014
Louie, P.K.K., Chow, J.C., Chen, L.-W.A., Watson, J.G., Leung, G., Sin, D.W.M., 2005. PM2.5 chemical composition in Hong Kong: urban and regional variations. Science of The Total Environment 338, 267–281. https://doi.org/10.1016/j.scitotenv.2004.07.021
Louvaris, E.E., Karnezi, E., Kostenidou, E., Kaltsonoudis, C., Pandis, S.N., 2017. Estimation of the volatility distribution of organic aerosol combining thermodenuder and isothermal dilution measurements. Atmospheric Measurement Techniques 10, 3909–3918. https://doi.org/10.5194/amt-10-3909-2017
Lyu, X., Huo, Y., Yang, J., Yao, D., Li, K., Lu, H., Zeren, Y., Guo, H., 2021. Real-time molecular characterization of air pollutants in a Hong Kong residence: Implication of indoor source emissions and heterogeneous chemistry. Indoor Air 31, 1340–1352. https://doi.org/10.1111/ina.12826
Manousakas, M.I., Florou, K., Pandis, S.N., 2020. Source Apportionment of Fine Organic and Inorganic Atmospheric Aerosol in an Urban Background Area in Greece. Atmosphere 11, 330. https://doi.org/10.3390/atmos11040330
Marcinkowska, M.A., Jeleń, H.H., 2022. Role of Sulfur Compounds in Vegetable and Mushroom Aroma. Molecules 27, 6116. https://doi.org/10.3390/molecules27186116
Marcy, T.P., Gao, R.S., Northway, M.J., Popp, P.J., Stark, H., Fahey, D.W., 2005. Using chemical ionization mass spectrometry for detection of HNO3, HCl, and ClONO2 in the atmosphere. International Journal of Mass Spectrometry 243, 63–70. https://doi.org/10.1016/j.ijms.2004.11.012
Marjanen, P., Kuittinen, N., Karjalainen, P., Saarikoski, S., Westerholm, M., Pettinen, R., Aurela, M., Lintusaari, H., Simonen, P., Markkula, L., Kalliokoski, J., Wihersaari, H., Timonen, H., Rönkkö, T., 2022. Exhaust emissions from a prototype non-road natural gas engine. Fuel 316, 123387. https://doi.org/10.1016/j.fuel.2022.123387
Martínez, M., Fuentes, M., Franco, N., Sánchez, J., de Miguel, C., 2014. Fatty Acid Profiles of Virgin Olive Oils from the Five Olive-Growing Zones of Extremadura (Spain). J Am Oil Chem Soc 91, 1921–1929. https://doi.org/10.1007/s11746-014-2528-9
Masoud, C.G., Li, Y., Wang, D.S., Katz, E.F., DeCarlo, P.F., Farmer, D.K., Vance, M.E., Shiraiwa, M., Hildebrandt Ruiz, L., 2022a. Molecular composition and gas-particle partitioning of indoor cooking aerosol: Insights from a FIGAERO-CIMS and kinetic aerosol modeling. Aerosol Science and Technology 0, 1–18. https://doi.org/10.1080/02786826.2022.2133593
Masoud, C.G., Li, Y., Wang, D.S., Katz, E.F., DeCarlo, P.F., Farmer, D.K., Vance, M.E., Shiraiwa, M., Hildebrandt Ruiz, L., 2022b. Molecular composition and gas-particle partitioning of indoor cooking

aerosol: Insights from a FIGAERO-CIMS and kinetic aerosol modeling. Aerosol Science and Technology 56, 1156–1173. https://doi.org/10.1080/02786826.2022.2133593
Masoud, C.G., Ruiz, L.H., 2021. Chlorine-Initiated Oxidation of α-Pinene: Formation of Secondary Organic Aerosol and Highly Oxygenated Organic Molecules. ACS Earth Space Chem. 5, 2307–2319. https://doi.org/10.1021/acsearthspacechem.1c00150
May, A.A., Presto, A.A., Hennigan, C.J., Nguyen, N.T., Gordon, T.D., Robinson, A.L., 2013. Gas-particle partitioning of primary organic aerosol emissions: (1) Gasoline vehicle exhaust. Atmospheric Environment 77, 128–139. https://doi.org/10.1016/j.atmosenv.2013.04.060
McDonald, B.C., de Gouw, J.A., Gilman, J.B., Jathar, S.H., Akherati, A., Cappa, C.D., Jimenez, J.L., Lee-Taylor, J., Hayes, P.L., McKeen, S.A., Cui, Y.Y., Kim, S.-W., Gentner, D.R., Isaacman-VanWertz, G., Goldstein, A.H., Harley, R.A., Frost, G.J., Roberts, J.M., Ryerson, T.B., Trainer, M., 2018. Volatile chemical products emerging as largest petrochemical source of urban organic emissions. Science 359, 760–764. https://doi.org/10.1126/science.aaq0524
Mehra, A., Canagaratna, M., Bannan, T.J., Worrall, S.D., Bacak, A., Priestley, M., Liu, D., Zhao, J., Xu, W., Sun, Y., Hamilton, J.F., Squires, F.A., Lee, J., Bryant, D.J., Hopkins, J.R., Elzein, A., Budisulistiorini, S.H., Cheng, X., Chen, Q., Wang, Y., Wang, L., Stark, H., Krechmer, J.E., Brean, J., Slater, E., Whalley, L., Heard, D., Ouyang, B., Acton, W.J.F., Hewitt, C.N., Wang, X., Fu, P., Jayne, J., Worsnop, D., Allan, J., Percival, C., Coe, H., 2021. Using highly time-resolved online mass spectrometry to examine biogenic and anthropogenic contributions to organic aerosol in Beijing. Faraday Discuss. 226, 382–408. https://doi.org/10.1039/D0FD00080A
Milic, A., Miljevic, B., Alroe, J., Mallet, M., Canonaco, F., Prevot, A.S.H., Ristovski, Z.D., 2016. The ambient aerosol characterization during the prescribed bushfire season in Brisbane 2013. Science of The Total Environment 560–561, 225–232. https://doi.org/10.1016/j.scitotenv.2016.04.036
Mohr, C., DeCarlo, P.F., Heringa, M.F., Chirico, R., Slowik, J.G., Richter, R., Reche, C., Alastuey, A., Querol, X., Seco, R., Peñuelas, J., Jiménez, J.L., Crippa, M., Zimmermann, R., Baltensperger, U., Prévôt, A.S.H., 2012. Identification and quantification of organic aerosol from cooking and other sources in Barcelona using aerosol mass spectrometer data. Atmospheric Chemistry and Physics 12, 1649–1665. https://doi.org/10.5194/acp-12-1649-2012
Mohr, C., Huffman, J.A., Cubison, M.J., Aiken, A.C., Docherty, K.S., Kimmel, J.R., Ulbrich, I.M., Hannigan, M., Jimenez, J.L., 2009. Characterization of Primary Organic Aerosol Emissions from Meat Cooking, Trash Burning, and Motor Vehicles with High-Resolution Aerosol Mass Spectrometry and Comparison with Ambient and Chamber Observations. Environ. Sci. Technol. 43, 2443–2449. https://doi.org/10.1021/es8011518
Mohr, C., Richter, R., DeCarlo, P.F., Prévôt, A.S.H., Baltensperger, U., 2011. Spatial variation of chemical composition and sources of submicron aerosol in Zurich during wintertime using mobile aerosol mass spectrometer data. Atmospheric Chemistry and Physics 11, 7465–7482. https://doi.org/10.5194/acp-11-7465-2011
Mohr, C., Thornton, J.A., Heitto, A., Lopez-Hilfiker, F.D., Lutz, A., Riipinen, I., Hong, J., Donahue, N.M., Hallquist, M., Petäjä, T., Kulmala, M., Yli-Juuti, T., 2019. Molecular identification of organic vapors driving atmospheric nanoparticle growth. Nat Commun 10, 4442. https://doi.org/10.1038/s41467-019-12473-2
Monfreda, M., Gobbi, L., Grippa, A., 2014. Blends of olive oil and seeds oils: Characterisation and olive oil quantification using fatty acids composition and chemometric tools. Part II. Food Chemistry 145, 584–592. https://doi.org/10.1016/j.foodchem.2013.07.141
Moutinho, J.L., Liang, D., Golan, R., Sarnat, S.E., Weber, R., Sarnat, J.A., Russell, A.G., 2020. Near-road vehicle emissions air quality monitoring for exposure modeling. Atmospheric Environment 224, 117318. https://doi.org/10.1016/j.atmosenv.2020.117318

Murphy, B.N., Donahue, N.M., Fountoukis, C., Pandis, S.N., 2011. Simulating the oxygen content of ambient organic aerosol with the 2D volatility basis set. Atmospheric Chemistry and Physics 11, 7859–7873. https://doi.org/10.5194/acp-11-7859-2011

Ng, N.L., Canagaratna, M.R., Zhang, Q., Jimenez, J.L., Tian, J., Ulbrich, I.M., Kroll, J.H., Docherty, K.S., Chhabra, P.S., Bahreini, R., Murphy, S.M., Seinfeld, J.H., Hildebrandt, L., Donahue, N.M., DeCarlo, P.F., Lanz, V.A., Prévôt, A.S.H., Dinar, E., Rudich, Y., Worsnop, D.R., 2010. Organic aerosol components observed in Northern Hemispheric datasets from Aerosol Mass Spectrometry. Atmospheric Chemistry and Physics 10, 4625–4641. https://doi.org/10.5194/acp-10-4625-2010
Niu, S., Liu, R., Zhao, Q., Gagan, S., Dodero, A., Ying, Q., Ma, X., Cheng, Z., China, S., Canagaratna, M., Zhang, Y., 2024. Quantifying the Chemical Composition and Real-Time Mass Loading of Nanoplastic Particles in the Atmosphere Using Aerosol Mass Spectrometry. Environ. Sci. Technol. 58, 3363–3374. https://doi.org/10.1021/acs.est.3c10286
Northway, M.J., Jayne, J.T., Toohey, D.W., Canagaratna, M.R., Trimborn, A., Akiyama, K.I., Shimono, A., Jimenez, J.L., DeCarlo, P.F., Wilson, K.R., Worsnop, D.R., 2007. Demonstration of a VUV Lamp Photoionization Source for Improved Organic Speciation in an Aerosol Mass Spectrometer. Aerosol Science and Technology 41, 828–839. https://doi.org/10.1080/02786820701496587
N. Pandis, S., Skyllakou, K., Florou, K., Kostenidou, E., Kaltsonoudis, C., Hasa, E., A. Presto, A., 2016. Urban particulate matter pollution: a tale of five cities. Faraday Discussions 189, 277–290. https://doi.org/10.1039/C5FD00212E
Ochieng', I.O., Gitari, H.I., Mochoge, B., Rezaei-Chiyaneh, E., Gweyi-Onyango, J.P., 2021. Optimizing Maize Yield, Nitrogen Efficacy and Grain Protein Content under Different N Forms and Rates. J Soil Sci Plant Nutr 21, 1867–1880. https://doi.org/10.1007/s42729-021-00486-0
Omelekhina, Y., Eriksson, A., Canonaco, F., H. Prevot, A.S., Nilsson, P., Isaxon, C., Pagels, J., Wierzbicka, A., 2020. Cooking and electronic cigarettes leading to large differences between indoor and outdoor particle composition and concentration measured by aerosol mass spectrometry. Environmental Science: Processes & Impacts 22, 1382–1396. https://doi.org/10.1039/D0EM00061B
Paulin, L.M., Diette, G.B., Scott, M., McCormack, M.C., Matsui, E.C., Curtin-Brosnan, J., Williams, D.L., Kidd-Taylor, A., Shea, M., Breysse, P.N., Hansel, N.N., 2014. Home interventions are effective at decreasing indoor nitrogen dioxide concentrations. Indoor Air 24, 416–424. https://doi.org/10.1111/ina.12085
Peräkylä, O., Riva, M., Heikkinen, L., Quéléver, L., Roldin, P., Ehn, M., 2020. Experimental investigation into the volatilities of highly oxygenated organic molecules (HOMs). Atmospheric Chemistry and Physics 20, 649–669. https://doi.org/10.5194/acp-20-649-2020
Pileidis, F.D., Titirici, M.-M., 2016. Corrigendum: Levulinic Acid Biorefineries: New Challenges for Efficient Utilization of Biomass. ChemSusChem 9, 652–655. https://doi.org/10.1002/cssc.201600272
Pye, H.O.T., Pouliot, G.A., 2012. Modeling the Role of Alkanes, Polycyclic Aromatic Hydrocarbons, and Their Oligomers in Secondary Organic Aerosol Formation. Environ. Sci. Technol. 46, 6041–6047. https://doi.org/10.1021/es300409w
Raatikainen, T., Vaattovaara, P., Tiitta, P., Miettinen, P., Rautiainen, J., Ehn, M., Kulmala, M., Laaksonen, A., Worsnop, D.R., 2010. Physicochemical properties and origin of organic groups detected in boreal forest using an aerosol mass spectrometer. Atmospheric Chemistry and Physics 10, 2063–2077. https://doi.org/10.5194/acp-10-2063-2010
Räty, M., Peräkylä, O., Riva, M., Quéléver, L., Garmash, O., Rissanen, M., Ehn, M., 2021. Measurement report: Effects of NOx and seed aerosol on highly oxygenated organic molecules (HOMs) from cyclohexene ozonolysis. Atmospheric Chemistry and Physics 21, 7357–7372. https://doi.org/10.5194/acp-21-7357-2021
Reitze, A.W.Jr., 1999. The Legislative History of U.S. Air Pollution Control. Hous. L. Rev. 36, 679–742.
Renzi, M., Marchetti, S., de' Donato, F., Pappagallo, M., Scortichini, M., Davoli, M., Frova, L., Michelozzi, P., Stafoggia, M., 2021. Acute Effects of Particulate Matter on All-Cause Mortality in Urban, Rural, and Suburban Areas, Italy. International Journal of Environmental Research and Public Health 18, 12895. https://doi.org/10.3390/ijerph182412895
Reyes-Villegas, E., Bannan, T., Le Breton, M., Mehra, A., Priestley, M., Percival, C., Coe, H., Allan, J.D., 2018a. Online Chemical Characterization of Food-Cooking Organic Aerosols: Implications for Source Apportionment. Environ. Sci. Technol. 52, 5308–5318. https://doi.org/10.1021/acs.est.7b06278

Reyes-Villegas, E., Bannan, T., Le Breton, M., Mehra, A., Priestley, M., Percival, C., Coe, H., Allan, J.D., 2018b. Online Chemical Characterization of Food-Cooking Organic Aerosols: Implications for Source Apportionment. Environ. Sci. Technol. 52, 5308–5318. https://doi.org/10.1021/acs.est.7b06278
Rissanen, M.P., Mikkilä, J., Iyer, S., Hakala, J., 2019. Multi-scheme chemical ionization inlet (MION) for fast switching of reagent ion chemistry in atmospheric pressure chemical ionization mass spectrometry (CIMS) applications. Atmospheric Measurement Techniques 12, 6635–6646. https://doi.org/10.5194/amt-12-6635-2019
Rivellini, L.-H., Adam, M.G., Kasthuriarachchi, N., Lee, A.K.Y., 2020. Characterization of carbonaceous aerosols in Singapore: insight from black carbon fragments and trace metal ions detected by a soot particle aerosol mass spectrometer. Atmospheric Chemistry and Physics 20, 5977–5993. https://doi.org/10.5194/acp-20-5977-2020
Robinson, A.L., Subramanian, R., Donahue, N.M., Bernardo-Bricker, A., Rogge, W.F., 2006. Source Apportionment of Molecular Markers and Organic Aerosol. 3. Food Cooking Emissions. Environ. Sci. Technol. 40, 7820–7827. https://doi.org/10.1021/es060781p
Rocchetti, G., Miragoli, F., Zacconi, C., Lucini, L., Rebecchi, A., 2019. Impact of cooking and fermentation by lactic acid bacteria on phenolic profile of quinoa and buckwheat seeds. Food Research International 119, 886–894. https://doi.org/10.1016/j.foodres.2018.10.073
Rogge, W.F., Hildemann, L.M., Mazurek, M.A., Cass, G.R., Simoneit, B.R.T., 1991a. Sources of fine organic aerosol. 1. Charbroilers and meat cooking operations. Environ. Sci. Technol. 25, 1112–1125. https://doi.org/10.1021/es00018a015
Rogge, W.F., Hildemann, L.M., Mazurek, M.A., Cass, G.R., Simoneit, B.R.T., 1991b. Sources of fine organic aerosol. 1. Charbroilers and meat cooking operations. Environ. Sci. Technol. 25, 1112–1125. https://doi.org/10.1021/es00018a015
Rose Eilenberg, S., Subramanian, R., Malings, C., Hauryliuk, A., Presto, A.A., Robinson, A.L., 2020. Using a network of lower-cost monitors to identify the influence of modifiable factors driving spatial patterns in fine particulate matter concentrations in an urban environment. J Expo Sci Environ Epidemiol 30, 949–961. https://doi.org/10.1038/s41370-020-0255-x
Ruggeri, G., Takahama, S., 2016. Technical Note: Development of chemoinformatic tools to enumerate functional groups in molecules for organic aerosol characterization. Atmospheric Chemistry and Physics 16, 4401–4422. https://doi.org/10.5194/acp-16-4401-2016
Saarikoski, S., Carbone, S., Decesari, S., Giulianelli, L., Angelini, F., Canagaratna, M., Ng, N.L., Trimborn, A., Facchini, M.C., Fuzzi, S., Hillamo, R., Worsnop, D., 2012. Chemical characterization of springtime submicrometer aerosol in Po Valley, Italy. Atmospheric Chemistry and Physics 12, 8401–8421. https://doi.org/10.5194/acp-12-8401-2012
Saha, P.K., Sengupta, S., Adams, P., Robinson, A.L., Presto, A.A., 2020. Spatial Correlation of Ultrafine Particle Number and Fine Particle Mass at Urban Scales: Implications for Health Assessment. Environ. Sci. Technol. 54, 9295–9304. https://doi.org/10.1021/acs.est.0c02763
Saha, P.K., Zimmerman, N., Malings, C., Hauryliuk, A., Li, Z., Snell, L., Subramanian, R., Lipsky, E., Apte, J.S., Robinson, A.L., Presto, A.A., 2019. Quantifying high-resolution spatial variations and local source impacts of urban ultrafine particle concentrations. Science of The Total Environment 655, 473–481. https://doi.org/10.1016/j.scitotenv.2018.11.197
Samuelsen, S., Zhu, S., Kinnon, M.M., Yang, O.K., Dabdub, D., Brouwer, J., 2021. An Episodic Assessment of Vehicle Emission Regulations on Saving Lives in California. Environ. Sci. Technol. 55, 547–552. https://doi.org/10.1021/acs.est.0c04060
Schauer, J.J., Kleeman, M.J., Cass, G.R., Simoneit, B.R.T., 2002a. Measurement of Emissions from Air Pollution Sources. 4. C1−C27 Organic Compounds from Cooking with Seed Oils. Environ. Sci. Technol. 36, 567–575. https://doi.org/10.1021/es002053m
Schauer, J.J., Kleeman, M.J., Cass, G.R., Simoneit, B.R.T., 2002b. Measurement of Emissions from Air Pollution Sources. 5. C1−C32 Organic Compounds from Gasoline-Powered Motor Vehicles. Environ. Sci. Technol. 36, 1169–1180. https://doi.org/10.1021/es0108077

Schauer, J.J., Rogge, W.F., Hildemann, L.M., Mazurek, M.A., Cass, G.R., Simoneit, B.R.T., 1996. Source apportionment of airborne particulate matter using organic compounds as tracers. Atmospheric Environment 30, 3837–3855. https://doi.org/10.1016/1352-2310(96)00085-4
Schueneman, M.K., Nault, B.A., Campuzano-Jost, P., Jo, D.S., Day, D.A., Schroder, J.C., Palm, B.B., Hodzic, A., Dibb, J.E., Jimenez, J.L., 2021. Aerosol pH indicator and organosulfate detectability from aerosol mass spectrometry measurements. Atmospheric Measurement Techniques 14, 2237–2260. https://doi.org/10.5194/amt-14-2237-2021
Seltzer, K.M., Murphy, B.N., Pennington, E.A., Allen, C., Talgo, K., Pye, H.O.T., 2022. Volatile Chemical Product Enhancements to Criteria Pollutants in the United States. Environ. Sci. Technol. 56, 6905–6913. https://doi.org/10.1021/acs.est.1c04298
Setyan, A., Zhang, Q., Merkel, M., Knighton, W.B., Sun, Y., Song, C., Shilling, J.E., Onasch, T.B., Herndon, S.C., Worsnop, D.R., Fast, J.D., Zaveri, R.A., Berg, L.K., Wiedensohler, A., Flowers, B.A., Dubey, M.K., Subramanian, R., 2012. Characterization of submicron particles influenced by mixed biogenic and anthropogenic emissions using high-resolution aerosol mass spectrometry: results from CARES. Atmospheric Chemistry and Physics 12, 8131–8156. https://doi.org/10.5194/acp-12-8131-2012
Shah, R.U., Robinson, E.S., Gu, P., Robinson, A.L., Apte, J.S., Presto, A.A., 2018a. High-spatial-resolution mapping and source apportionment of aerosol composition in Oakland, California, using mobile aerosol mass spectrometry. Atmospheric Chemistry and Physics 18, 16325–16344. https://doi.org/10.5194/acp-18-16325-2018
Shah, R.U., Robinson, E.S., Gu, P., Robinson, A.L., Apte, J.S., Presto, A.A., 2018b. High-spatial-resolution mapping and source apportionment of aerosol composition in Oakland, California, using mobile aerosol mass spectrometry. Atmospheric Chemistry and Physics 18, 16325–16344. https://doi.org/10.5194/acp-18-16325-2018
Shao, Y., Voliotis, A., Du, M., Wang, Y., Pereira, K., Hamilton, J., Alfarra, M.R., McFiggans, G., 2022. Chemical composition of secondary organic aerosol particles formed from mixtures of anthropogenic and biogenic precursors. Atmospheric Chemistry and Physics 22, 9799–9826. https://doi.org/10.5194/acp-22-9799-2022
Siegel, K., Karlsson, L., Zieger, P., Baccarini, A., Schmale, J., Lawler, M., Salter, M., Leck, C., L. Ekman, A.M., Riipinen, I., Mohr, C., 2021. Insights into the molecular composition of semi-volatile aerosols in the summertime central Arctic Ocean using FIGAERO-CIMS. Environmental Science: Atmospheres 1, 161–175. https://doi.org/10.1039/D0EA00023J
Song, R., Presto, A.A., Saha, P., Zimmerman, N., Ellis, A., Subramanian, R., 2021a. Spatial variations in urban air pollution: impacts of diesel bus traffic and restaurant cooking at small scales. Air Qual Atmos Health 14, 2059–2072. https://doi.org/10.1007/s11869-021-01078-8
Song, R., Presto, A.A., Saha, P., Zimmerman, N., Ellis, A., Subramanian, R., 2021b. Spatial variations in urban air pollution: impacts of diesel bus traffic and restaurant cooking at small scales. Air Qual Atmos Health. https://doi.org/10.1007/s11869-021-01078-8
Stolzenburg, D., Wang, M., Schervish, M., Donahue, N.M., 2022. Tutorial: Dynamic organic growth modeling with a volatility basis set. Journal of Aerosol Science 166, 106063. https://doi.org/10.1016/j.jaerosci.2022.106063
Stout, S.A., Magar, V.S., Uhler, R.M., Ickes, J., Abbott, J., Brenner, R., 2001. Characterization of Naturally-occurring and Anthropogenic PAHs in Urban Sediments-Wycoff/Eagle Harbor Superfund Site. Environmental Forensics 2, 287–300. https://doi.org/10.1080/713848281
Sturm, P.J., Baltensperger, U., Bacher, M., Lechner, B., Hausberger, S., Heiden, B., Imhof, D., Weingartner, E., Prevot, A.S.H., Kurtenbach, R., Wiesen, P., 2003. Roadside measurements of particulate matter size distribution. Atmospheric Environment, 11th International Symposium, Transport and Air Pollution 37, 5273–5281. https://doi.org/10.1016/j.atmosenv.2003.05.006
Sun, Y.L., Wang, Z.F., Fu, P.Q., Yang, T., Jiang, Q., Dong, H.B., Li, J., Jia, J.J., 2013. Aerosol composition, sources and processes during wintertime in Beijing, China. Atmospheric Chemistry and Physics 13, 4577–4592. https://doi.org/10.5194/acp-13-4577-2013

Sun, Y.L., Zhang, Q., Schwab, J.J., Yang, T., Ng, N.L., Demerjian, K.L., 2012. Factor analysis of combined organic and inorganic aerosol mass spectra from high resolution aerosol mass spectrometer measurements. Atmospheric Chemistry and Physics 12, 8537–8551. https://doi.org/10.5194/acp-12-8537-2012
Surratt, J.D., Kroll, J.H., Kleindienst, T.E., Edney, E.O., Claeys, M., Sorooshian, A., Ng, N.L., Offenberg, J.H., Lewandowski, M., Jaoui, M., Flagan, R.C., Seinfeld, J.H., 2007. Evidence for Organosulfates in Secondary Organic Aerosol. Environ. Sci. Technol. 41, 517–527. https://doi.org/10.1021/es062081q
Takegawa, N., Miyakawa, T., Watanabe, M., Kondo, Y., Miyazaki, Y., Han, S., Zhao, Y., van Pinxteren, D., Bruggemann, E., Gnauk, T., Herrmann, H., Xiao, R., Deng, Z., Hu, M., Zhu, T., Zhang, Y., 2009. Performance of an Aerodyne Aerosol Mass Spectrometer (AMS) during Intensive Campaigns in China in the Summer of 2006. Aerosol Science and Technology 43, 189–204. https://doi.org/10.1080/02786820802582251
Takhar, M., Li, Y., Chan, A.W.H., 2021. Characterization of secondary organic aerosol from heated-cooking-oil emissions: evolution in composition and volatility. Atmospheric Chemistry and Physics 21, 5137–5149. https://doi.org/10.5194/acp-21-5137-2021
Takhar, M., Stroud, C.A., Chan, A.W.H., 2019. Volatility Distribution and Evaporation Rates of Organic Aerosol from Cooking Oils and their Evolution upon Heterogeneous Oxidation. ACS Earth Space Chem. 3, 1717–1728. https://doi.org/10.1021/acsearthspacechem.9b00110
Tan, Y., Dallmann, T.R., Robinson, A.L., Presto, A.A., 2016. Application of plume analysis to build land use regression models from mobile sampling to improve model transferability. Atmospheric Environment 134, 51–60. https://doi.org/10.1016/j.atmosenv.2016.03.032
Tanzer, R., Malings, C., Hauryliuk, A., Subramanian, R., Presto, A.A., 2019. Demonstration of a Low-Cost Multi-Pollutant Network to Quantify Intra-Urban Spatial Variations in Air Pollutant Source Impacts and to Evaluate Environmental Justice. International Journal of Environmental Research and Public Health 16, 2523. https://doi.org/10.3390/ijerph16142523
The, S.V., Snyder, R., Tegeder, M., 2021. Targeting Nitrogen Metabolism and Transport Processes to Improve Plant Nitrogen Use Efficiency. Front. Plant Sci. 11. https://doi.org/10.3389/fpls.2020.628366
Thompson, S.L., Yatavelli, R.L.N., Stark, H., Kimmel, J.R., Krechmer, J.E., Day, D.A., Hu, W., Isaacman-VanWertz, G., Yee, L., Goldstein, A.H., Khan, M.A.H., Holzinger, R., Kreisberg, N., Lopez-Hilfiker, F.D., Mohr, C., Thornton, J.A., Jayne, J.T., Canagaratna, M., Worsnop, D.R., Jimenez, J.L., 2017. Field intercomparison of the gas/particle partitioning of oxygenated organics during the Southern Oxidant and Aerosol Study (SOAS) in 2013. Aerosol Science and Technology 51, 30–56. https://doi.org/10.1080/02786826.2016.1254719
Thornton, J.A., Mohr, C., Schobesberger, S., D'Ambro, E.L., Lee, B.H., Lopez-Hilfiker, F.D., 2020. Evaluating Organic Aerosol Sources and Evolution with a Combined Molecular Composition and Volatility Framework Using the Filter Inlet for Gases and Aerosols (FIGAERO). Acc. Chem. Res. 53, 1415–1426. https://doi.org/10.1021/acs.accounts.0c00259
Tikkanen, O.-P., Buchholz, A., Ylisirniö, A., Schobesberger, S., Virtanen, A., Yli-Juuti, T., 2020. Comparing secondary organic aerosol (SOA) volatility distributions derived from isothermal SOA particle evaporation data and FIGAERO–CIMS measurements. Atmospheric Chemistry and Physics 20, 10441–10458. https://doi.org/10.5194/acp-20-10441-2020
Torkmahalleh, M.A., Goldasteh, I., Zhao, Y., Udochu, N.M., Rossner, A., Hopke, P.K., Ferro, A.R., 2012. PM2.5 and ultrafine particles emitted during heating of commercial cooking oils. Indoor Air 22, 483–491. https://doi.org/10.1111/j.1600-0668.2012.00783.x
Tsimpidi, A.P., Karydis, V.A., Pandis, S.N., Lelieveld, J., 2016. Global combustion sources of organic aerosols: model comparison with 84 AMS factor-analysis data sets. Atmospheric Chemistry and Physics 16, 8939–8962. https://doi.org/10.5194/acp-16-8939-2016
Ulbrich, I.M., Canagaratna, M.R., Zhang, Q., Worsnop, D.R., Jimenez, J.L., 2009. Interpretation of organic components from Positive Matrix Factorization of aerosol mass spectrometric data. Atmospheric Chemistry and Physics 9, 2891–2918. https://doi.org/10.5194/acp-9-2891-2009

Utami, U., Nadiya, R.A., Harianie, L., 2024. The effect of molasses and yeast extract concentration on yeast growth as leavening agent for bread. IOP Conf. Ser.: Earth Environ. Sci. 1312, 012062. https://doi.org/10.1088/1755-1315/1312/1/012062
Vaughan, E.J., Wilson, S.K., Howlett, S.J., Parravicini, V., Williams, G.J., Graham, N.A.J., 2021. Nitrogen enrichment in macroalgae following mass coral mortality. Coral Reefs 40, 767–776. https://doi.org/10.1007/s00338-021-02079-w
Vicente, E.D., Vicente, A., Evtyugina, M., Carvalho, R., Tarelho, L.A.C., Oduber, F.I., Alves, C., 2018. Particulate and gaseous emissions from charcoal combustion in barbecue grills. Fuel Processing Technology 176, 296–306. https://doi.org/10.1016/j.fuproc.2018.03.004
Vodička, P., Kawamura, K., Schwarz, J., Ždímal, V., 2022. Seasonal changes in stable carbon isotopic composition in the bulk aerosol and gas phases at a suburban site in Prague. Science of The Total Environment 803, 149767. https://doi.org/10.1016/j.scitotenv.2021.149767
Voliotis, A., Du, M., Wang, Y., Shao, Y., Alfarra, M.R., Bannan, T.J., Hu, D., Pereira, K.L., Hamilton, J.F., Hallquist, M., Mentel, T.F., McFiggans, G., 2022. Chamber investigation of the formation and transformation of secondary organic aerosol in mixtures of biogenic and anthropogenic volatile organic compounds. Atmospheric Chemistry and Physics 22, 14147–14175. https://doi.org/10.5194/acp-22-14147-2022
Wallace, L.A., Emmerich, S.J., Howard-Reed, C., 2004. Source Strengths of Ultrafine and Fine Particles Due to Cooking with a Gas Stove. Environ. Sci. Technol. 38, 2304–2311. https://doi.org/10.1021/es0306260
Wan, M.-P., Wu, C.-L., Sze To, G.-N., Chan, T.-C., Chao, C.Y.H., 2011. Ultrafine particles, and PM2.5 generated from cooking in homes. Atmospheric Environment 45, 6141–6148. https://doi.org/10.1016/j.atmosenv.2011.08.036
Wang, J., Sha, Z., Zhang, J., Qin, W., Xu, W., Goulding, K., Liu, X., 2023. Improving nitrogen fertilizer use efficiency and minimizing losses and global warming potential by optimizing applications and using nitrogen synergists in a maize-wheat rotation. Agriculture, Ecosystems & Environment 353, 108538. https://doi.org/10.1016/j.agee.2023.108538
Wang, J., Ye, J., Liu, D., Wu, Y., Zhao, J., Xu, W., Xie, C., Shen, F., Zhang, J., Ohno, P.E., Qin, Y., Zhao, X., Martin, S.T., Lee, A.K.Y., Fu, P., Jacob, D.J., Zhang, Q., Sun, Y., Chen, M., Ge, X., 2020. Characterization of submicron organic particles in Beijing during summertime: comparison between SP-AMS and HR-AMS. Atmospheric Chemistry and Physics 20, 14091–14102. https://doi.org/10.5194/acp-20-14091-2020
Wang, L., Zhang, L., Ristovski, Z., Zheng, X., Wang, H., Li, L., Gao, J., Salimi, F., Gao, Y., Jing, S., Wang, Lin, Chen, J., Stevanovic, S., 2020. Assessing the Effect of Reactive Oxygen Species and Volatile Organic Compound Profiles Coming from Certain Types of Chinese Cooking on the Toxicity of Human Bronchial Epithelial Cells. Environ. Sci. Technol. 54, 8868–8877. https://doi.org/10.1021/acs.est.9b07553
Wang, S., Gao, S., Li, S., Feng, K., 2020. Strategizing the relation between urbanization and air pollution: Empirical evidence from global countries. Journal of Cleaner Production 243, 118615. https://doi.org/10.1016/j.jclepro.2019.118615
Wang, Y., Bechle, M.J., Kim, S.-Y., Adams, P.J., Pandis, S.N., Pope, C.A., Robinson, A.L., Sheppard, L., Szpiro, A.A., Marshall, J.D., 2020. Spatial decomposition analysis of NO2 and PM2.5 air pollution in the United States. Atmospheric Environment 241, 117470. https://doi.org/10.1016/j.atmosenv.2020.117470
Wang, Y., Yao, L., Xu, Y., Sun, S., Li, T., 2021. Potential heterogeneity in the relationship between urbanization and air pollution, from the perspective of urban agglomeration. Journal of Cleaner Production 298, 126822. https://doi.org/10.1016/j.jclepro.2021.126822
Wang, Y., Zhu, Y., Salinas, R., Ramirez, D., Karnae, S., John, K., 2008. Roadside Measurements of Ultrafine Particles at a Busy Urban Intersection. Journal of the Air & Waste Management Association 58, 1449–1457. https://doi.org/10.3155/1047-3289.58.11.1449
Wang, Y., Zhuang, G., Chen, S., An, Z., Zheng, A., 2007. Characteristics and sources of formic, acetic and oxalic acids in PM2.5 and PM10 aerosols in Beijing, China. Atmospheric Research 84, 169–181. https://doi.org/10.1016/j.atmosres.2006.07.001

Wang, Zixuan, Xing, A., Shen, H., 2023. Effects of nitrogen addition on the combined global warming potential of three major soil greenhouse gases: A global meta-analysis. Environmental Pollution 334, 121848. https://doi.org/10.1016/j.envpol.2023.121848
Wang, Zhibo, Yu, D., Morota, G., Dhakal, K., Singer, W., Lord, N., Huang, H., Chen, P., Mozzoni, L., Li, S., Zhang, B., 2023. Genome-wide association analysis of sucrose and alanine contents in edamame beans. Front. Plant Sci. 13. https://doi.org/10.3389/fpls.2022.1086007
Weidner, L., Cannas, J.V., Rychlik, M., Schmitt-Kopplin, P., 2023. Molecular Characterization of Cooking Processes: A Metabolomics Decoding of Vaporous Emissions for Food Markers and Thermal Reaction Indicators. J. Agric. Food Chem. 71, 17442–17454. https://doi.org/10.1021/acs.jafc.3c05383
Wood, C.W., Torbert, H.A., Weaver, D.B., 1993. Nitrogen Fertilizer Effects on Soybean Growth, Yield, and Seed Composition. Journal of Production Agriculture 6, 354–360. https://doi.org/10.2134/jpa1993.0354
Wu, C.L., Chao, C.Y.H., Sze-To, G.N., Wan, M.P., Chan, T.C., 2012. Ultrafine Particle Emissions from Cigarette Smouldering, Incense Burning, Vacuum Cleaner Motor Operation and Cooking. Indoor and Built Environment 21, 782–796. https://doi.org/10.1177/1420326X11421356
Xu, J., Zhang, Q., Chen, M., Ge, X., Ren, J., Qin, D., 2014. Chemical composition, sources, and processes of urban aerosols during summertime in northwest China: insights from high-resolution aerosol mass spectrometry. Atmospheric Chemistry and Physics 14, 12593–12611. https://doi.org/10.5194/acp-14-12593-2014
Xu, L., Coggon, M.M., Stockwell, C.E., Gilman, J.B., Robinson, M.A., Breitenlechner, M., Lamplugh, A., Crounse, J.D., Wennberg, P.O., Neuman, J.A., Novak, G.A., Veres, P.R., Brown, S.S., Warneke, C., 2022. Chemical ionization mass spectrometry utilizing ammonium ions (NH4+ CIMS) for measurements of organic compounds in the atmosphere. Atmospheric Measurement Techniques 15, 7353–7373. https://doi.org/10.5194/amt-15-7353-2022
Xu, W., Lambe, A., Silva, P., Hu, W., Onasch, T., Williams, L., Croteau, P., Zhang, X., Renbaum-Wolff, L., Fortner, E., Jimenez, J.L., Jayne, J., Worsnop, D., Canagaratna, M., 2018. Laboratory evaluation of species-dependent relative ionization efficiencies in the Aerodyne Aerosol Mass Spectrometer. Aerosol Science and Technology 52, 626–641. https://doi.org/10.1080/02786826.2018.1439570
Yang, L.H., Takeuchi, M., Chen, Y., Ng, N.L., 2021. Characterization of thermal decomposition of oxygenated organic compounds in FIGAERO-CIMS. Aerosol Science and Technology 55, 1321–1342. https://doi.org/10.1080/02786826.2021.1945529
Yao, D., Lyu, X., Lu, H., Zeng, L., Liu, T., Chan, C.K., Guo, H., 2021. Characteristics, sources and evolution processes of atmospheric organic aerosols at a roadside site in Hong Kong. Atmospheric Environment 252, 118298. https://doi.org/10.1016/j.atmosenv.2021.118298
Yao, X., Lau, N.T., Fang, M., Chan, C.K., 2005. Real-Time Observation of the Transformation of Ultrafine Atmospheric Particle Modes. Aerosol Science and Technology 39, 831–841. https://doi.org/10.1080/02786820500295248
Ye, C., Yuan, B., Lin, Y., Wang, Z., Hu, W., Li, T., Chen, W., Wu, C., Wang, Chaomin, Huang, S., Qi, J., Wang, B., Wang, Chen, Song, W., Wang, Xinming, Zheng, E., Krechmer, J.E., Ye, P., Zhang, Z., Wang, Xuemei, Worsnop, D.R., Shao, M., 2021. Chemical characterization of oxygenated organic compounds in the gas phase and particle phase using iodide CIMS with FIGAERO in urban air. Atmospheric Chemistry and Physics 21, 8455–8478. https://doi.org/10.5194/acp-21-8455-2021
Ye, Q., Gu, P., Li, H.Z., Robinson, E.S., Lipsky, E., Kaltsonoudis, C., Lee, A.K.Y., Apte, J.S., Robinson, A.L., Sullivan, R.C., Presto, A.A., Donahue, N.M., 2018a. Spatial Variability of Sources and Mixing State of Atmospheric Particles in a Metropolitan Area. Environ. Sci. Technol. 52, 6807–6815. https://doi.org/10.1021/acs.est.8b01011
Ye, Q., Gu, P., Li, H.Z., Robinson, E.S., Lipsky, E., Kaltsonoudis, C., Lee, A.K.Y., Apte, J.S., Robinson, A.L., Sullivan, R.C., Presto, A.A., Donahue, N.M., 2018b. Spatial Variability of Sources and Mixing State of Atmospheric Particles in a Metropolitan Area. Environ. Sci. Technol. 52, 6807–6815. https://doi.org/10.1021/acs.est.8b01011

Yokelson, R.J., Goode, J.G., Ward, D.E., Susott, R.A., Babbitt, R.E., Wade, D.D., Bertschi, I., Griffith, D.W.T., Hao, W.M., 1999. Emissions of formaldehyde, acetic acid, methanol, and other trace gases from biomass fires in North Carolina measured by airborne Fourier transform infrared spectroscopy. Journal of Geophysical Research: Atmospheres 104, 30109–30125. https://doi.org/10.1029/1999JD900817
Yoon, S., Ortiz, S.M., Clark, A.E., Barrett, T.E., Usenko, S., Duvall, R.M., Ruiz, L.H., Bean, J.K., Faxon, C.B., Flynn, J.H., Lefer, B.L., Leong, Y.J., Griffin, R.J., Sheesley, R.J., 2021. Apportioned primary and secondary organic aerosol during pollution events of DISCOVER-AQ Houston. Atmospheric Environment 244, 117954. https://doi.org/10.1016/j.atmosenv.2020.117954
Yu, X., Li, Q., Liao, K., Li, Y., Wang, X., Zhou, Y., Liang, Y., Yu, J.Z., 2024. New measurements reveal a large contribution of nitrogenous molecules to ambient organic aerosol. npj Clim Atmos Sci 7, 1–9. https://doi.org/10.1038/s41612-024-00620-6
Zareie, Z., Moayedi, A., Garavand, F., Tabar-Heydar, K., Khomeiri, M., Maghsoudlou, Y., 2023. Probiotic Properties, Safety Assessment, and Aroma-Generating Attributes of Some Lactic Acid Bacteria Isolated from Iranian Traditional Cheese. Fermentation 9, 338. https://doi.org/10.3390/fermentation9040338
Zhang, H., Han, X., Wei, C., Bao, J., 2017. Oxidative production of xylonic acid using xylose in distillation stillage of cellulosic ethanol fermentation broth by Gluconobacter oxydans. Bioresource Technology 224, 573–580. https://doi.org/10.1016/j.biortech.2016.11.039
Zhang, H., Yee, L.D., Lee, B.H., Curtis, M.P., Worton, D.R., Isaacman-VanWertz, G., Offenberg, J.H., Lewandowski, M., Kleindienst, T.E., Beaver, M.R., Holder, A.L., Lonneman, W.A., Docherty, K.S., Jaoui, M., Pye, H.O.T., Hu, W., Day, D.A., Campuzano-Jost, P., Jimenez, J.L., Guo, H., Weber, R.J., de Gouw, J., Koss, A.R., Edgerton, E.S., Brune, W., Mohr, C., Lopez-Hilfiker, F.D., Lutz, A., Kreisberg, N.M., Spielman, S.R., Hering, S.V., Wilson, K.R., Thornton, J.A., Goldstein, A.H., 2018. Monoterpenes are the largest source of summertime organic aerosol in the southeastern United States. Proceedings of the National Academy of Sciences 115, 2038–2043. https://doi.org/10.1073/pnas.1717513115
Zhang, J., Li, K., Wang, T., Gammelsæter, E., Cheung, R.K.Y., Surdu, M., Bogler, S., Bhattu, D., Wang, D.S., Cui, T., Qi, L., Lamkaddam, H., El Haddad, I., Slowik, J.G., Prevot, A.S.H., Bell, D.M., 2023. Bulk and molecular-level composition of primary organic aerosol from wood, straw, cow dung, and plastic burning. Atmospheric Chemistry and Physics 23, 14561–14576. https://doi.org/10.5194/acp-23-14561-2023
Zhang, L., You, S., Zhang, M., Zhang, S., Yi, S., Zhou, B., 2022. The effects of urbanization on air pollution based on a spatial perspective: Evidence from China. Front. Environ. Sci. 10. https://doi.org/10.3389/fenvs.2022.1058009
Zhang, Q., Alfarra, M.R., Worsnop, D.R., Allan, J.D., Coe, H., Canagaratna, M.R., Jimenez, J.L., 2005. Deconvolution and Quantification of Hydrocarbon-like and Oxygenated Organic Aerosols Based on Aerosol Mass Spectrometry. Environ. Sci. Technol. 39, 4938–4952. https://doi.org/10.1021/es048568l
Zhang, Q., Jimenez, J.L., Canagaratna, M.R., Ulbrich, I.M., Ng, N.L., Worsnop, D.R., Sun, Y., 2011. Understanding atmospheric organic aerosols via factor analysis of aerosol mass spectrometry: a review. Anal Bioanal Chem 401, 3045–3067. https://doi.org/10.1007/s00216-011-5355-y
Zhang, W., Yu, H., Hettiyadura, A.P.S., Verma, V., Laskin, A., 2022. Field evidence for enhanced generation of reactive oxygen species in atmospheric aerosol containing quinoline components. Atmospheric Environment 291, 119406. https://doi.org/10.1016/j.atmosenv.2022.119406
Zhang, X., Han, L., Wei, H., Tan, X., Zhou, W., Li, W., Qian, Y., 2022. Linking urbanization and air quality together: A review and a perspective on the future sustainable urban development. Journal of Cleaner Production 346, 130988. https://doi.org/10.1016/j.jclepro.2022.130988
Zhang, Y., Liu, R., Yang, D., Guo, Y., Li, M., Hou, K., 2023. Chemical ionization mass spectrometry: Developments and applications for on-line characterization of atmospheric aerosols and trace gases. TrAC Trends in Analytical Chemistry 168, 117353. https://doi.org/10.1016/j.trac.2023.117353
Zhang, Y., Tang, L., Yu, H., Wang, Z., Sun, Y., Qin, W., Chen, W., Chen, Changhong, Ding, A., Wu, J., Ge, S., Chen, Cheng, Zhou, H., 2015. Chemical composition, sources and evolution processes of aerosol at an urban site in Yangtze River Delta, China during wintertime. Atmospheric Environment, PM2.5

Research in the Yangtze River Delta: Observations, processes, modeling and Health effects 123, 339–349. https://doi.org/10.1016/j.atmosenv.2015.08.017
Zhang, Z., Zhu, W., Hu, M., Wang, H., Chen, Z., Shen, R., Yu, Y., Tan, R., Guo, S., 2021a. Secondary Organic Aerosol from Typical Chinese Domestic Cooking Emissions. Environ. Sci. Technol. Lett. 8, 24–31. https://doi.org/10.1021/acs.estlett.0c00754
Zhang, Z., Zhu, W., Hu, M., Wang, H., Chen, Z., Shen, R., Yu, Y., Tan, R., Guo, S., 2021b. Secondary Organic Aerosol from Typical Chinese Domestic Cooking Emissions. Environ. Sci. Technol. Lett. 8, 24–31. https://doi.org/10.1021/acs.estlett.0c00754
Zhang, Zirui, Zhu, W., Hu, M., Liu, K., Wang, H., Tang, R., Shen, R., Yu, Y., Tan, R., Song, K., Li, Y., Zhang, W., Zhang, Zhou, Xu, H., Shuai, S., Li, S., Chen, Y., Li, J., Wang, Y., Guo, S., 2021c. Formation and evolution of secondary organic aerosols derived from urban-lifestyle sources: vehicle exhaust and cooking emissions. Atmospheric Chemistry and Physics 21, 15221–15237. https://doi.org/10.5194/acp-21-15221-2021
Zhao, H., Yuan, M., Strokal, M., Wu, H.C., Liu, X., Murk, A., Kroeze, C., Osinga, R., 2021. Impacts of nitrogen pollution on corals in the context of global climate change and potential strategies to conserve coral reefs. Science of The Total Environment 774, 145017. https://doi.org/10.1016/j.scitotenv.2021.145017
Zhao, Y., Hu, M., Slanina, S., Zhang, Y., 2007a. Chemical Compositions of Fine Particulate Organic Matter Emitted from Chinese Cooking. Environ. Sci. Technol. 41, 99–105. https://doi.org/10.1021/es0614518
Zhao, Y., Hu, M., Slanina, S., Zhang, Y., 2007b. The molecular distribution of fine particulate organic matter emitted from Western-style fast food cooking. Atmospheric Environment 41, 8163–8171. https://doi.org/10.1016/j.atmosenv.2007.06.029
Zhao, Y., Hu, M., Slanina, S., Zhang, Y., 2007c. Chemical Compositions of Fine Particulate Organic Matter Emitted from Chinese Cooking. Environ. Sci. Technol. 41, 99–105. https://doi.org/10.1021/es0614518
Zhou, W., Xu, W., Kim, H., Zhang, Q., Fu, P., R. Worsnop, D., Sun, Y., 2020. A review of aerosol chemistry in Asia: insights from aerosol mass spectrometer measurements. Environmental Science: Processes & Impacts 22, 1616–1653. https://doi.org/10.1039/D0EM00212G
Zhu, Q., Huang, X.-F., Cao, L.-M., Wei, L.-T., Zhang, B., He, L.-Y., Elser, M., Canonaco, F., Slowik, J.G., Bozzetti, C., El-Haddad, I., Prévôt, A.S.H., 2018. Improved source apportionment of organic aerosols in complex urban air pollution using the multilinear engine (ME-2). Atmospheric Measurement Techniques 11, 1049–1060. https://doi.org/10.5194/amt-11-1049-2018